LNCIS
Lecture Notes in Control and Information Sciences
414

Hocine Imine
Leonid Fridman
Hassan Shraim
Mohamed Djemai

Sliding Mode Based Analysis and Identification of Vehicle Dynamics

Springer

Lecture Notes in Control and Information Sciences 414

Editors: M. Thoma, F. Allgöwer, M. Morari

Hocine Imine, Leonid Fridman, Hassan Shraim,
and Mohamed Djemai

Sliding Mode Based Analysis and Identification of Vehicle Dynamics

Springer

Authors

Dr. Hocine Imine
Laboratoire d'Expliotation, Perception,
Simulateurs et Silulations (LEPSIS)
Institut Français des Sciences et Technologies des
Transports, de l'Aménagement
et des Réseaux (IFSTTAR)
LCPC/INRETS, 58 Boulevard Lefebvre
75732 Paris, France
E-mail: hocine.imine@ifsttar.fr

Dr. Leonid Fridman
Universidad Nacional Autonoma de Mexico
Departamento de Ingeniería de Control y Robótica
División de Ingeniería Eléctrica
Facultad de Ingeniería UNAM
04510, Mexico, D.F. Mexico
E-mail: lfridman@servidor.unam.mx

Dr. Hassan Shraim
University of Paul Cezanne
BR Laboratory of Sciences of Informations
and of Systems
LSIS UMR 6168
Escadrille de Normandie, Niemen
Aix-Marseille III Av
13397, Marseille Cedex 20, France
E-mail: hassanshraim@yahoo.fr

Dr. Mohamed Djemai
University of Valenciennes and
Hainaut-Cambrésis (UVHC)
Laboratory LAMIH, UMR CNRS 8530
Valenciennes 59300, France
E-mail: mohamed.djemai@univ-valenciennes.fr

ISBN 978-3-642-22223-8 e-ISBN 978-3-642-22224-5

DOI 10.1007/978-3-642-22224-5

Lecture Notes in Control and Information Sciences ISSN 0170-8643

Library of Congress Control Number: 2011932321

Typeset & Cover Design: Scientific Publishing Services Pvt. Ltd., Chennai, India.

Printed on acid-free paper

9 8 7 6 5 4 3 2 1

springer.com

We dedicate this book to all researchers who work in the field of vehicle dynamics and Variable Structure System.

Acknowledgements

This work has been supported, for M. Djemai, by International Campus on Safety and Intermodality in Transportation, the European Community, the Delegation Regionale à la Recherche et à la Technologie, the Ministere de l'Enseignement superieur et de la Recherche, the Region Nord Pas de Calais and the Centre National de la Recherche Scientifique.

The authors gratefully acknowledge Professor Hajjaji for his great help and his interest to this research work.

Contents

1 Introduction ... 1

2 Observation and Identification via HOSM-Observers ... 5
- 2.1 Motivation ... 5
- 2.2 Mechanical Systems ... 6
  - 2.2.1 Super-Twisting Based Observer ... 7
  - 2.2.2 Differentiation vs. Observation ... 11
  - 2.2.3 Equivalent Output Injection Analysis ... 13
  - 2.2.4 Parameter Identification ... 15
  - 2.2.5 Example ... 19
- 2.3 Conclusion ... 24

3 Vehicle Modeling ... 25
- 3.1 Introduction ... 25
- 3.2 Coordinate Systems ... 28
  - 3.2.1 Fixed Coordinate System R_0 ... 28
  - 3.2.2 Center of Gravity Coordinate System R_c ... 29
- 3.3 Chassis Modeling ... 32
  - 3.3.1 Translation Motion ... 32
  - 3.3.2 Rotational Motion ... 33
  - 3.3.3 Side Slip Angle ... 33
- 3.4 Suspension Model ... 35
- 3.5 Wheel/Road Interaction ... 37
  - 3.5.1 Contact Surface ... 37
  - 3.5.2 Vertical Forces ... 38
  - 3.5.3 Longitudinal Forces ... 39
  - 3.5.4 Lateral Forces ... 46
  - 3.5.5 Aerodynamic Forces ... 47
  - 3.5.6 Angular Motions of the Wheels ... 47

3.6 Model Validation ... 48
3.6.1 Simulator Description ... 49
3.6.2 Vehicle Instrumentation ... 49
3.6.3 Validation Results ... 55
3.7 Conclusion ... 59

4 States and Parameters Estimation ... 61
4.1 Introduction ... 61
4.2 Problem Statement ... 64
4.3 A Second Order Sliding Mode Observer Design ... 66
4.3.1 Unknown Parameter Identification ... 66
4.3.2 Simulation Results ... 67
4.4 Side Slip Angle ... 70
4.4.1 Two Track Model and Observability Study ... 73
4.4.2 Comparison between the Observers ... 76
4.4.3 Simulation Results and Discussions ... 76
4.5 Conclusion ... 81

5 Estimation of Road Profile and External Forces as Unknown Inputs ... 83
5.1 Introduction ... 83
5.2 Vehicle Modeling ... 84
5.3 Sliding Mode Observer and Estimation of Unknown Inputs ... 86
5.3.1 Observability Study ... 86
5.3.2 Observer Design ... 87
5.3.3 Convergence Study ... 88
5.3.4 Estimation Results ... 90
5.4 Unknown Forces Estimation ... 94
5.4.1 Convergence Study ... 96
5.4.2 Experimental Results ... 98
5.5 Conclusion ... 102

6 Conclusions ... 103

References ... 105

A Recalls on Sliding Modes Techniques ... 113

B Equivalent Control Concept ... 117
B.1 Motivation ... 117
B.2 Equivalent Control Method ... 117

C Vehicle Parameters Description ... 125
C.1 Vehicle Data ... 125
C.2 Friction Parameters Characteristics ... 125

D Matrices Definitions ... 127

Chapter 1
Introduction

Vehicles are complex mechanical systems with strong nonlinear characteristics and which can present some uncertainties due to their dynamic parameters such as masses, inertias, suspension springs, tires side slip coefficients, etc.

A vehicle is composed of many parts, namely the unsprung mass, the sprung mass, the suspension which makes the link between these two masses and therefore ensures passenger comfort, and also the pneumatic which absorbs the energy coming from the road and ensures contact between the vehicle and the road. In addition to its complexity and the presence of many nonlinearities and uncertainties, the presence of some external perturbations, such as the wind and the road inputs with its own characteristics (radius of curvature, longitudinal and lateral slop, road profile and skid resistance) can cause risks not only to the vehicle but also to passengers and other road users.

Many methods have been developed in order to understand the behavior of a vehicle (light and heavy vehicle), control it and assist the driver in order to avoid possible lane departures, rollover or jackknifing risks, to ensure a better passenger comfort by means of a suspension control and/or to estimate a safety speed and trajectory ([KN05], [SOA05a], [ID07], [ISM08], [AFTV10], [KID10c]).

The main specific features of vehicles as control systems are:

- The absence of exact models of the vehicle as the system and all its subsystems.
- The state variables of the models are sometimes difficult to measure.
- These parameters of the known models are often not well known (for, example, because they are not provided by the companies working with vehicle manufacturers) and have to be identified.
- The parameters of the vehicles are time varying.
  That is why in the last years, many techniques of robust control have been used in order to ensure the safety and comfort of passengers and road users. Such techniques are able to control and observe the vehicle dynamics,

H. Imine et al.: Sliding Mode Based Analysis, LNCIS 414, pp. 1–4.

especially when we need to identify uncertainties and parameters online with the best possible accuracy.

The algorithms for control, observation and identification based on sliding modes are a special technique ensuring theoretically exact convergence of the error even in the presence of uncertainties and disturbances([Eme67], [Utk77], [Utk92], [SLD+06], [EFT07]).

The first order sliding mode based controllers and observers have already been successfully employed and experimentally illustrated for control, observation and identification of vehicle dynamics ([KR95], [CH99], [ILMD02b]).

Other applications of classical sliding mode techniques related to vehicle dynamics such as estimation of the tire road contact friction and control wheel slip, can be found in the literature ([CH99], [HCB+01], [HCM01], [AFTV10]). Omar and al have developed methods using sliding mode observer for heavy duty vehicle tyre forces estimation ([KID10a], [KID10b], [KID10c]).

Moreover, Imine and al ([ILMD01], [ILMD02a], [IF08]) have developed sliding mode observers with unknown inputs in order to estimate the road profile identifying it as an unknown input of the vehicle model. Marouf and al ([MDSP10], [NMS+10]) have developed sliding mode observers with unknown inputs in order to estimate road reaction force of an electric power assisted steering.

Other authors have developed warning systems based on sliding modes in order to control the trajectory of the vehicle ([SH97], [UK99], [MNMSm00], [Mam02], [SOF07]).

Sliding mode techniques can also be used in order to estimate the unknown parameters of the vehicle such us tire cornering stiffness, spring stiffness, etc. ([Sie97], [HCBM01], [SAF+06],).

Fault detection and diagnosis is also another application of sliding modes in the field of vehicle dynamics ([YS95], [GMR01], [MYWL02], [FBPD04], [SOA05b], [SFAO07]).

In this book we will also deal with recently developed higher order sliding mode (HOSM) algorithms ([Lev85], [EKL93], [Lev98], [FLD08]). Such algorithms allow ensuring the maximal possible asymptotic precision in terms of the sampling step and measurement noises in the sense of Kolmogorov [Kol62] and overcome the need of the sliding mode surface design.

Furthermore, HOSM differentiators ([Lev98], [Lev03]) and HOSM based observers ([DFL05a], [FB06], [FLD07]) ensure theoretically exact convergence to the exact system states and unknown inputs for systems which satisfy the sufficient and necessary conditions of strong observability. Moreover, the state estimation and unknown inputs identification may be reached *without filtration.* The use of HOSM differentiators in these observers ensure the maximal possible asymptotic precision in terms of the sampling step and measurement noises in the sense of Kolmogoroff [Kol62].

The continuous nature of vehicles as mechanical systems require continuous methods for uncertainties and parameter identification. That is why the continuous version of the Least Square Method for time invariant and time varying parameters was proposed in ([PSF+06], [BFP07]).

The present book is an attempt to show how the above mentioned HOSM based observation, uncertainties identification and parameter estimation may be applied in the control of vehicle dynamics as well as for parameter and perturbations estimation.

The aim of the presented work is to propose an interesting tool for researchers and students working in the field of vehicle dynamics and estimation.

Firstly, the HOSM observation methodology for mechanical systems is revisited. Then, a dynamic model of a vehicle is presented and validated through experimental tests.

The quality of HOSM observation and identification techniques is tested in the estimation of road profiles and external forces as the unknown inputs.

This book is composed of four chapters described as follows:

- **Chapter 1: Observation and Identification via HOSM-Observers**

The methods for state observation and identification based on higher-order sliding mode algorithms will be presented in the first chapter. The super-twisting based second-order sliding mode (SOSM) observers for mechanical systems are presented. The precision of the convergence of the proposed observers is discussed.

Two different methodologies of unknown inputs estimation are presented. First, an SOSM based observer which requires filtration but allows identifying bounded measurable perturbations is discussed. Then a third order sliding mode based observer is developed which allows estimating Lipschitz perturbations *without filtration*.

Finally, the continuous version of the Least Square Method for time invariant parameters identification is proposed.

- **Chapter 2: Vehicle Modeling**

The second chapter devoted to vehicle modeling. The car model is divided into different parts. Each part of the model, such as pneumatic, suspension and wheels, is developed in detail.

Simulation results done with Matlab-Simulink software and experimental results done with an instrumented vehicle rolling on a track are presented and compared in order to show the validity of the proposed model.

- **Chapter 3: Observation and Estimation of States and Parameters**

In the third chapter, sliding mode observers are proposed for the estimation of tire forces, side slip angle and the states of a complete vehicle. The estimations of the longitudinal forces are based on the assumption that they are considered as unknown inputs. These unknown inputs are estimated using a second order sliding mode observer based on the super-twisting algorithm and then filtered through a low-pass filter. In the second part, the estimated longitudinal forces are injected in the reduced state space equations representing the vehicle, which contain the side slip angle and the yaw rate of the center of gravity. Estimation in this part is based on the principles of the classical sliding mode observer. Velocities of the center of gravity are deduced directly after the side slip angle, and then lateral forces can be easily obtained. The vertical force of each wheel can be estimated using accelerometer measurements and the vertical position of the center of gravity.

- **Chapter 4: Estimation of Road Profile and External Forces as Unknown Inputs**

In the fourth chapter, an application of sliding mode observers is developed in order to estimate the unknown inputs of the road profile. Vehicle motion simulation accuracy, such as in accident reconstruction or vehicle controllability analysis on real roads, can be obtained only if valid road profile and tire-road friction models are available. Regarding road profiles, a new method based on Sliding Mode Observers has been developed and is compared to two inertial methods. Experimental results are shown and discussed to evaluate the robustness and the quality of the proposed approach.

The external forces, namely the longitudinal forcer of the wheels which are a function of the road adhesion coefficient, are considered as unknown states to be estimated. This it the second objective ensured in this chapter.

- **Conclusion**

Some analysis and remarks concerning the application of sliding mode technique to vehicle dynamics, as well as the different presented results, are given in this chapter. Some perspectives and new solutions are also given in order to improve the quality of the proposed work.

How to read this book?

Readers which already know about HOSM observation techniques can go directly to Chapter 2.

Those readers interested in car models can read Chapter 2 only.

Finally, readers which are familiar with car modeling and HOSM observation techniques can read Chapters 3 and 4 only.

Hocine Imine
Leonid Fridman
Hassam Shraim
Mohamed Djemai

April, 2011

Chapter 2
Observation and Identification via HOSM-Observers

2.1 Motivation

The idea of using a dynamical system to generate estimates of the system states was proposed in 1963 by Luenberger for linear systems [Lue64]. In spite of the extensive development of robust control techniques, sliding mode control (SMC) remains a key choice for handling Boundedness uncertainties/disturbances and unmodeled dynamics in both control and estimation problems. During the last decade, SMC techniques have been widely used to design observers (sliding mode observers) suitable for robust state estimation even in the presence of unknown inputs.

In absence of external disturbances, Luenberger observers can be applied directly for asymptotical reconstruction of the system states. However, in the presence of disturbances, the standard technique is not accurate; the Luenberger observer can only ensure the convergence to a bounded region near the real value of the state.

Sliding Mode Based Observers are presented as an alternative to the problem of observation of perturbed systems. In particular, High Order Sliding Mode (HOSM) Based Observers can be considered as a successful technique for the state observation of perturbed systems due their high precision and robust behavior with respect to parametric uncertainties.

The existence of a direct relation between differentiation and the observability problem makes Sliding Mode Based Differentiators a technique that can be applied directly for state reconstruction. Even when the differentiators appears as a natural solution to the observation problem, the use of the system knowledge for the design of an observation strategy results in a reduction of the gains for the sliding mode compensation terms. This reduction is evidenced in the improvement of the accuracy. Moreover, the complete or partial knowledge of the system model can give place to the application of techniques for parametric reconstruction or disturbance reconstruction. In this chapter we will show how the higher order sliding mode concept can be applied for

H. Imine et al.: Sliding Mode Based Analysis, LNCIS 414, pp. 5–24.
springerlink.com

observation of uncertainties or parameter identification of mechanical system following ([DFL05a], [DFP06]).

2.2 Mechanical Systems

Consider the mathematical model of a mechanical system in the form:

$$M(\mathbf{q})\ddot{\mathbf{q}} + C(\mathbf{q},\dot{\mathbf{q}})\dot{\mathbf{q}} + P(\dot{\mathbf{q}}) + G(\mathbf{q}) + \Delta(t,\mathbf{q},\dot{\mathbf{q}}) = \tau, \tag{2.1}$$

where $\mathbf{q} \in R^n$ is a vector of generalized coordinates, $M(\mathbf{q})$ is the inertia matrix, $C(\mathbf{q},\dot{\mathbf{q}})$ is the matrix of Coriolis and centrifugal forces, $P(\dot{\mathbf{q}})$ is the Coulomb friction, which possibly contains relay terms depending on $\dot{\mathbf{q}}$, $G(\mathbf{q})$ is the term of gravitational forces, $\Delta(t,\mathbf{q},\dot{\mathbf{q}})$ is an uncertainty term and τ is the generalized torque/force produced by the actuators. The control input τ is assumed to be given by some known feedback function. Note that $M(\mathbf{q})$ is invertible, since $M(\mathbf{q}) = M^T(\mathbf{q})$ is strictly positive definite. Furthermore other terms are assumed to be uncertain, but the corresponding nominal functions $M_n(\mathbf{q})$, $C_n(\mathbf{q},\dot{\mathbf{q}})$, $P_n(\dot{\mathbf{q}})$, $G_n(\mathbf{q})$ are assumed known.

Introducing the variables $x_1 = \mathbf{q}$, $x_2 = \dot{\mathbf{q}}$, $u = \tau$, the model (2.1) can be rewritten in the state-space form as

$$\begin{aligned} &\dot{x}_1 = x_2, \\ &\dot{x}_2 = f(t,x_1,x_2,u) + \xi(t,x_1,x_2,u), \qquad u = U(t,x_1,x_2), \\ &y = x_1, \end{aligned} \tag{2.2}$$

where the nominal part of the system dynamics is represented by the function

$$f(t,x_1,x_2,u) = -M_n^{-1}(x_1)[C_n(x_1,x_2)x_2 + P(x_2) + G_n(x_1) - u]$$

containing the known nominal functions M_n, C_n, G_n, P, while the uncertainties are concentrated in the term $\xi(t,x_1,x_2,u)$. The solutions to system (2.2) are understood in Filippov's sense [Fil88]. It is assumed that the function $f(t,x_1,x_2,U(t,x_1,x_2))$ and the uncertainty $\xi(t,x_1,x_2,U(t,x_1,x_2))$ are Lebesgue-measurable and uniformly bounded in any compact region of the state space x_1, x_2 .

In order to apply a state feedback controller or to simply perform system monitoring, the complete knowledge of the coordinate x_2 is required. Moreover, in the general case, for the design of a controller it is necessary to know the parameters of the system. The tasks are to design a finite-time convergent observer of the velocity $\dot{\mathbf{q}}$ for the original system (2.1) when only the position $\mathbf{q}$ and the nominal model are available, and an identification algorithm to obtain the system parameters, with only the knowledge of the state $\mathbf{x}_1$ and the input $u(t)$. Only the scalar case $x_1, x_2 \in R$ is considered for the sake of simplicity. In the vector case the observers are constructed in parallel for each position variable x_{1j} in exactly the same way.

2.2.1 Super-Twisting Based Observer

The proposed super-twisting observer has the form

$$\begin{aligned} \dot{\hat{x}}_1 &= \hat{x}_2 + z_1 \\ \dot{\hat{x}}_2 &= f(t, x_1, \hat{x}_2, u) + z_2 \end{aligned} \tag{2.3}$$

where $\hat{x}_1$ and $\hat{x}_2$ are the state estimations, and the correction variables z_1 and z_2 are output injections of the form:

$$\begin{aligned} z_1 &= \lambda |x_1 - \hat{x}_1|^{1/2}\, sign(x_1 - \hat{x}_1) \\ z_2 &= \alpha\, sign(x_1 - \hat{x}_1). \end{aligned} \tag{2.4}$$

It is assumed that at the initial moment $\hat{x}_1 = x_1$ and $\hat{x}_2 = 0$. Taking $\tilde{x}_1 = x_1 - \hat{x}_1$ and $\tilde{x}_2 = x_2 - \hat{x}_2$ we obtain the error equations

$$\begin{aligned} \dot{\tilde{x}}_1 &= \tilde{x}_2 - \lambda |\tilde{x}_1|^{1/2}\, sign(\tilde{x}_1) \\ \dot{\tilde{x}}_2 &= F(t, x_1, x_2, \hat{x}_2) - \alpha\, sign(\tilde{x}_1) \end{aligned} \tag{2.5}$$

where $F(t, x_1, x_2, \hat{x}_2) = f(t, x_1, x_2, U(t, x_1, x_2)) - f(t, x_1, \hat{x}_2, U(t, x_1, x_2)) + \xi(t, x_1, x_2, U(t, x_1, x_2))$. Suppose that the system states can be assumed bounded, then the existence of a constant f^+ is ensured such that the inequality

$$|F(t, x_1, x_2, \hat{x}_2)| < f^+ \tag{2.6}$$

holds for any possible t, x_1, x_2 and $|\hat{x}_2| \leq 2 \sup |x_2|$.

Remark 1. When the accelerations in the mechanical system are bounded, the constant f^+ can be found as the double maximal possible acceleration of the system. Moreover. the estimation constant f^+ does not depend on the nominal elasticity or control terms. Such assumption of the state boundedness is true as well, if, for example, system (2.2) is BIBS stable, and the control input $u = U(t, x_1, x_2)$ is bounded.

Let α and λ satisfy the inequalities

$$\begin{aligned} &\alpha > f^+, \\ &\lambda > \sqrt{\tfrac{2}{\alpha - f^+}} \tfrac{(\alpha + f^+)(1+p)}{(1-p)}, \end{aligned} \tag{2.7}$$

where p is some chosen constant, $0 < p < 1$.

Theorem 2.1. *[DFL05d] Suppose that the parameters of the observer (2.3), (2.4) are selected according to (2.7), and condition (2.6) holds for system (2.2). Then the variables of the observer (2.3),(2.4) converge in finite time to the states of system (2.2), i.e.* $(\hat{x}_1, \hat{x}_2) \to (x_1, x_2)$.

Remark 2. Finite-time convergence of the observer allows designing the observer and the control law separately, i.e. the separation principle is satisfied. The only requirement for its implementation is the boundedness of the function $F(t, x_1, x_2, \hat{x}_2, u)$ in the operational domain. If the applied controller is known to stabilize the process, one of the admissible ways is to choose the observer dynamics fast enough to provide for the exact evaluation of the velocity before leaving some preliminarily chosen area, where the stabilization is assured. This is easily performed through simulation (see the example below).

Remark 3. The standard 2-sliding-mode-based differentiator [Lev98] can also be implemented here to estimate the velocity. At the same time, the proposed observer requires smaller gains and is more accurate, i.e. the elasticity term $M^{-1}(\mathbf{q})G(\mathbf{q})$ does not influence the gain choice.

Remark 4. Another way to choose α and λ is to take $\alpha = a_1 f^+$, $\lambda = a_2\,(f^+)^{1/2}$ with some predetermined proper a_1, a_2. In particular, $a_1 = 1.1$, $a_2 = 1.5$ is a valid choice [Lev98].

2.2.1.1 Example

Consider a pendulum system with Coulomb friction and external perturbation given by the equation

$$\ddot{\theta} = \frac{1}{J}\tau - \frac{MgL}{J}\sin\theta - \frac{V_s}{J}\dot{\theta} - \frac{P_s}{J}\,sign(\dot{\theta}) + v, \tag{2.8}$$

where the values $M = 1.1$, $g = 9.815$, $L = 0.9$, $J = ML^2 = 0.891$, $V_S = 0.18$, $P_s = 0.45$ were taken and v is an uncertain external perturbation, $|v| \leq 1$. $v = 0.5\sin 2t + 0.5\cos 5t$ was chosen in simulation. Let the system be driven by the twisting controller

$$\tau = -30\,sign(\theta - \theta_d) - 15\,sign(\dot{\theta} - \dot{\theta}_d), \tag{2.9}$$

where $\theta_d = \sin t$ and $\dot{\theta}_d = \cos t$ are the reference signals. The system can be rewritten as

$$\begin{aligned} \dot{x}_1 &= x_2, \\ \dot{x}_2 &= \tfrac{1}{J}\tau - \tfrac{MgL}{J}\sin x_1 - \tfrac{V_s}{J}x_2 - \tfrac{P_s}{J}\,sign(x_2) + v. \end{aligned}$$

Thus, the proposed velocity observer (see Remark 3) has the form

$$\begin{aligned} \dot{\hat{x}}_1 &= \hat{x}_2 + 1.5(f^+)^{1/2}|\tilde{x}_1|^{1/2}\,sign(x_1 - \hat{x}_1), \\ \dot{\hat{x}}_2 &= \tfrac{1}{J_n}\tau - \tfrac{M_n g L_n}{J_n}\sin x_1 - \tfrac{V_{sn}}{J_n}\hat{x}_2 + 1.1 f^+\,sign(x_1 - \hat{x}_1), \end{aligned}$$

where $M_n = 1$, $L_n = 1$, $J_n = M_n L_n^2 = 1$, $V_{sn} = 0.2$, $P_{sn} = 0.5$ are the "known" nominal values of the parameters, and f^+ is to be assigned. Assume also that it is known that the real parameters differ from the known values by no more than 10%. The initial values $\theta = x_1 = \hat{x}_1 = 0$ and $\dot{\theta} = x_2 = 1$, $\hat{x}_2 = 0$ were taken at $t = 0$. Identifying 0 and 2π obtain that θ belongs to a compact set (a ring). Thus, obviously, the dynamic system (2.8) is BIBS stable. Easy calculation shows that the given controller provides for $|\tau| \le 45$, and the inequality $|\dot{\theta}| \le 70$ is ensured when the nominal values of parameters and their maximal possible deviations are taken into account. Taking $|x_2| \le 70$, $|\hat{x}_2| \le 140$ obtain that $|F| = |\frac{1}{J}\tau - \frac{g}{L}\sin x_1 - \frac{V_s}{J}x_2 - \frac{P_s}{J}\,sign(x_2) + v - \frac{1}{J_n}\tau + \frac{g}{L_n}\sin x_1 + \frac{V_{sn}}{J_n}\hat{x}_2| < 60 = f^+$. Therefore, the observer parameters $\alpha = 66$ and $\lambda = 11.7$ were chosen . Simulation adjustment (see Remark 1) shows that $f^+ = 6$ and the respective values $\alpha = 6.6$ and $\lambda = 4$ are sufficient. Note that the terms $\frac{MgL}{J}\sin x_1$ and $\frac{1}{J}\tau$ would be fully taken into account for the choice of the differentiator parameters [Lev98] causing much larger coefficients to be used. The performance of the observer is shown in Fig. 2.1.

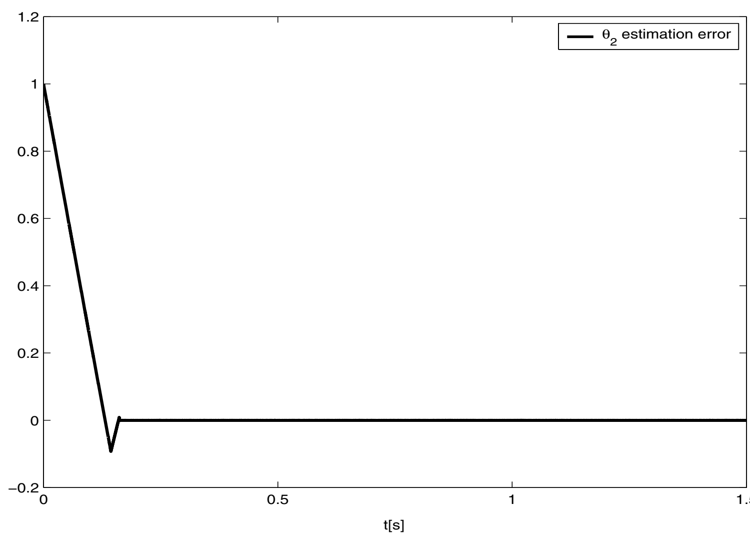

Fig. 2.1 Estimation error for x_2.

The finite-time convergence of the estimated velocity to the real one is demonstrated in Fig. 2.2, and Fig. 2.3 shows the convergence in the plane $\tilde{x}_1$ vs $\tilde{x}_2$.

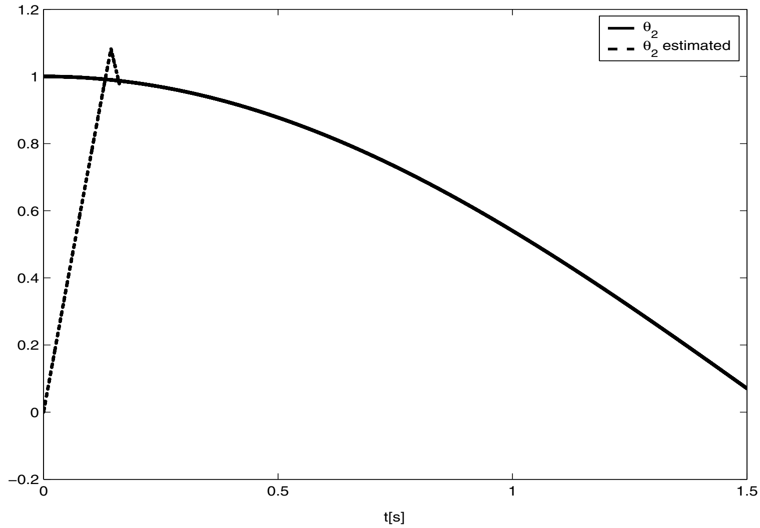

Fig. 2.2 Real and estimated velocity.

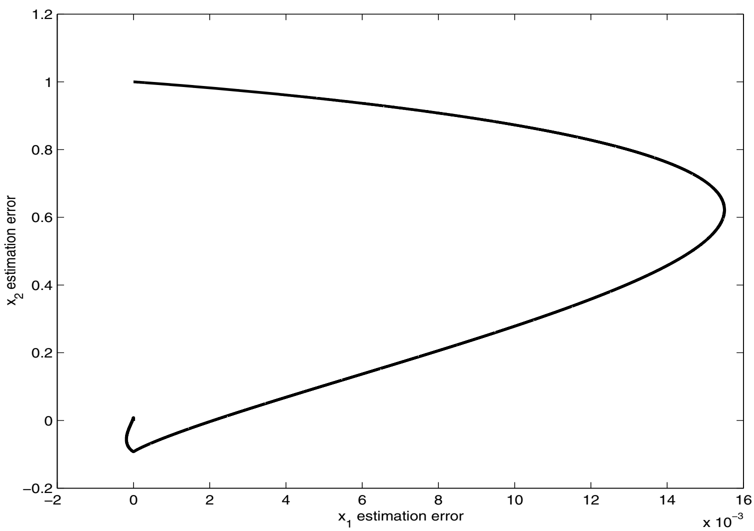

Fig. 2.3 Graph of $\tilde{x}_1$ vs $\tilde{x}_2$.

2.2.2 Differentiation vs. Observation

In the last example the state x_2 is the derivative of the state x_1. Why don't use differentiators instead of observers?

Consider again system (2.8). Let us apply the first order differentiator to recover the state x_2. The state estimation obtained by differentiation is shown in Fig. 2.4.

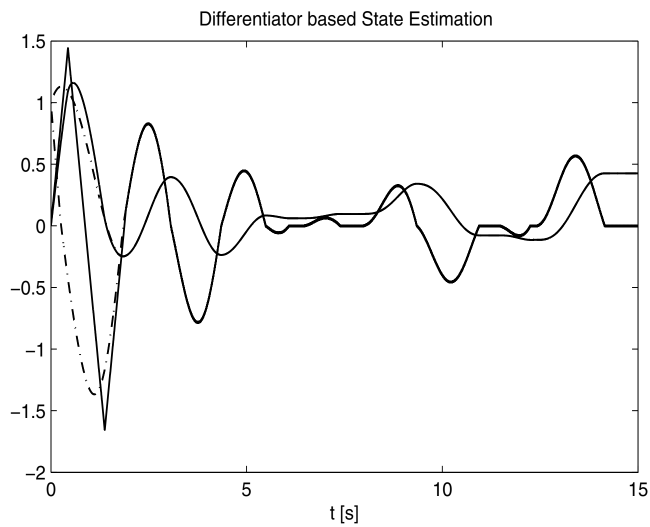

Fig. 2.4 System states (doted line) and their estimation using differentiators (continuous line).

It is clear that exact reconstruction is achieved. However, lets compare this result with the observer based approach.

Consider that the observer takes on the form:

$$\dot{\hat{x}}_1 = \hat{x}_2 + 1.5(3)^{1/2}|\tilde{x}_1|^{1/2}\, sign(x_1 - \hat{x}_1),$$
$$\dot{\hat{x}}_2 = \frac{1}{J}\tau - \frac{MgL}{J}\sin x_1 - \frac{V_{sn}}{J_n}\hat{x}_2 + 3.3\, sign(x_1 - \hat{x}_1),$$

Notice that the Coulomb friction term is not taken into account for the design of the observer.

The state observation is presented in Fig. 2.5.

The state reconstruction is exact and apparently it preserves the same convergence features that the reconstruction made by differentiation.

In Fig. 2.6 both estimation errors, the one obtained by differentiation and the one obtained by observation, are presented.

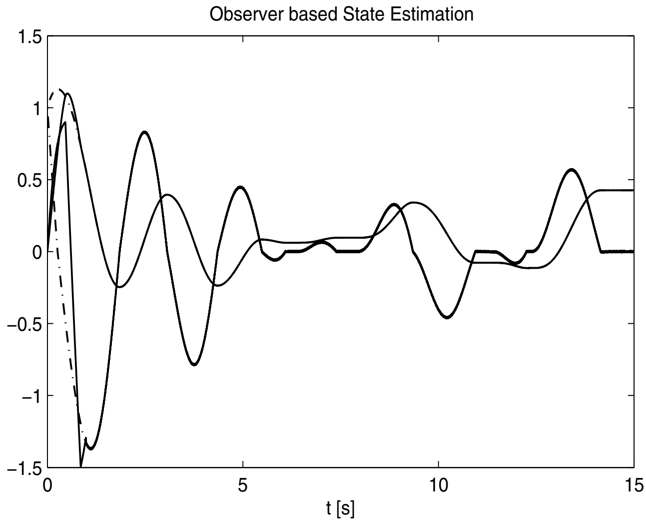

Fig. 2.5 System states (dotted line) and their estimation using observers (continuous line).

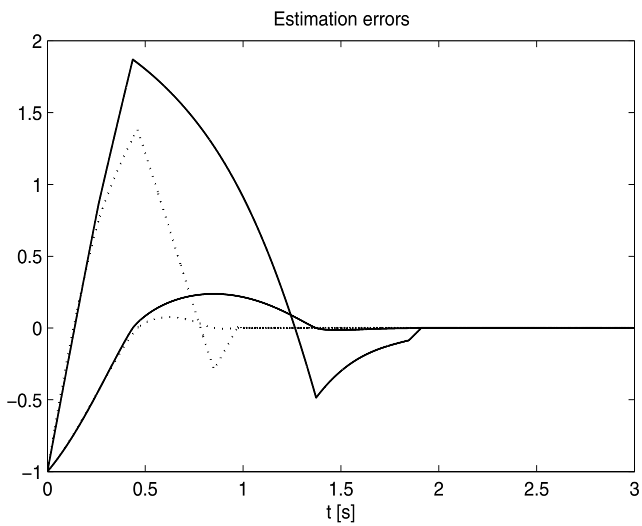

Fig. 2.6 Estimation error comparative of differentiation and state observation.

Even when the gains are the same in both approaches, the convergence time is smaller for the observer. Additionally, one of the main features of the sliding mode approach, the equivalent output injection, can be exploited when the observer is applied (see subsection 2.2.3).

2.2.3 Equivalent Output Injection Analysis

2.2.3.1 Equivalent Output Injection

Standard Procedure

The finite time convergence to the second order sliding mode set ensures that there exists a time constant $t_0 > 0$ such that for all $t \geq t_0$ the following identity holds

$$0 \equiv \dot{\tilde{x}}_2 \equiv F(t, x_1, x_2, \hat{x}_2, u) + \xi(t, x_1, x_2, u) - \alpha_1 sign(\tilde{x}_1),$$

Notice that $F(t, x_1, x_2, \hat{x}_2, u) = f(t, x_1, x_2, u) - f(t, x_1, \hat{x}_2, u) = 0$ because $\hat{x}_2 = x_2$. Then the equivalent output injection z_{eq} is given by

$$z_{eq}(t) \equiv \alpha_1 sign(\tilde{x}_1) \equiv \xi(t, x_1, x_2, u). \tag{2.10}$$

We said before that the term $\xi(t, x_1, x_2, u)$ is composed of uncertainties and perturbations. This term may be written as

$$\xi(t, x_1, x_2, u) = \zeta(t) + \Delta F(t, x_1, x_2, u) \tag{2.11}$$

where $\zeta(t)$ is an external perturbation term and $\Delta F(t, x_1, x_2, u)$ concentrates the parameter uncertainties.

Theoretically, the equivalent output injection is the result of an infinite switching frequency of the discontinuous term $\alpha_1 sign(\tilde{x}_1)$. Nevertheless, the realization of the observer produces a high (finite) switching frequency making the application of a filter necessary. To eliminate the high frequency component we will use the filter of the form

$$\tau \dot{\bar{z}}_{eq}(t) = -\bar{z}_{eq}(t) + z_{eq}(t)$$

where $\tau \in \mathbb{R}$ and $h << \tau << 1$, being h a sampling step.

It is possible to rewrite z_{eq} as result of the filtering process in the following form

$$z_{eq}(t) = \bar{z}_{eq}(t) + \varepsilon(t) \tag{2.12}$$

where $\varepsilon(t) \in \mathbb{R}^n$ is the difference caused by the filtration and $\bar{z}_{eq}(t)$ is the filtered version of $z_{eq}(t)$.

Nevertheless, as it is shown in ([Utk92], [Fri99]) that

$$\lim_{\substack{\tau \to 0 \\ h/\tau \to 0}} \bar{z}_{eq}(\tau, h) = z_{eq}(t),$$

Thus, it is possible to assume that the equivalent output injection is equal to the output of the filter.

Extended Order Approach

Suppose that the perturbation/uncertainty therm $\xi(t, x_1(t), x_2(t), u(t))$ is a smooth function of t. Lets differentiate the second equation of (2.2) and introduce the new state variable $x_3 = \dot{x}_2$. System (2.2) can be written in an equivalent form as

$$\begin{aligned} \dot{x}_1 &= x_2, \\ \dot{x}_2 &= x_3, \\ \dot{x}_3 &= \dot{f}(t, x_1, x_2, u) + \frac{d}{dt}\xi(t, x_1(t), x_2(t), u(t)) \end{aligned} \tag{2.13}$$

The extension of the system dynamics implies a new requirement for $\dot{f}(t, x_1, x_2, u) + \dot{\xi}(t, x_1, x_2, u)$ to be bounded.

If this new requirement is satisfied, it is possible to apply the third order differentiator [Lev03]:

$$\begin{aligned} \dot{z}_1 &= w_1 = -\alpha_3 M^{1/3} |z_1 - x_1|^{2/3} \operatorname{sign}(z_1 - x_1) + z_2 \\ \dot{z}_2 &= w_2 = -\alpha_2 M^{1/2} |z_2 - w_1|^{1/2} \operatorname{sign}(z_2 - w_1) + z_3 \\ \dot{z}_3 &= -\alpha_1 M \operatorname{sign}(z_3 - w_2) \end{aligned} \tag{2.14}$$

Now, the differentiator variables z_1, z_2, z_3 are the estimates of the states x_1, x_2, x_3 of the extended system (2.13) respectively.

Since (2.13) is only another representation of (2.2), then after convergence of the differentiator the equality $\dot{z}_2 = \dot{x}_2$ holds, and given the equivalence between (2.2) and (2.13), the following equality is satisfied:

$$f(t, x_1, x_2, u) + \xi(t, x_1, x_2, u) + \alpha_2 M^{1/2} |z_2 - w_1|^{1/2} \operatorname{sign}(z_2 - w_1) - z_3 = 0,$$

The third term of the above mentioned equality is equal to zero as a result of the differentiator convergence, so it is possible to obtain the equivalent output injection as:

$$z_{eq} = z_3 = f(t, x_1, x_2, u) + \xi(t, x_1, x_2, u)$$

In this case z_3 is a continuous term, and no filtration is required to obtain the equivalent output injection. This is an important fact, because given the finite time convergence of the differentiator, we are able now to reconstruct in finite time the equivalent output injection. Moreover, the variable z_3 is not affected by any filtration process, hence z_3 is an exact estimation of $f(t, x_1, x_2, u) + \xi(t, x_1, x_2, u)$.

Below we will refer to this as the exact method to obtain the *smooth* equivalent output injection, while the method described in the past subsection will be referred to as the standard method.

2.2.3.2 Perturbation Identification

Consider the case where the nominal model is totally known, i.e. for all $t > t_0$ the uncertain part $\Delta F(t, x_1, x_2, u) = 0$. The equivalent output injection takes the form

$$\bar{z}_{eq}(t) = z_2 = \zeta(t). \tag{2.15}$$

For the standard method to obtain z_{eq}, the result of the filtering process will yield

$$\lim_{\substack{\tau \to 0 \\ h/\tau \to 0}} \bar{z}_{eq}(\tau) = \zeta(t),$$

Then, any bounded perturbation can be identified directly using the filter output, however the maximal frequency allowed will be restricted by the filter cutoff frequency.

For the exact method, the perturbation can be identified using both the term z_{eq} and the knowledge of the system as

$$\hat{\zeta} = z_{eq} - f(t, \hat{x}_1, \hat{x}_2, u)$$

The maximal frequency allowed for the perturbation will be restricted by the constant of the differentiator (2.14)

$$M > \dot{\zeta}(t)$$

Notice that, in this case, even when perturbation is not required to be bounded its frequency should be bounded to allow the design of the observer.

2.2.4 Parameter Identification

2.2.4.1 Regressor Form

Let us consider the unperturbed case when $\zeta(t) = 0$ and $\xi(t, x_1, x_2, u) = \Delta F(t, x_1, x_2, u)$. The system acceleration (i.e. $\dot{x}_2$) can be represented as a sum of a well-known part and an uncertain part,

$$\dot{x}_2 = f(t, x_1, x_2, u) + \Delta F(t, x_1, x_2, u),$$

where $f(t, x_1, x_2, u) \in \mathbb{R}^n$ is a completely known part of the system and $\Delta F(t, x_1, x_2, u)$ is an uncertain part. Using the regressor notation [SS89] we can write the uncertain part as

$$\Delta F(t, x_1, x_2, u) = \theta(t)\varphi(t, x_1, x_2, u)$$

where $\theta(t) \in \mathbb{R}^{n \times l}$ is a matrix composed by the value of the uncertain parameters of the functions M, C, G, P and $\varphi(t, x_1, x_2, u) \in \mathbb{R}^l$ is a known nonlinear functions vector. System (2.2) takes the form

$$\begin{aligned} &\dot{x}_1 = x_2, \\ &\dot{x}_2 = f(t, x_1, x_2, u) + \theta(t)\varphi(t, x_1, x_2, u), \quad u = U(t, x_1, x_2), \\ &y = x_1, \end{aligned} \tag{2.16}$$

and the observer can be rewritten as

$$\begin{aligned} \dot{\hat{x}}_1 &= \hat{x}_2 + \alpha_2 \lambda(\tilde{x}_1) sign(\tilde{x}_1) \\ \dot{\hat{x}}_2 &= f(t, x_1, \hat{x}_2, u) + \bar{\theta}(t)\varphi(t, x_1, \hat{x}_2, u) + \alpha_1 sign(\tilde{x}_1), \end{aligned} \tag{2.17}$$

where $\bar{\theta} \in \mathbb{R}^{n \times l}$ is a matrix of nominal values of the parameter matrix $\theta(t)$. The error dynamics for all $t \geq t_0$, becomes

$$\begin{aligned} \dot{\tilde{x}}_1 &= \tilde{x}_2 - \alpha_2 \lambda(\tilde{x}_1) sign(\tilde{x}_1) \\ \dot{\tilde{x}}_2 &= (\theta(t) - \bar{\theta}(t))\varphi(t, x_1, x_2, u) - \alpha_1 sign(\tilde{x}_1) \end{aligned} \tag{2.18}$$

Note that parameter uncertainties are concentrated in the first part of the model $(\theta(t) - \bar{\theta}(t))\varphi(t, x_1, x_2, u)$.

The task is to design an algorithm which provides parameter identification for the original system (2.1), when only the position x_1 is measurable and the nominal model $\bar{\theta}(t)\varphi(t, x_1, x_2, u)$ is known.

2.2.4.2 Time-Invariant Parameters Identification

Consider the case when the system parameters are time invariant, i.e. $\theta(t) = \theta$. Now, the equivalent output injection can be represented in the form

$$\bar{z}_{eq}(t) = \alpha_1 sign(\tilde{x}_1) = (\theta - \bar{\theta})\varphi(t, x_1, x_2, u) \tag{2.19}$$

Notice that $\alpha_1 sign(\tilde{x}_1)$ is a known term and the finite time convergence of the observer guarantees the knowledge of all the state vector i.e. $\varphi(t, x_1, \hat{x}_2, u) = \varphi(t, x_1, x_2, u)$ for all $t \geq t_0$. Equation (2.19) represents a linear regression model where the vector parameters to be estimated are $(\theta - \bar{\theta})$. To obtain the real system parameters θ a linear regression algorithm may be proposed from equation (2.19).

The recursive LSM algorithm (see for example [SS89]) applied for parameter identification of dynamical systems is usually designed using discretization of the regressor and derivatives of the states in order to obtain the regressor form. Then the algorithm is applied in a discrete form. Notice that the linear regressor form in [SS89] can be directly obtained from (2.19).

In mechanical system observation and identification, we deal with data sets of a continuous-time nature. That is why an implementation of any standard discretization scheme is related to unavoidable losses of existing information. This produces a systematical error basically caused by the estimation of derivatives of the considered process. As it is shown above, the proposed second-order sliding mode technique provides an estimation of derivatives converging in a finite time that permits avoiding an additional error arising during any standard discretization scheme implementation. Below we present the continuous-time version of the LS-algorithm based on the proposed second-order sliding mode observation scheme. Notice that the proposed algorithm can be implemented in analog devices directly.

Define $\Delta\theta := \theta - \bar{\theta}$ and post-multiply (2.19) by $\varphi^T(t, x_1, x_2, u)$ (for short notation function $\varphi(t, x_1, x_2, u)$ will be called $\varphi(t)$). Now, using the auxiliary variable σ for integration in time, the average values of equation (2.19) take the form

$$\frac{1}{t}\int_0^t \bar{z}_{eq}(\sigma)\varphi^T(\sigma)d\sigma = \Delta\theta\frac{1}{t}\int_0^t \varphi(\sigma)\varphi(\sigma)^T d\sigma \tag{2.20}$$

Therefore, the system parameters can be estimated from (2.20) by

$$\widehat{\Delta\theta} = \left[\int_0^t \bar{z}_{eq}(\sigma)\varphi^T(\sigma)d\sigma\right]\left[\int_0^t \varphi(\sigma)\varphi^T(\sigma)d\sigma\right]^{-1} \tag{2.21}$$

where $\widehat{\Delta\theta}$ is the estimation of $\Delta\theta$. For any square matrix the next equalities hold

$$\begin{gathered} \Gamma^{-1}(t)\Gamma(t) = I, \\ \Gamma^{-1}(t)\dot{\Gamma}(t) + \dot{\Gamma}^{-1}(t)\Gamma(t) = 0 \end{gathered} \tag{2.22}$$

Let us define $\Gamma(t) = \left[\int_0^t \varphi(\sigma)\varphi^T(\sigma)d\sigma\right]^{-1}$. Using (2.22) we can rewrite (2.21) in the form:

$$\dot{\widehat{\Delta\theta}} = \left[\int_0^t \bar{z}_{eq}(\sigma)\varphi^T(\sigma)d\sigma\right]\dot{\Gamma}(t) + z_{eq}(t)\varphi^T(t)\Gamma(t)$$

Now, using equation (2.20) we can write

$$\dot{\widehat{\Delta\theta}} = \widehat{\Delta\theta}\Gamma^{-1}(t)\dot{\Gamma}(t) + \bar{z}_{eq}(t)\varphi^T(t)\Gamma(t)$$

The equalities (2.22) allow us to write a dynamic expression to compute $\Delta\theta$ as

$$\dot{\widehat{\Delta\theta}} = \left[-\widehat{\Delta\theta}\varphi(t) + \bar{z}_{eq}(t)\right]\varphi^T(t)\Gamma(t). \tag{2.23}$$

In the same way, a dynamic form to find $\Gamma(t)$ is given by

$$\dot{\Gamma}(t) = -\Gamma(t)\varphi(t)\varphi^T(t)\Gamma(t) \tag{2.24}$$

The average values of the real $z_{eq}(t)$, without filtering, satisfy the equality

$$\int_0^t z_{eq}(\sigma)\varphi^T(\sigma)d\sigma = \Delta\theta \int_0^t \varphi(\sigma)\varphi^T(\sigma)d\sigma$$

then

$$\Delta\theta = \left[\int_0^t z_{eq}(\sigma)\varphi^T(\sigma)d\sigma\right]\Gamma(t).$$

Substituting equation (2.12), the real values of parameters vector $\Delta\theta$ holds

$$\Delta\theta = \left[\int_0^t \bar{z}_{eq}(\sigma)\varphi^T(\sigma)d\sigma + \int_0^t \varepsilon(\sigma)\varphi^T(\sigma)d\sigma\right]\Gamma(t). \tag{2.25}$$

Let us assume $\bar{z}_{eq}(t) = \widehat{\Delta\theta}\varphi(t)$. In this case equation (2.25) becomes

$$\Delta\theta = \left[\widehat{\Delta\theta}\int_0^t \varphi(\sigma)\varphi^T(\sigma)d\sigma + \int_0^t \varepsilon(\sigma)\varphi^T(\sigma)d\sigma\right]\Gamma(t),$$

which can be written as

$$\Delta\theta = \widehat{\Delta\theta} + \left[\int_0^t \varepsilon(\sigma)\varphi^T(\sigma)d\sigma\right]\Gamma(t). \tag{2.26}$$

From equations (2.21) and (2.26) it is possible to define the convergence conditions

$$\sup ||t\Gamma(t)|| < \infty, \tag{2.27}$$

$$||\frac{1}{t}\int_0^t \varepsilon(\sigma)\varphi^T(\sigma)d\sigma|| \to 0 \quad \text{as} \quad t \to \infty. \tag{2.28}$$

Condition (2.27), known as the persistent excitation condition (see for example, [SS89]), requires the non-singularity of the matrix $\Gamma^{-1}(t) = \int_0^t \varphi(\sigma)\varphi^T(\sigma)d\sigma$. To avoid this restriction let us introduce the term ρI where $0 < \rho << 1$ and I is the unitary matrix and redefine $\Gamma^{-1}(t)$ as

$$\Gamma^{-1}(t) = \int_0^t \big(\varphi(\sigma)\varphi^T(\sigma)d\sigma\big) + \rho I$$

In this case the value of $\Gamma^{-1}(t)$ is always non-singular.

Notice that the introduction of the term ρI is equivalent to setting the initial conditions of (2.24) as

$$\Gamma(0) = \rho^{-1} I, \quad 0 < \rho\text{-small enough}$$

The introduction of the term ρ ensures the condition $sup \|t\Gamma(t)\| < \infty$ but does not guarantee the convergence of the estimated parameters to the real values. The convergence of the estimated values to the real ones is ensured by the *persistent excitation condition*

$$\liminf_{t \to \infty} \frac{1}{t} \int_0^t \left(\varphi(\sigma) \varphi(\sigma)^T d\sigma \right) > 0$$

The condition (2.28) refers to the filtering process, and it gives the convergence quality of the identification. As fast as term $\frac{1}{t} \int_0^t \varepsilon(\sigma)\varphi(\sigma)^T d\sigma$ converges to zero, the estimated parameters will tend to the real parameters values. The above can be summarized in Theorem 2.2.

Theorem 2.2. *The algorithm (2.23), (2.24) ensures the convergence of $\widehat{\Delta\theta} \to \Delta\theta$ under the conditions (2.27), (2.28).*

Remark 1. The effect of noise sensitivity of the suggested procedure can be easily seen from (23):

$$\frac{1}{t} \int_0^t \varepsilon(\sigma) \varphi^T(\sigma) d\sigma \to 0 \text{ when } t \to \infty$$

There $\varepsilon(t)$ is given by (9) and includes all error effects caused by observation noises (if there are any), error in the realization of the equivalent output injection and etc. One can see that if $\varepsilon(t)$ and $\varphi(t)$ are uncorrelated and "on average" equal to zero, i.e.,

$$\frac{1}{t} \int_0^t \varepsilon(\sigma) d\sigma \to 0, \ \frac{1}{t} \int_0^t \varphi(\sigma) d\sigma \to 0$$

then the noise effect vanishes.

2.2.5 Example

2.2.5.1 Perturbation Identification

Consider the mathematical model of a pendulum given by

$$\ddot{\theta} = \frac{1}{J} u - \frac{MgL}{2J} \sin\theta - \frac{V_s}{J} \dot{\theta} + v(t)$$

where $M = 1.1[Kg]$ is the pendulum mass, $g = 9.815[m/s^2]$ is the gravitational force, $L = 0.9[m]$ is the pendulum length, $J = ML^2 = 0.891[Kg * m^2]$ is the arm inertia, $V_S = 0.18[Kg * m^2/s]$ is the pendulum viscous friction coefficient, and $v(t)$ is a bounded disturbance term. Assume that the angle θ is available for measurement. Introducing the variables $x_1 = \theta$, $x_2 = \dot{\theta}$ and the measured output $y = \theta$ the pendulum equation can be written in the state space form as

$$\begin{aligned} \dot{x}_1 &= x_2, \\ \dot{x}_2 &= \frac{1}{J}u - \frac{MgL}{2J}\sin x_1 - \frac{V_s}{J}x_2 + v(t), \\ y &= x_1 \end{aligned}$$

Suppose that all the system parameters ($M = 1.1$, $g = 9.815$, $L = 0.9$, $J = ML^2 = 0.891$, $V_S = 0.18$) are well-known. The super-twisting observer for this system has the form

$$\begin{aligned} \dot{\hat{x}}_1 &= \hat{x}_2 + \alpha_2|\tilde{x}_1|^{1/2}\, sign(\tilde{x}_1), \\ \dot{\hat{x}}_2 &= \frac{1}{J}u - \frac{MgL}{2J}\sin x_1 - \frac{V_s}{J}\hat{x}_2 + \alpha_1\, sign(\tilde{x}_1), \\ \tilde{x}_1 &= y - \hat{x}_1 \end{aligned}$$

The equivalent output injection in this case is given by

$$z_{eq} = \alpha_1 sign(\tilde{x}_1) = v(t)$$

Using the standard method with a low-pass filter with $\tau = 0.02[s]$ for a sinusoidal external perturbation the identification is shown in Fig. 2.7.

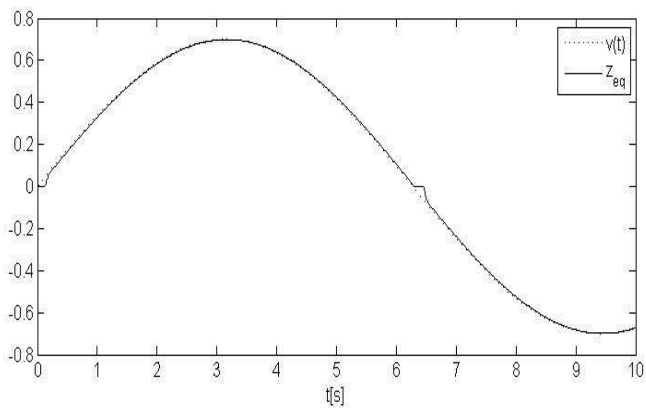

Fig. 2.7 Sinusoidal external perturbation identification using the filtering method

Using the standard method with a filter with time constant $\tau = 0.002[s]$ the perturbation identification for a discontinuous signal is shown in Fig. 2.8.

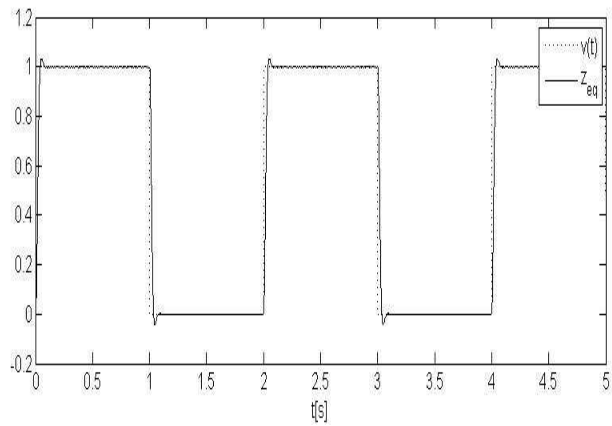

Fig. 2.8 Discontinuous perturbation identification using the filtering method

The sinusoidal signal reconstruction obtained by the exact method is shown in Fig. 2.9.

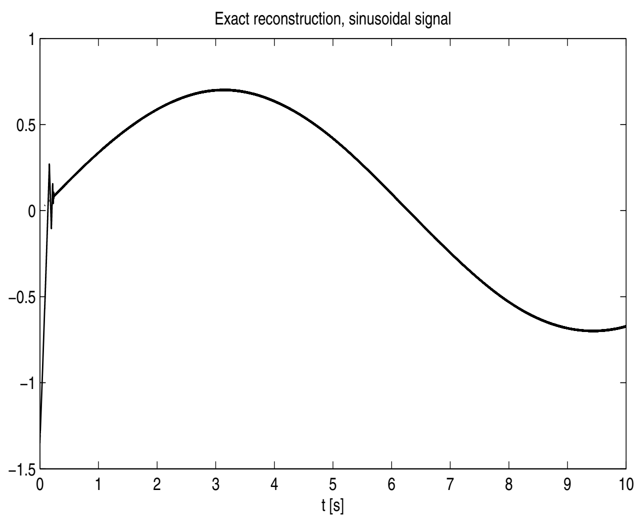

Fig. 2.9 Exact identification of a sinusoidal external perturbation using the exact method.

In Fig. 2.10 the reconstruction of a discontinuous signal using the exact method is shown.

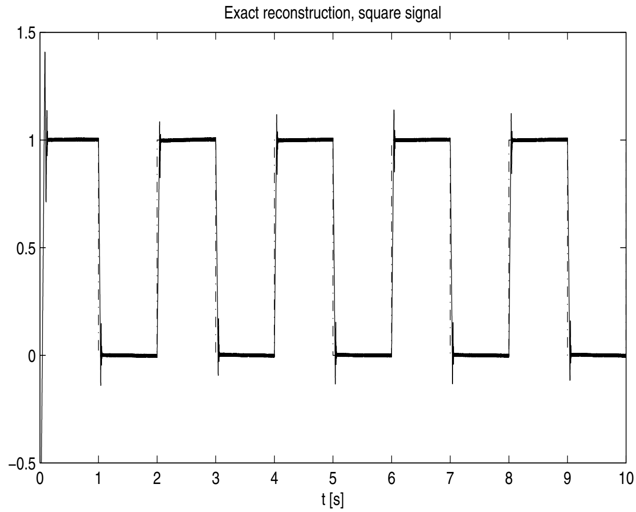

Fig. 2.10 Discontinuous perturbation identification using the exact method.

In this figure it is clear that even when the signal presents abrupt changes, the exact method provides a good reconstruction of the perturbation. After each abrupt change of the signal, the differentiator should converge and as a result the reconstruction exhibits a small transient.

2.2.5.2 Time Invariant Parameter Identification

Consider the model of a pendulum with Coulomb friction given by the equation

$$\ddot{\theta} = \frac{1}{J}u - \frac{MgL}{2J}\sin\theta - \frac{V_s}{J}\dot{\theta} - \frac{P_s}{J}\,sign(\dot{\theta})$$

where $M = 1.1[Kg]$ is the pendulum mass, $g = 9.815[m/s^2]$ is the gravitational force, $L = 0.9[m]$ is the arm length, $J = ML^2 = 0.891[Kg * m^2]$ is the arm inertia, $V_S = 0.18[Kg * m^2/s]$ is the viscous friction coefficient, $P_s = 0.45[Kg * m^2/s^2]$ is the Coulomb friction coefficient. Suppose that the angle θ is available for measurement. Introducing the variables $x_1 = \theta$, $x_2 = \dot{\theta}$, the state space form representation for the system becomes

$$\begin{aligned}
\dot{x}_1 &= x_2,\\
\dot{x}_2 &= \frac{1}{J}u - \frac{MgL}{2J}\sin x_1 - \frac{V_s}{J}x_2 - \frac{P_s}{J}\,sign(x_2),\\
y &= x_1
\end{aligned}$$

where $a_1 = \frac{MgL}{2J} = 5.4528, a_2 = \frac{V_s}{J} = 0.2020, a_3 = \frac{P_s}{J} = 0.5051$ are the unknown parameters. Let us design the super-twisting based observer as

$$\dot{\hat{x}}_1 = \hat{x}_2 + \alpha_2 |\tilde{x}_1|^{1/2}\, sign(\tilde{x}_1),$$
$$\dot{\hat{x}}_2 = \frac{1}{J}u - \bar{a}_1 \sin x_1 - \bar{a}_2 \hat{x}_2 - \bar{a}_3\, sign(x_2) + \alpha_1\, sign(\tilde{x}_1),$$
$$\tilde{x}_1 = y - \hat{x}_1$$

where $\bar{a}_1 = 2$,$\bar{a}_2 = \bar{a}_3 = 0.1$ are the nominal values of the unknown parameters. Let the control signal be generated by the twisting controller

$$u = -30\, sign(\theta - \theta_d) - 15\, sign(\dot{\theta} - \dot{\theta}_d), \tag{2.29}$$

where the reference signal is $\theta_d = 0.3\sin(3t + \pi/4) + 0.3\sin(1/2t + \pi)$.

For a sampling time of $\delta = 0.0001$ the state estimation error is shown in Fig. 2.11.

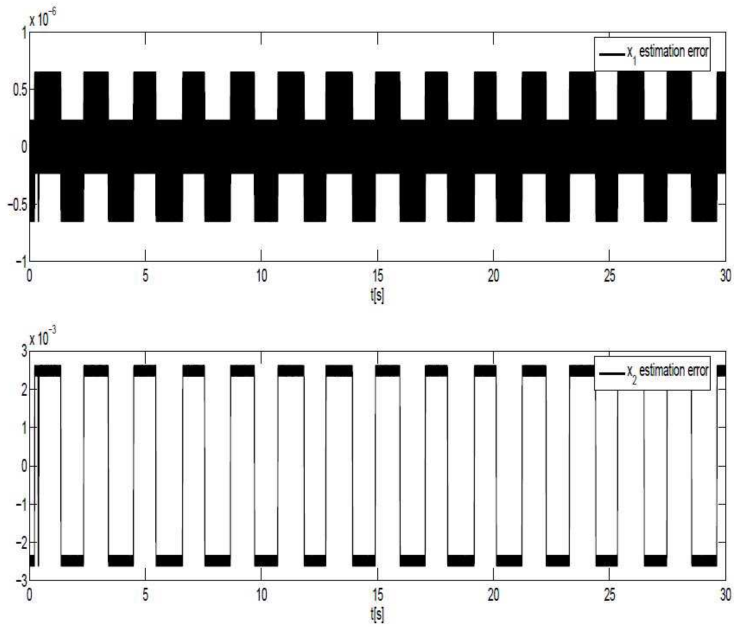

Fig. 2.11 x1, x2 estimation error for the LTI case.

In this case, the identification variables are given by:

$$
\begin{aligned}
z_{eq} &= \alpha_1 sign\tilde{x}_1 \\
\Delta_\theta &= [-a_1 + \bar{a}_1 \quad - a_2 + \bar{a}_2 \quad - a_3 + \bar{a}_3] \\
\Delta_\theta &= [-3.4528 \quad - 0.1020 \quad - 0.4051] \\
\varphi &= \begin{bmatrix} \sin x_1 \\ x_2 \\ sign(x_2) \end{bmatrix}
\end{aligned}
$$

Let us apply algorithm (2.23). The Fig. 2.12 shows the convergence of the estimated parameters to the real parameters values.

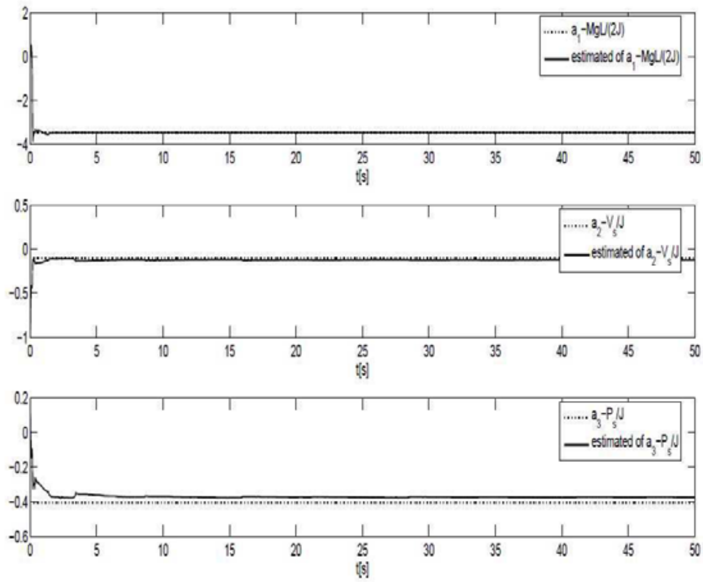

Fig. 2.12 Parameter identification for the LTI case

2.3 Conclusion

In this section we have shown the utility of high order sliding mode for estimation of uncertainties or parameter identification of mechanical system following. Some simulation example have been given in order to show the quality of this concept. In the next chapters, the same idea is applied in order to estimate the dynamics of vehicle and to identify its unknown inputs.

Chapter 3
Vehicle Modeling

Abstract. This chapter is devoted to vehicle modeling. The car is modelized using matlab simulink. Differents parts of the model such as pneumatic, suspension and wheels are developed. Simulation and experimental results are presented to show the validity and the quality of the proposed model.

3.1 Introduction

The increasing worldwide use of automobiles has motivated the need to develop vehicles that optimize the use of highway and fuel resources, provide safe and comfortable transportation and at the same time have minimal impact on the environment. It is a great challenge to develop vehicles that can satisfy these diverse and often conflicting requirements. To meet this challenge, automobiles are increasingly relying on electromechanical sub-systems that employ sensors, actuators and feedback control. Advances in solid state electronics, sensors, computer technology and control systems during the last two decades have also played an enabling role in promoting this trend. In order to develop new strategies for the estimation, diagnosis and control for the vehicle, it is necessary to develop a modeling stage. This step is a fundamental aspect for all applied sciences. Its aim is to establish the relationships between characteristic variables of the vehicle system. These relations should represent as accurately as possible the actual behavior of the vehicle.

To theoretically analyze the vehicle dynamics and to design algorithms for observation and control, the equations of motion must be known and physical interactions between the various sub-systems must be written in the form of mathematical equations. For this purpose, two main approaches may be used: the alternative approach and the physical approach. If the purpose is to obtain a precise model, methods of theoretical physics are used, if not, the alternative approach will be implemented.

H. Imine et al.: Sliding Mode Based Analysis, LNCIS 414, pp. 25–59.
springerlink.com

Table 3.1 Nomenclature.

Symbol	Physical Meaning
Ω_i	angular velocity of the wheel
M	total mass of the vehicle
r_i	radius of the wheel i
COG	centre of gravity of the vehicle
r_{1i}	dynamical radius of the wheel i
Fz_i	vertical force at wheel i
Fx_i	longitudinal force applied at the wheel i
Fy_i	lateral force applied at the wheel i
C_{Fi}	braking torque applied at wheel i
C_{Mi}	motor torque applied at wheel i
$Torque_i$	$C_{Mi} - C_{Fi}$
I_Z	moment of inertia around the Z axis
ψ	yaw angle
$\dot{\psi}$	yaw velocity
δ_f	front steering angle
δ_r	rear steering angle
δ_i	deflection in the tire i
Vx	longitudinal velocity of the center of gravity
Vy	lateral velocity of the center of gravity
I_{ri}	moment of inertia of the wheel i
v_{COG}	total velocity of the center of gravity
L_1	distance between COG and the front axis
L_2	distance between COG and the rear axis
L	$L_1 + L_2$
h_{COG}	height of COG
t_f	front half gauge
t_r	rear half gauge
l	$t_f + t_r$
F_{xwind}	air resistance in the longitudinal direction
F_{ywind}	air resistance in the lateral direction
A_L	front vehicle area
ρ	air density
C_{aer}	coefficient of aerodynamic drag
α_i	slip angle at the wheel i
β	side slip angle at the COG
μ_i	friction coefficient at the wheel i
X_t	length of the contact patch for the wheel i
$X_{adherencei}$	length of the adhesion patch for the wheel i
$X_{slidingi}$	length of the sliding patch for the wheel i
Vx_i	Longitudinal velocity of the wheel i
p_i	inflation pressure of the tire i
K_{1i}	constant depending on the deformation of the tire
K_{2i}	constant depending on the deformation of the tire

Despite the use of the alternative approach in many publications, it is based on a simplified vehicle model using the smallest possible calculation time. The approach used in this chapter follows the physical method to obtain a precise model taking into account the variation of some physical parameters that influence the stability of the vehicle.

During its motion, the vehicle is subject to moments of different origins that affect many parts of its structure.

The vehicle motion is mainly determined by the interaction forces between the tires and the road. These interactions can be decomposed in the contact surface plane in the form of lateral, longitudinal forces, braking or acceleration, and also a couple of self alignment. Before discussing the origin of these forces, we can say that their amplitudes depend mainly on the vertical forces and the adherence of the road. These vertical forces vary with time under the influence of longitudinal and lateral accelerations.

Several studies found in the literature deal with the problem of vehicle modeling and dynamics ([Gil92], [Dix96], [KN05], [Imi03], [SNA05], [RMFD06]). In these references we find models with different degrees of freedom and different complexity levels (quarter of a vehicle, half a vehicle, and a complete vehicle). Different developed strategies for control and observation are done based on these models. The influence of the tire-road interaction on the vehicle dynamic behavior has been widely studied ([DS70], [BSW77] and [CBW90]). Analytical models based on the physical description of the tire contact area deformation phenomenon have been presented in several references ([GN90], [ZWR90], [ZEP95], [CB98], [CH99], [dwTV+03]).

On the other hand, due to the complexity of the contact area phenomenon, empirical models have been described by means of experiments ([BNP87], [Pac89]).

The proposed dynamic vehicle model is nonlinear. Moreover, the kinematic elements can greatly influence the vehicle dynamic behavior. This is due to the existing interconnection between different parts of the vehicle. However, for the sake of simplicity, the complexity of the model may be reduced depending on the type of application and the purpose of modeling. Due to the complexity of a complete vehicle model, we limit our work to five interconnected subsystems: the chassis, suspension, wheels and their interaction with the ground, the driver controls and aerodynamic forces. Six degrees of freedom are considered for the chassis, including three for translation along the longitudinal axis, lateral and vertical and three for rotations (roll, pitch and yaw) and four for the vertical translation of the suspension system and four for wheel rotation.

Model validation

The model has been validated by two different manners:

- By the simulator (ve)-dynamics developed by the (TESIS) Group [SNA05] which is a software specially designed for simulating vehicle dynamics in real-time applications and offline studies. The validation of this model includes validation of all the forces acting on each wheel (horizontal, vertical and lateral), accelerations, velocities and positions of the center of gravity (translation and rotation), drift angle, the position and rotation velocity of each wheel.

- By real measurements (which will be presented in the chapter).

In both cases, the model has given reasonable and acceptable results.

Chapter Structure
This chapter is structured as follows: first some conventions (references, axes) have been introduced and the overall vehicle model is developed. Indeed, the various motions (translations and rotations) of the center of gravity have been described. To model these motions, the wheel-road interaction, the suspension system, the input of the driver and the influence of aerodynamics on the vehicle behavior should be modeled. These models require studies of the contact surface, the longitudinal forces, lateral and vertical. In the modeling of these forces, we consider the inflation pressure, sliding, the friction coefficient, drift angle and velocity (linear and angular) of each wheel and the rolling resistance. After modeling these components, we present a model for the vehicle side slip angle. Then, some experimental results using an instrumented vehicle in order to validate the model have been given and finally and finally the conclusions of this chapter are presented.

3.2 Coordinate Systems

In any mechanical study, the choice of the coordinate systems is essential in order to apply the theorems of classical mechanics. Work in vehicle dynamics uses both world-fixed and vehicle-fixed coordinate systems. It is often necessary to use matrix transformation methods to convert back and forth between the two systems. The following two subsections detail the two coordinate systems used for vehicle modeling.

3.2.1 Fixed Coordinate System R_0

In the reference system R_0, traditionally X_0 is used for the longitudinal axis, Y_0 for the lateral axis, and Z_0 for the vertical axis. The axes X_0, Y_0 and Z_0 form a direct trihedral

(see Fig. 3.1).

$$R_0(O, X_0, Y_0, Z_0)$$

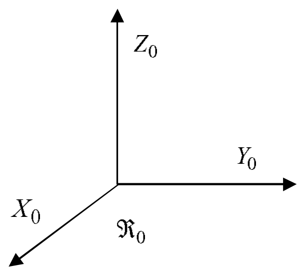

Fig. 3.1 Fixed coordinate system

3.2.2 Center of Gravity Coordinate System R_c

The center of gravity coordinate system which has its origin at the vehicle center of gravity is of the utmost importance.

All the vehicle motions are given with reference to this coordinate system. The equations of motion in vehicle dynamics are usually expressed in the center of gravity coordinate system, attached to the vehicle center of gravity. The X_c axis is a longitudinal axis passing through G and directed forward. The Y_c axis goes laterally to the left from the driver's viewpoint. The Z_c axis makes the coordinate system a righthand triad. To show the vehicle orientation, we use three angles: a roll angle θ about the X_c axis, a pitch angle ϕ about the Y_c axis, and a yaw angle ψ about the Z_c axis.

$$R_c = (G, X_c, Y_c, Z_c)$$

In order to make the transformation from the fixed coordinate system R_0 to the center of gravity coordinate system R_c, a transformation matrix must be constructed. This transformation matrix is represented by T_r:

$$T_r = R_\psi \times R_\phi \times R_\theta \tag{3.1}$$

where R_ψ, R_ϕ and R_θ are respectively the transformation matrices around ψ, θ and ϕ which are calculated as follows.

The transition matrix R_ψ around the axis Z_0 is defined as (Fig. 3.2) :

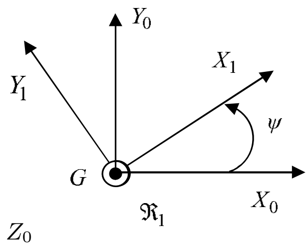

Fig. 3.2 Rotation around Z_0

$$R_\psi = \begin{pmatrix} cos(\psi) & sin(\psi) & 0 \\ -sin(\psi) & cos(\psi) & 0 \\ 0 & 0 & 1 \end{pmatrix} \tag{3.2}$$

The transformation matrix R_ϕ around the axis Y_1 is illustrated in the Fig. 3.3.

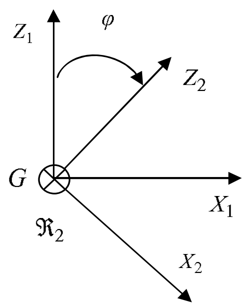

Fig. 3.3 Rotation of R_1 around Y_1

One obtains:

$$R_\phi = \begin{pmatrix} cos(\phi) & 0 & -sin(\phi) \\ 0 & 1 & 0 \\ sin(\phi) & 0 & cos(\phi) \end{pmatrix} \tag{3.3}$$

The transformation matrix R_θ around the axis X_1 is illustrated in the Fig. 3.4.

$$R_\theta = \begin{pmatrix} 1 & 0 & 0 \\ 0 & cos(\theta) & sin(\theta) \\ 0 & -sin(\theta) & cos(\theta) \end{pmatrix} \tag{3.4}$$

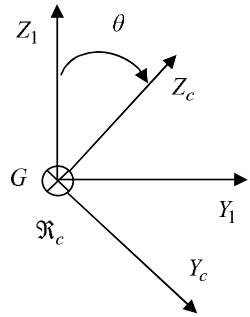

Fig. 3.4 Rotation of R_2 around X_1

Finally we get:

$$T_r = \begin{pmatrix} cos(\psi)cos(\phi) & \begin{matrix}(-sin(\psi)cos(\phi)\\ -cos(\psi)sin(\theta)sin(\phi))\end{matrix} & \begin{matrix}(sin(\psi)sin(\phi)\\ +cos(\psi)sin(\theta)cos(\phi))\end{matrix} \\ sin(\psi)cos(\theta) & \begin{matrix}(cos(\psi)cos(\phi)\\ +sin(\psi)sin(\theta)sin(\phi))\end{matrix} & \begin{matrix}(-cos(\psi)sin(\phi)\\ -sin(\psi)sin(\theta)cos(\phi))\end{matrix} \\ sin(\theta) & cos(\phi)sin(\theta) & cos(\theta)sin(\phi) \end{pmatrix} \quad (3.5)$$

To integrate the inclination angle of the road θ_{road} and the slope angle of the road ϕ_{road}, we replace ϕ by $(\phi - \phi_{road})$ and θ by $(\theta - \theta_{road})$ in the transformation matrix.

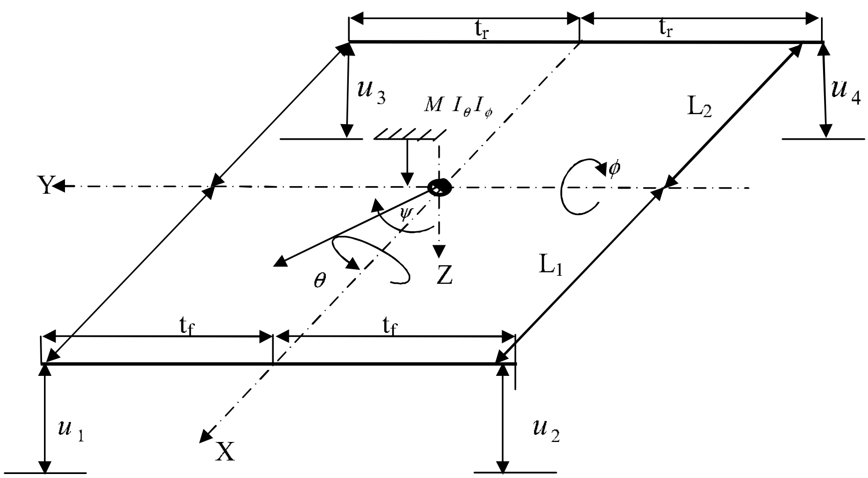

Fig. 3.5 Vehicle representation

In order to simulate the vehicle motion, this chapter is focused on the modeling of the complete vehicle (see Fig. 3.5).

For this reason, the several components that strongly influence the vehicle dynamics and their characteristic quantities are all presented. Firstly the chassis, then the wheel-road interaction (the tire and suspension system), then the controls of the driver applied to the vehicle, i.e. the braking torque, the acceleration torque and steering angle.

3.3 Chassis Modeling

High rigidity of the vehicle chassis can limit the chassis flexibility study and its influence on the suspension system and the wheels system. In most cases, and also in this work, the chassis is considered as rigid. The rigidity of the chassis helps in supporting axes with articulations of the elastic type. Therefore it can be considered as a suspended mass. The inertial parameters of the body are generally represented by:

- Its mass M,
- Position of the center of gravity G,
- Matrix of inertia I.

The equations of motion of the chassis are obtained by applying the fundamental principles of classical physics. This leads to three ordinary differential equations for the translational motion of the center of gravity and three ordinary differential equations for the rotation.

3.3.1 Translation Motion

The sum of external forces applied to a solid body in motion is equal to its mass M multiplied by its acceleration:

$$M\dot{v}_{COG} = \sum F_{External forces} \tag{3.6}$$

The equilibrium of these forces along the three axes leads to the following relation:

$$M \begin{pmatrix} \dot{V}_x \\ \dot{V}_y \\ \dot{V}_z \end{pmatrix} = T_r \times \begin{pmatrix} \sum_{i=1}^{4} FX_i + F_{aeroX} + F_{GX} \\ \sum_{i=1}^{4} FY_i + F_{aeroY} + F_{GY} \\ \sum_{i=1}^{4} Fz_{ic} + F_{aeroZ} + F_{GZ} \end{pmatrix} \tag{3.7}$$

with

$$\begin{pmatrix} FX_1 = Fx_1 cos(\delta_f) - Fy_1 sin(\delta_f) \\ FY_1 = Fx_1 cos(\delta_f) + Fy_1 sin(\delta_f) \\ FX_2 = Fx_2 cos(\delta_f) - Fy_2 sin(\delta_f) \\ FY_2 = Fx_2 cos(\delta_f) + Fy_2 sin(\delta_f) \\ FX_3 = Fx_3 \\ FY_3 = Fy_3 \\ FX_4 = Fx_4 \\ FY_4 = Fy_4 \end{pmatrix} \tag{3.8}$$

and

$$\begin{pmatrix} F_{GX} \\ F_{GY} \\ F_{GZ} \end{pmatrix} = \begin{pmatrix} cos(\phi_{road}) & sin(\phi_{road})sin(\theta_{road}) & sin(\phi_{road})cos(\theta_{road}) \\ 0 & cos(\theta_{road}) & -sin(\theta_{road}) \\ -sin(\phi_{road}) & cos(\phi_{road})sin(\theta_{road}) & cos(\phi_{road})cos(\theta_{road}) \end{pmatrix} \begin{pmatrix} 0 \\ 0 \\ mg \end{pmatrix} \tag{3.9}$$

In order to apply these equations we need to know the rotation angles (ψ, θ, θ_{road}, ϕ, ϕ_{road}), the contact forces (Fx_i, Fy_i and Fz_{ic}) and also the aerodynamic forces(F_{aeroX}, F_{aeroY} and F_{aeroZ}).

3.3.2 Rotational Motion

The equilibrium of the moments around the three axes (X_c, Y_c, Z_c) gives:

$$I \times \begin{pmatrix} \ddot{\theta} \\ \ddot{\phi} \\ \ddot{\psi} \end{pmatrix} = \begin{pmatrix} (Fz_1 - Fz_2)t_f + (Fz_3 - Fz_4)t_r - Ma_y h \\ -(Fz_1 + Fz_2)L_1 + (Fz_3 + Fz_4)L_2 + Ma_x h \\ (Fy_1 + Fy_2)L_1 - (Fy_3 + Fy_4)L_2 + \\ (Fx_2 - Fx_1)t_f + (Fx_4 - Fx_3)t_f \end{pmatrix} \tag{3.10}$$

where $[\ddot{\theta}, \ddot{\phi}, \ddot{\psi}]$ represents respectively the accelerations of the roll angle, the pitch angle, and the yaw angle. The vehicle matrix of inertia in the frame R_c is given by:

$$I = \begin{pmatrix} I_\theta & 0 & 0 \\ 0 & I_\phi & 0 \\ 0 & 0 & I_\psi \end{pmatrix} \tag{3.11}$$

The cross moments of inertia are neglected.

3.3.3 Side Slip Angle

When the vehicle is in motion, a deviation between its longitudinal axis and its motion direction may be produced. This deviation is characterized by the side slip angle β. This angle is very important to determine the stability of the vehicle.

In the electronic control systems, such as Electronic Stability Program (ESP), or the Dynamic Stability Control (DSC), this angle is used as the control input reference.

When the vehicle is in a turn, a centripetal force is produced. This force is expressed as follows:

$$F_{CP} = -Mv_{COG}(\dot{\beta} + \dot{\psi}) \tag{3.12}$$

Based on the vehicle dynamic modeling in the (X, Y) plane (see Fig. 3.6), we obtain :

$$\begin{cases} M\dot{V}_x = M\dot{\psi}V_Y - F_{CP}sin(\beta) + cos(\delta_f)(Fx_1 + Fx_2) \\ +cos(\delta_r)(Fx_3 + Fx_4) \\ M\dot{V}_y = -M\dot{\psi}V_x - F_{CP}cos(\beta) + sin(\delta_f)(Fx_1 + Fx_2) \\ +sin(\delta_r)(Fx_3 + Fx_4) \end{cases} \tag{3.13}$$

The longitudinal and the lateral velocities are written as a function of the side slip angle:

$$\begin{cases} Vx = v_{COG}cos(\beta) \\ Vy = v_{COG}sin(\beta) \end{cases} \tag{3.14}$$

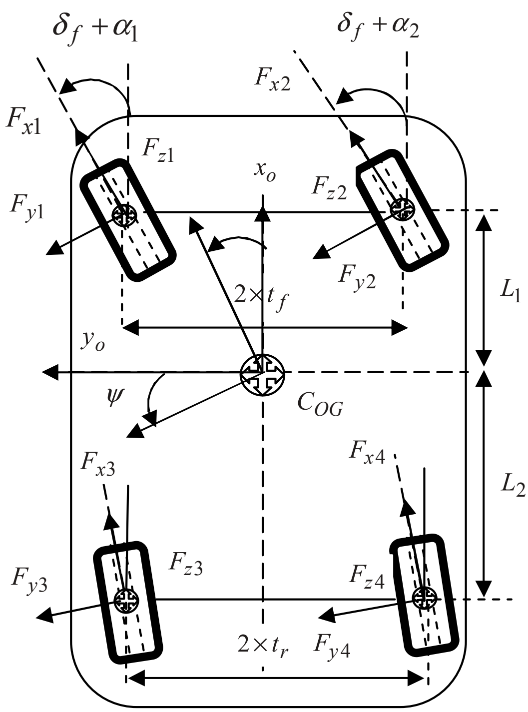

Fig. 3.6 2D vehicle representation

Then, we obtain:

$$\dot{\beta} = \frac{1}{Mv_{COG}} \left(cos(\beta) \sum F_S - sin(\beta) \sum F_L \right) - \dot{\psi} \tag{3.15}$$

with

$$\begin{aligned} \sum F_L = {} & cos(\delta_f)(Fx_1 + Fx_2) + cos(\delta_r)(Fx_3 + Fx_4) - \\ & sin(\delta_f)(Fy_1 + Fy_2) - sin(\delta_r)(Fy_3 + Fy_4) \end{aligned} \tag{3.16}$$

and

$$\begin{aligned} \sum F_S = {} & sin(\delta_f)(Fx_1 + Fx_2) + sin(\delta_r)(Fx_3 + Fx_4) + \\ & cos(\delta_f)(Fy_1 + Fy_2) + cos(\delta_r)(Fy_3 + Fy_4) \end{aligned} \tag{3.17}$$

3.4 Suspension Model

The suspension system is part of the vehicle that ensures passenger comfort. Generally, a good suspension should provide a comfortable ride and good handling in a reasonable margin of travel. For this, it must keep the wheels in contact with the road, filter out the irregularities in the road and limit the amplitudes of deflections [GFP02].

The control system absorbs the road irregularities and ensures the control due to the flexibility of the suspension. The springs are most often deformed metallic elements, but there are also rubber, synthetic elastomeric springs... and air springs, whose elasticity is ensured by air or nitrogen. The hydraulic shock absorbers are equipped with a piston moving inside a cylinder filled with oil, whose motion is hampered by narrow orifices and elastic valves. They help reduce the oscillations of the suspension.

On modern cars, the wheels are suspended from the body independently, because this type of structure eliminates some vibration noise that may occur during the motion of the vehicle. The suspension model is represented in Fig. 3.7.

The stiffness and damping coefficients of the wheels are represented respectively by the variables K_i and B_i, $i = 1..4$.

The anti-roll bar generally serves to limit the motion of body roll in curves and contributes in the improvement of the vehicle stability and good cornering behavior. If the front wheels go up or down simultaneously, the anti-roll bar turns freely on its hinge and makes no effort. However, if one of the front wheels goes up while the other one goes down, the anti-roll bar front will be twisted and thus exerts a force which tends to oppose the deflection difference (same scenario for the rear anti-roll bar).

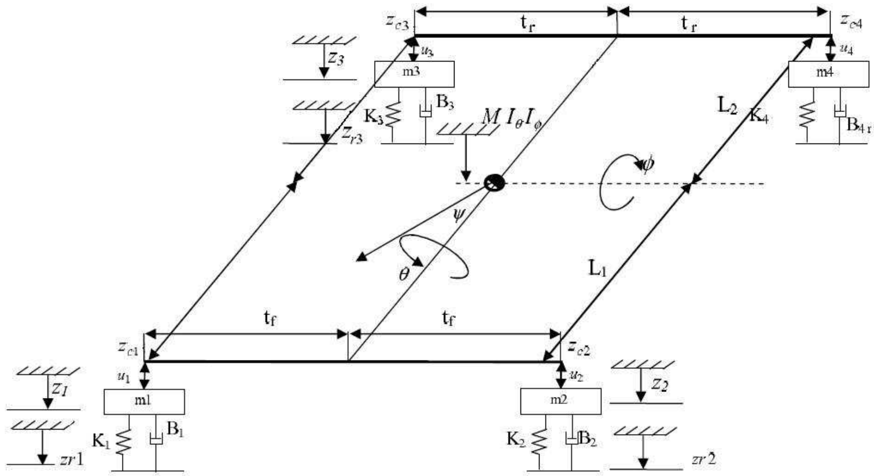

Fig. 3.7 Vehicle with suspension model

The system includes four road inputs Z_{r1}, Z_{r2}, Z_{r3} and Z_{r4}. The vertical displacements of the corners Z_{c1}, Z_{c2}, Z_{c3} and Z_{c4} which depend on the angles ϕ and θ and the vertical displacement z of the sprung mass as shown in the following equations:

$$\begin{cases} Z_{c1} = z - t_f sin(\theta) + L_1 sin(\phi) \\ Z_{c2} = z + t_f sin(\theta) + L_1 sin(\phi) \\ Z_{c3} = z - t_r sin(\theta) - L_2 sin(\phi) \\ Z_{c4} = z + t_r sin(\theta) - L_2 sin(\phi) \end{cases} \tag{3.18}$$

The vertical displacement z_i of each side of the sprung mass can be represented as:

- Front left :

$$\begin{aligned} m_1\ddot{z}_1 = {} & K_1 z + B_1\dot{z} - (B_1 + B_{1road})\dot{z}_1 - (K_1 + K_{1road})z_1 \\ & + K_{1road}Z_{r1} + B_{1road}\dot{Z}_{r1} - B_1 t_f\dot{\theta}cos(\theta) \\ & + B_1 L_1\dot{\phi}cos(\phi) + K_1 L_1 sin(\phi) - K_1 t_f sin(\theta) \end{aligned} \tag{3.19}$$

- Front right:

$$
\begin{aligned}
m_2\ddot{z}_2 = {} & K_2 z + B_2\dot{z} - (B_2 + B_{2road})\dot{z}_2 - (K_2 + K_{2road})z_2 \\
& +K_{2road}z_{r2} + B_{2road}\dot{Z}_{r2} + B_2 t_f\dot{\theta}cos(\theta) \\
& +B_2 L_1\dot{\phi}cos(\phi) + K_2 L_1 sin(\phi) + K_2 t_f sin(\theta)
\end{aligned}
\tag{3.20}
$$

- Rear left:

$$
\begin{aligned}
m_3\ddot{z}_3 = {} & K_3 z + B_3\dot{z} - (B_3 + B_{3road})\dot{z}_3 - (K_3 + K_{3road})z_3 \\
& +K_{3road}Z_{r3} + B_{3road}\dot{Z}_{r3} - B_3 t_r\dot{\theta}cos(\theta) \\
& -B_3 L_2\dot{\phi}cos(\phi) - K_3 L_2 sin(\phi) - K_3 t_r sin(\theta)
\end{aligned}
\tag{3.21}
$$

- Rear right:

$$
\begin{aligned}
m_4\ddot{z}_4 = {} & K_4 z + B_4\dot{z} - (B_4 + B_{4road})\dot{z}_4 - (K_4 + K_{4road})z_4 \\
& +K_{4road}Z_{r4} + B_{4roue}\dot{Z}_{r4} + B_4 t_r\dot{\theta}cos(\theta) \\
& -B_4 L_2\dot{\phi}cos(\phi) - K_4 L_2 sin(\phi) + K_4 t_r sin(\theta)
\end{aligned}
\tag{3.22}
$$

The rear and the front anti-roll bars are represented by their stiffness k_{arr} and k_{arf} respectively. They are used to restrict the vehicle rolling motion to stabilize the vehicle when cornering. The applied torque due to these anti-roll bars is given by:

$$
\Gamma = (k_{arr} + k_{arf})\theta \tag{3.23}
$$

3.5 Wheel/Road Interaction

All the external efforts that are applied on the vehicle, except for the aerodynamical forces, are generated at the wheel/road interaction. For that reason the surface of contact with the ground is an important factor.

3.5.1 Contact Surface

The contact surface between the wheel and the ground may be divided into two parts (brush model):

- The static region, or the adherence $X_{adherence}$,
- The dynamic part, or the sliding $X_{sliding}$.

The dimensions of this contact surface, where the contact forces are generated, are important factors needed to calculate these forces and to study the vehicle stability.

3.5.2 Vertical Forces

The vertical load supported by the wheels is not constant (see Fig. 3.8).

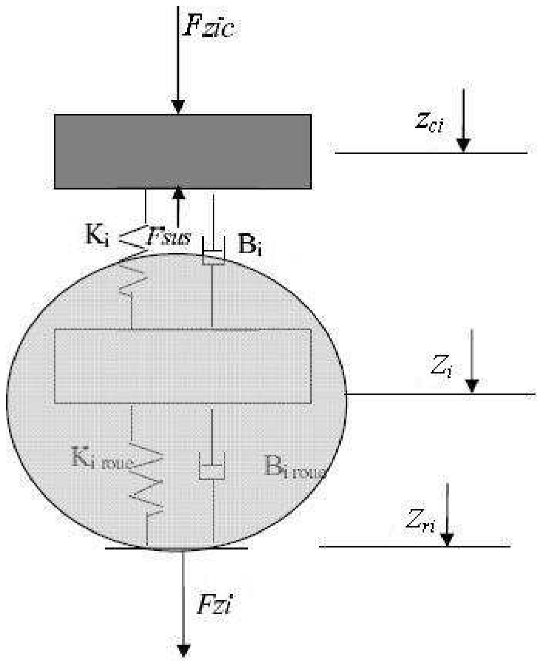

Fig. 3.8 Suspension model

In fact, many factors may cause the variation of this load such as vehicle acceleration (deceleration), when the vehicle is in a turn, non symmetrical distribution of the mass, aerodynamic forces, etc...

- The geometrical load transfer:
  The vertical loads are not identically distributed over the four wheels as described below:
  Front left wheel:

$$Fz_1 = \frac{M}{2L} \times \left(-L_2 \ddot{Y}_{COG} \frac{H}{l} - \ddot{X}_{COG} H + g L_2 \right) \tag{3.24}$$

  Front right wheel:

$$Fz_2 = \frac{M}{2L} \times \left(L_2 \ddot{Y}_{COG} \frac{H}{l} - \ddot{X}_{COG} H + g L_2 \right) \tag{3.25}$$

Rear left wheel:

$$Fz_3 = \frac{M}{2L} \times \left(-L_1 \ddot{Y}_{COG} \frac{H}{l} + \ddot{X}_{COG} H + g L_1 \right) \tag{3.26}$$

Rear right wheel:

$$Fz_4 = \frac{M}{2L} \times \left(L_1 \ddot{Y}_{COG} \frac{H}{l} + \ddot{X}_{COG} H + g L_1 \right) \tag{3.27}$$

with $L = L_1 + L_2$ and $H = h + z$,

- The elastic load transfer:
  The vertical force of the chassis is also expressed in terms of the suspension system of each wheel. For the wheel i :

$$Fzic = K_i(Z_i - z_{ci}) + B_i(\dot{Z}_i - \dot{z}_{ci}) \tag{3.28}$$

However, to find the vertical force, the suspension model is needed.

3.5.3 Longitudinal Forces

Since the forces applied on the tire then its deformation on a rigid surface is different from that on a deformed surface (ground). In this work, the road is assumed to be rigid and consequently no penetration in the road is considered.

The global longitudinal force applied on each wheel is equal to the sum of all the longitudinal forces acting on its contact surface with the ground. These forces are generated in the adhesion and the sliding areas.

A unit volume deformation is limited by the friction between the tire and the road. The maximal friction force acting on the contact surface is given by:

$$F_{imax} = \mu_i F z_i \tag{3.29}$$

So the element of the brush model begins to slide when the deformation reaches the value presented by the above equation. Therefore the force acting on the element is equal to $\mu F z_i$.

Then the simplified longitudinal force is given :

$$Fx_i = \mu_{xi} F z_i \tag{3.30}$$

The longitudinal force is thus a function of:

- The inflation pressure p_i,
- the wheel radius r_i,
- the vertical force Fz_i,
- the slipping λ_i,

- the coefficient of adherence μ_i,
- the side slip angle of each wheel α_i,
- the linear velocity of each wheel(Vx_i and Vy_i),
- the friction force F_{rri},
- the angular velocity of each wheel Ω_i.

3.5.3.1 Slipping

The relative velocity of the tire on the ground defines a dimensionless longitudinal slip at the tire-road interaction.
In the case of braking or constant velocity, the longitudinal sliding is expressed by:

$$\lambda_{xi} = \frac{Vx_i - r_{1i}\Omega_i}{Vx_i} \tag{3.31}$$

The longitudinal slip $\lambda_{xi} = 0$ characterizes the motion of a free wheel without longitudinal force. If the wheel is locked ($\Omega_i = 0$), then the slipping value is $\lambda_{xi} = 1$. However, any tire has a limit beyond which it cannot withstand additional transverse force [Pet03]. When the tire reaches the saturation limits, it slides transversely.

In case of braking or constant speed, the lateral slip is expressed by a function of the side slip angle:

$$\lambda_{yi} = tan(\alpha_i) \tag{3.32}$$

In the case of acceleration:

- The longitudinal slip
$$\lambda_{xi} = \frac{r_{1i}\Omega_i - Vx_i}{r_{1i}\Omega_i} \tag{3.33}$$
- The lateral slip
$$\lambda_{yi} = (1 - \lambda_{xi})\, tan(\alpha_i) \tag{3.34}$$

In both cases, the global slipping is given by:

$$\lambda_i = \sqrt{\lambda_{xi}^2 + \lambda_{yi}^2} \tag{3.35}$$

3.5.3.2 Road Adhesion

The road adhesion coefficient μ_i depends on the sliding of the wheel, its velocity and its slip angle [KN05]:

$$\mu_i(\lambda_i, v_{COG}) = (C_{1i}\,(1 - exp\,(-C_{2i}\lambda_i)) - C_{3i}\lambda_i)\, exp\,(-C_{4i}\lambda_i v_{COG}) \tag{3.36}$$

Several experiments have been realized. They allow showing how the friction coefficient varies in function of the vertical load.

This coefficient can be calculated as follows:

$$\mu_{xi}(\lambda_i, v_{COG}) = (C_{1i}\,(1 - exp\,(-C_{2i}\lambda_i)) - C_{3i}\lambda_i)\Delta \qquad (3.37)$$

where $\Delta = exp\,(-C_{4i}\lambda_i v_{COG})\,(1 - C_{5i}Fz_i^2)$.

This function depends essentially on the tire characteristics (quality, usage, inflation pressure, temperature, etc.), but also on the type of the road cover which is characterized by the coefficients C_{1i}, C_{2i} and C_{3i}. These coefficients are assumed known for different types of road cover and are defined as:

- C_{1i} is the maximal value of the friction curve,
- C_{2i} corresponds to the form of the friction curve,
- C_{3i} is the difference between the maximal value of the friction and its value when it is equal to 1,
- C_{4i} is known and it depends on the maximal velocity of the wheel i,
- C_{5i} determines the influence of the vertical load on the wheel i,
- The adherence coefficient has the following properties:

- $\mu_i(0, v_{COG}, \alpha_i) = 0$
- $\mu_i(0, v_{COG}, \alpha_i) > 0$ if $\lambda_i > 0$

Moreover, the variation of the tire friction coefficient μ_i according to the longitudinal slip of the wheel has two zones of distinct operations which we shall call the stable area ($0 < \lambda_{xi} < \ lambda_o$) and the unstable zone ($\lambda_o < \ lambda_{xi} < 1$) curve of Fig. 3.9.

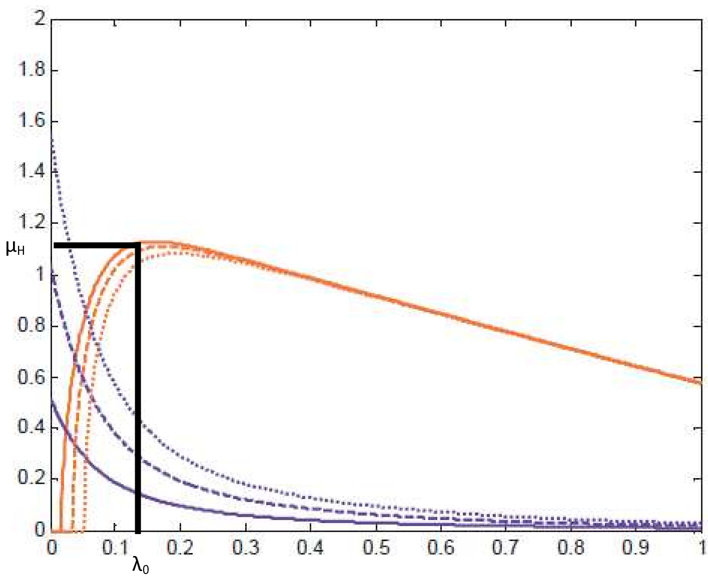

Fig. 3.9 Adherence coefficient

The existence of this unstable area justifies the need for braking control such as Antilock Braking System (ABS) or Anti Slip Regulation (ASR).

Fig. 3.9 shows how the friction coefficient increases with slipping until it reaches μ_H, or it reaches its maximum value. For higher values of slip, the friction coefficient will decrease to a minimum when the wheel is locked and only the sliding friction is acting on the wheel.

Fig. 3.10 shows the variation of the road adhesion coefficient versus the slip by varying the slip angle of the wheel.

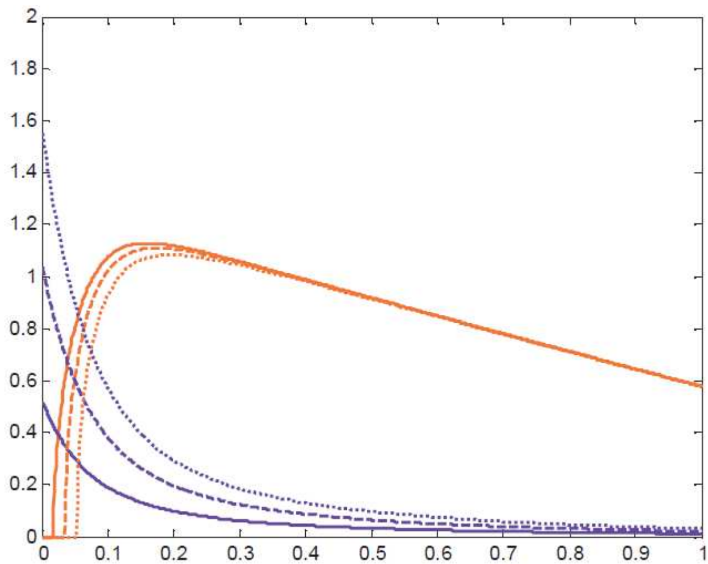

Fig. 3.10 Adherence coefficient by varing the side slip angle

where:

The solid line red corresponds to longitudinal friction with a side slip angle of 1 °.

The solid line blue corresponds to lateral friction with a side slip angle of 1 °.

The dashed line red corresponds to longitudinal friction with a side slip angle of 2 °.

The dashed line blue corresponds to lateral friction with a side slip angle of 2 °.

The dotted line red corresponds to longitudinal friction with a side slip angle of 3 °.

The dotted line blue corresponds to lateral friction with a side slip angle of 3 °.

The velocity of the center of gravity is 20 m/s

The type the road pavement is asphalt dry.

Fig. 3.11 shows the variation of the adhesion coefficient versus slip by varying the type of the road surface.

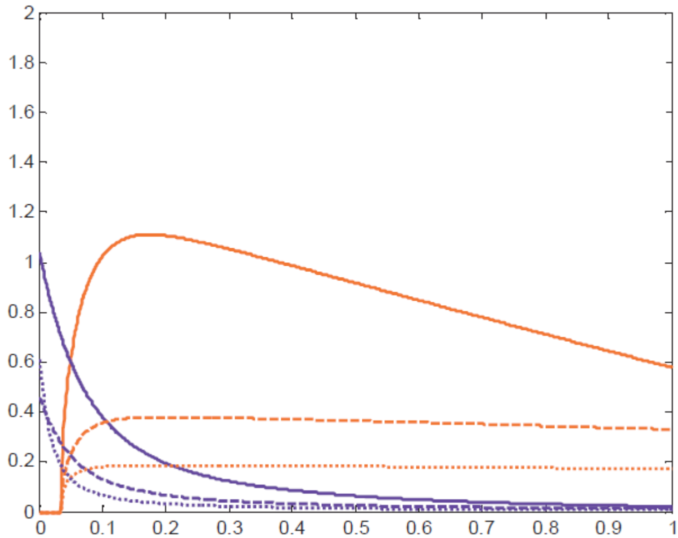

Fig. 3.11 Adherence coefficient by varing the road surface

where:

The solid line red corresponds to longitudinal friction (Dry asphalt).

The solid line blue corresponds to lateral friction (Dry asphalt).

The dashed line red corresponds to longitudinal friction (Dry Cobblestones).

The dashed line blue corresponds to lateral friction (Dry Cobblestones).

The dotted line red corresponds to longitudinal friction (Ice).

The dotted line blue corresponds to lateral friction (Ice)

The velocity of the center of gravity is 20 m/s

The type the road pavement is asphalt dry.

Fig. 3.12 shows the friction coefficient as function of the lateral adhesion

The angles found in the figure 3.12 correspond to the side slip angle of the wheel.

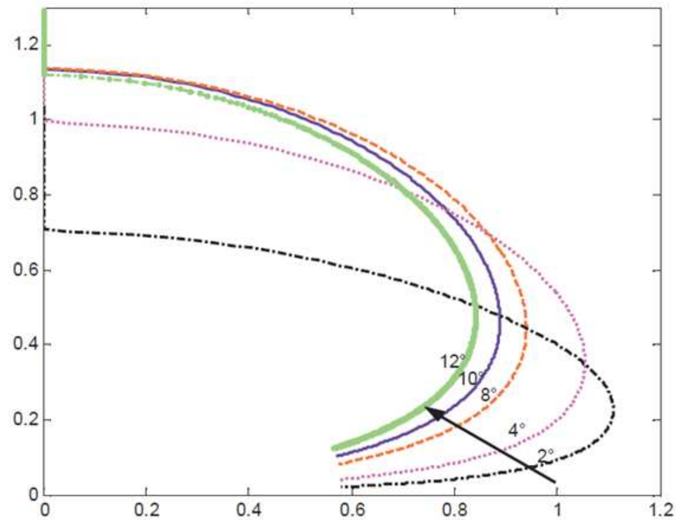

Fig. 3.12 Lateral adherence coefficient versus the longitudinal adherence coefficient

3.5.3.3 Wheel Slip Angle

When a rotating wheel is subject to lateral stress, it appears that the surface of the tire slides on the ground in a direction opposite to that effort.

The deformation of the contact surface creates an angle between the longitudinal axis of the wheel and the direction of motion as given in the figure 3.13.

This angle is called the slip angle of the tire. We then say that the tire is slipping when its trajectory makes an angle relative to its plane of symmetry.

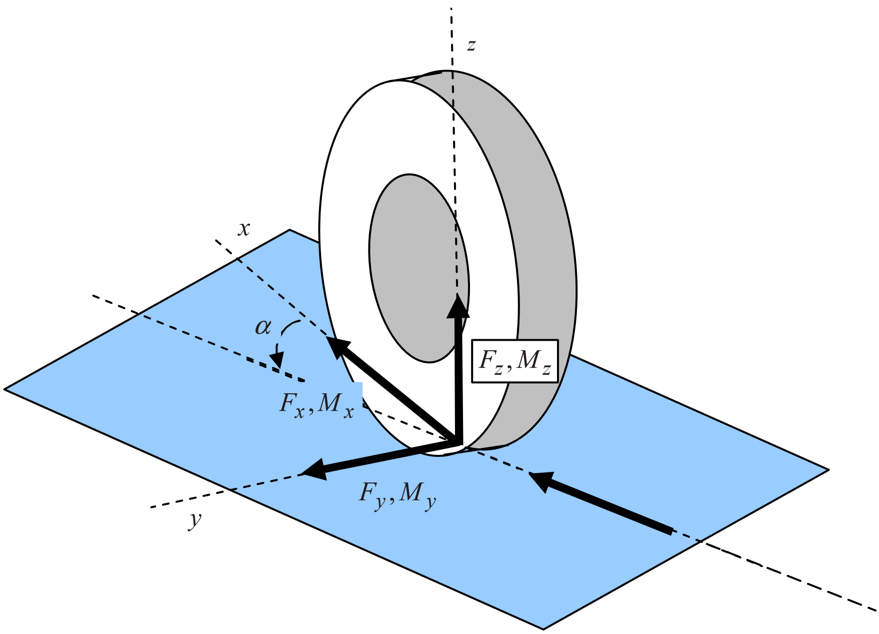

Fig. 3.13 Slip angle and the contact forces

The slip angle of each wheel is given by:

- front left wheel:

$$\alpha_1 = tan^{-1}\left(\frac{Vy + L_1\dot{\psi}}{Vx - t_f\dot{\psi}}\right) - \delta_f \tag{3.38}$$

- front right wheel:

$$\alpha_2 = tan^{-1}\left(\frac{Vy + L_1\dot{\psi}}{Vx + t_f\dot{\psi}}\right) - \delta_f \tag{3.39}$$

- rear left wheel :

$$\alpha_3 = tan^{-1}\left(\frac{Vy - L_2\dot{\psi}}{Vx - t_r\dot{\psi}}\right) - \delta_r \tag{3.40}$$

- rear right wheel:

$$\alpha_4 = tan^{-1}\left(\frac{Vy - L_2\dot{\psi}}{Vx + t_r\dot{\psi}}\right) - \delta_r \tag{3.41}$$

3.5.3.4 Velocities of the Wheels

The longitudinal and lateral velocities of each wheel are calculated by the following equations:

- front left wheel:

$$Vx_1 = \left(Vx - t_f\dot{\psi}\right) cos(\delta_f) + \left(Vy + L_1\dot{\psi}\right) sin(\delta_f) \tag{3.42}$$

$$Vy_1 = -\left(Vx - t_f\dot{\psi}\right) sin(\delta_f) + \left(Vy + L_1\dot{\psi}\right) cos(\delta_f) \tag{3.43}$$

- front right wheel:

$$Vx_2 = \left(Vx + t_f\dot{\psi}\right) cos(\delta_f) + \left(Vy + L_1\dot{\psi}\right) sin(\delta_f) \tag{3.44}$$

$$Vy_2 = -\left(Vx + t_f\dot{\psi}\right) sin(\delta_f) + \left(Vy + L_1\dot{\psi}\right) cos(\delta_f) \tag{3.45}$$

- rear left wheel:

$$Vx_3 = \left(Vx - t_r\dot{\psi}\right) cos(\delta_r) + \left(Vy - L_2\dot{\psi}\right) sin(\delta_r) \tag{3.46}$$

$$Vy_3 = -\left(Vx - t_r\dot{\psi}\right) sin(\delta_r) + \left(Vy - L_2\dot{\psi}\right) cos(\delta_r) \tag{3.47}$$

- rear right wheel:

$$Vx_4 = \left(Vx + t_r\dot{\psi}\right) cos(\delta_r) + \left(Vy - L_2\dot{\psi}\right) sin(\delta_r) \tag{3.48}$$

$$Vy_4 = -\left(Vx + t_r\dot{\psi}\right) sin(\delta_r) + \left(Vy - L_2\dot{\psi}\right) cos(\delta_r) \tag{3.49}$$

3.5.4 Lateral Forces

Based on the same idea shown in the description of the longitudinal forces, the lateral forces are represented by their simplified model. Thus the lateral force is given:

$$Fy_i = \mu_{yi} Fz_i \tag{3.50}$$

3.5.5 Aerodynamic Forces

As with any body moving through the air, six components of aerodynamic forces act on the vehicle: three efforts and three moments [GFP02]. These components depend on the width, length, surface contact with the air, the speed of the vehicle and some coefficients depending on the structure and external shape of the vehicle.

The equations representing the forces [KN05] are given by:

$$\begin{array}{c} F_{aeroX} = -c_{ventX} A_L \frac{\rho}{2} \left(V_x - V_{ventX} cos(\psi) - V_{ventY} sin(\psi)\right)^2 \\ F_{aeroX} = -c_{ventX} A_S \frac{\rho}{2} \left(V_Y - V^*_{vent}\right)^2 sign(-V^*_{vent}) \\ F_{aeroZ} = 0 \end{array} \tag{3.51}$$

where $V^*_{wind} = -V_{windX} sin(\psi) + V_{windY} cos(\psi)$.

The three moments are given by :

$$\left\{ \begin{array}{l} Mx_{aero} = \frac{1}{2}\rho V_r^2 SLC_{aermx} \\ My_{aero} = \frac{1}{2}\rho V_r^2 SLC_{aermy} \\ Mz_{aero} = \frac{1}{2}\rho V_r^2 SLC_{aermz} \end{array} \right| \tag{3.52}$$

with $V_r = V_x + V_a$ if the wind is coming from the front and $V_r = V_x - V_a$ otherwise.

3.5.6 Angular Motions of the Wheels

The wheel model is shown in Fig. 3.14.

The equilibrium of moments for each wheel are given by the following equations (see [KN05]):

$$\left\{ \begin{array}{l} Ir_1 \times \dot{\Omega}_1 = -r_{11} \times Fx_1 + Torque_1 \\ Ir_2 \times \dot{\Omega}_2 = -r_{21} \times Fx_2 + Torque_2 \\ Ir_3 \times \dot{\Omega}_3 = -r_{31} \times Fx_3 + Torque_3 \\ Ir_4 \times \dot{\Omega}_4 = -r_{41} \times Fx_4 + Torque_4 \end{array} \right| \tag{3.53}$$

where $Torque_i = C_{Mi} - C_{Fi}$, $i = 1..4$.

If the vehicle has two rear drive wheels $C_{M1} = C_{M2} = 0$, and if the two drive wheels are the front wheels then $C_{M3} = C_{M4} = 0$. Ir_i , $i = 1..4$, are the inertia of the wheels.

The motor and the braking torques are assumed to be the inputs of the model.

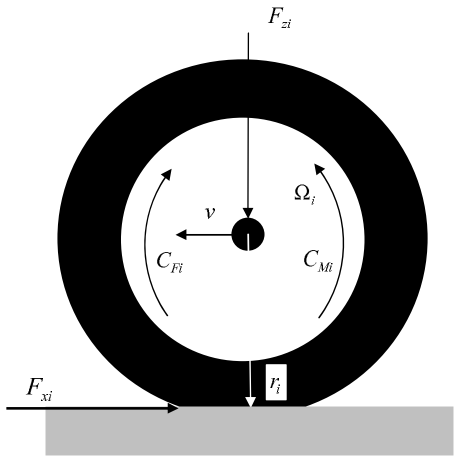

Fig. 3.14 Wheel representation

3.6 Model Validation

Once the model is completed, it should be validated. The most common method to validate a model is to simulate its behavior and analyze its response with respect to different inputs, and then to compare these results with those of the real system (prototype, validated simulator2026) having the same inputs. To realize this step, the following questions arise:

- Do the model outputs match the measured data?
- Is the model appropriate to the purpose for which it is built?

Before results analysis and validation, one must clearly understand the desired aim of the model. In other words, what output should have great precision, and where may some errors be tolerated?

Several test scenarios should be defined in order to validate the model and the chosen tests should represent the vehicle behavior in different significant situations. For example, if the model is needed in order to design the longitudinal control, a scenario of a straight line motion (acceleration, braking, constant velocity) should be prepared. For the lateral dynamics, a scenario of a two lane passage may be used.

The validation step includes:

- velocities (lateral, longitudinal)
- angles (roll, pitch and yaw) and the yaw rate,
- contact forces of each wheel (longitudinal, lateral and vertical)
- slip angle and the vehicle position in the (X, Y, Z) plane of the center of gravity of the vehicle,

3.6.1 Simulator Description

The vehicle model which has been developed using Matlab-Simulink is composed of many parts:

- The inputs of the driver: the steering angle, engine torque, acceleration load and brake pressures;
- aerodynamic resistance: this block is composed of aerodynamic forces;
- Suspensions forces;
- Pneumatic forces.

The validation consists in comparing the simulation results to the measurements done on the instrumented vehicle 406 in Nantes, France.

The system inputs are coming form driver (steering angle) and from the road (road profile).

3.6.2 Vehicle Instrumentation

The instrumented vehicle is a Peugeot 406 rolling on the track as shown in Fig. 3.15.

Fig. 3.15 Instrumented vehicle

The vehicle is equipped with different sensors such as Laser, accelerometer and inertial central in order to measure the dynamics of the vehicle (see Fig. 3.16).

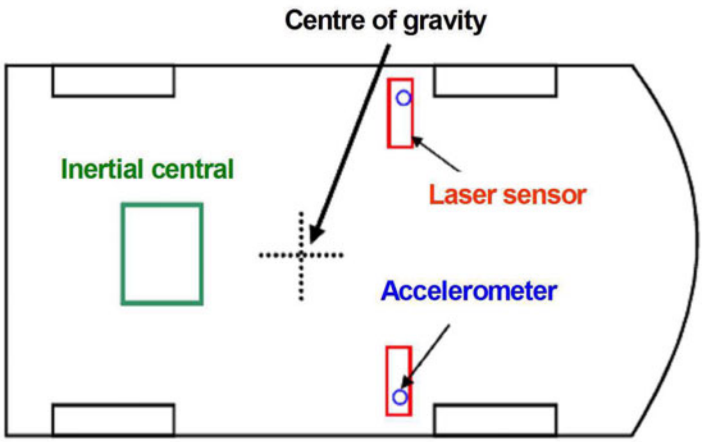

Fig. 3.16 Sensors emplacement

These sensors are described in the following subsections.

3.6.2.1 Translation Sensors

In order to record the translation motion, some sensors are installed in the vehicle. Two laser sensors (Fig. 3.17) are installed in the front of the vehicle.

They are used to measure the distance between the suspension and the road.

Fig. 3.17 Laser sensor

The accelerometers allow obtaining the vertical displacement of the suspension after double integration

3.6.2.2 Rotational Sensors

In order to measure the angular motion of the vehicle (roll, pitch and yaw motion), two gyrometers are placed in the front of the vehicle and two others in the rear of the vehicle. They measure the roll, pitch and yaw rate. We then need to integrate these speeds in order to obtain the angles. These positions are compared with those obtained by the software POS-MV provided by SIREHNA (3.18).

Fig. 3.18 Central Inertia

3.6.2.3 Displacements Sensors

A differential GPS is also installed in the vehicle, as we can see in Fig. 3.19.

We can then obtain the exact position of the vehicle according to a fixed reference and follow its trajectory. The vehicle speed is about $72 km/h$. It is measured by "correvit".

Fig. 3.19 Differential gps

To obtain the signals, the software POS-MV is used. It allows drawing the trajectory of the vehicle (positions, speeds...).

Fig. 3.20 and Fig. 3.21 show the installation of the acquisition materials in the vehicle.

Fig. 3.20 Acquisition material: front of vehicle

Fig. 3.21 Acquisition material: rear of vehicle

In order to have an indication on the road and to identify the position of the vehicle, cones are placed each $500m$ on the track as we can see in Fig. 3.22.

Fig. 3.22 Cone placement

The detection of the vehicle passing in front of the cone is done using an optic sensor (Fig. 3.23).

Fig. 3.23 Optic sensor

The detection cell is represented in Fig. 3.24. After each passage in front of a cone, one needs to reset this cell.

Fig. 3.24 Detection cell

Fig. 3.25 shows the passage time of the vehicle in front of the cones.

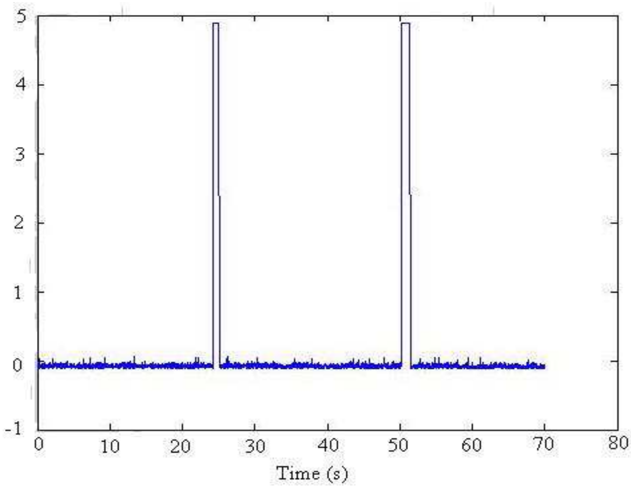

Fig. 3.25 cone detection

3.6.3 Validation Results

Many tests have been done with different speeds. In this section, the vehicle rolls at an average speed of $72km/h$ $(20m/s)$.

In Fig. 3.26 the longitudinal slip is shown.

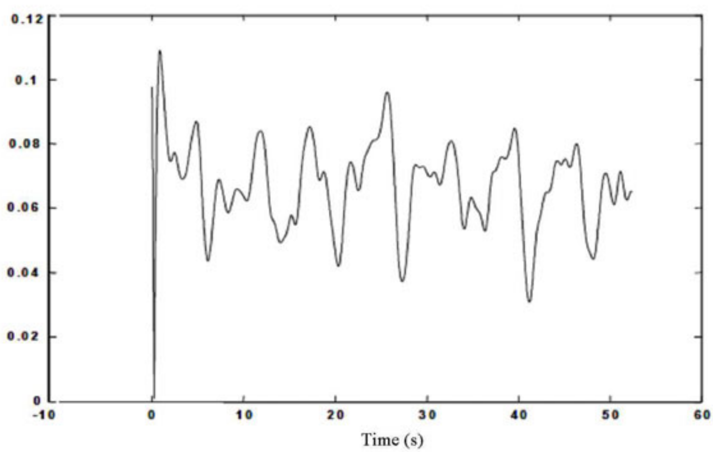

Fig. 3.26 Longitudinal slip

One remarks that this slip is very small. That is why a linearization can be done the road adhesion coefficient μ can be considered as proportional to the slip λ ($\mu = C\lambda$).

The measured vertical displacements of the four wheels are compared to those given by the mode in the Fig. 3.27.

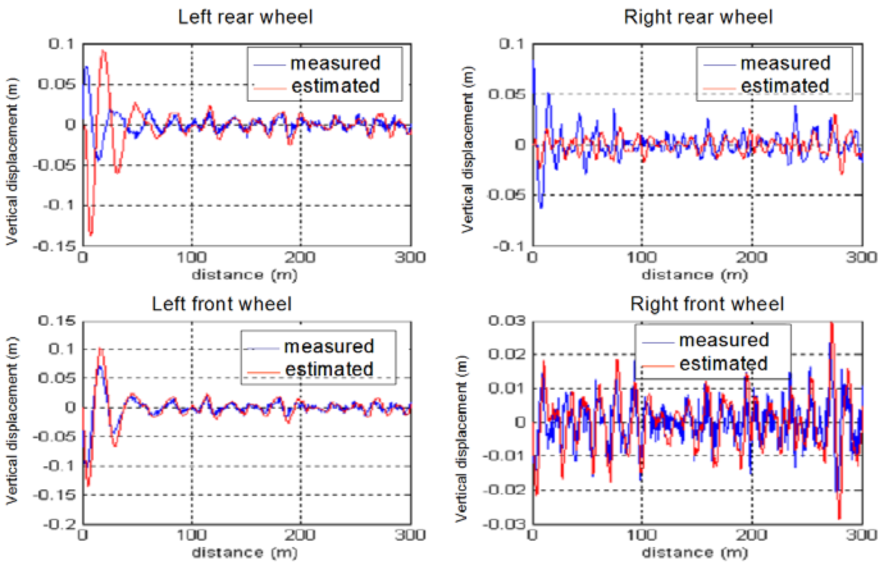

Fig. 3.27 Vertical displacements of the wheels

Fig. 3.28 shows the measured and estimated vertical displacement of the body.

One can note that the estimation of the vertical displacement of the chassis and the wheels are accurate compared with the measured ones.

The roll angle, pitch angle and its derivatives coming from the model are compared to those measured by the sensors. The result of this comparison is shown in the Fig 3.29.

One notices that the variables coming from the model convergence well toward the measures.

The estimation of the vertical accelerations of the wheels and the body are shown, respectively, in Fig. 3.30 and Fig. 3.31.

One remarks that the estimated acceleration coming from the model accurately follows the measured one after only $50m$ ($\simeq 2.5s$).

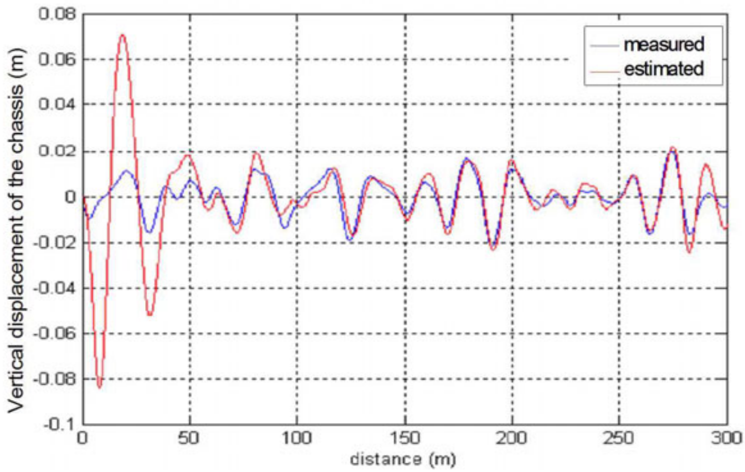

Fig. 3.28 Vertical displacement of the chassis

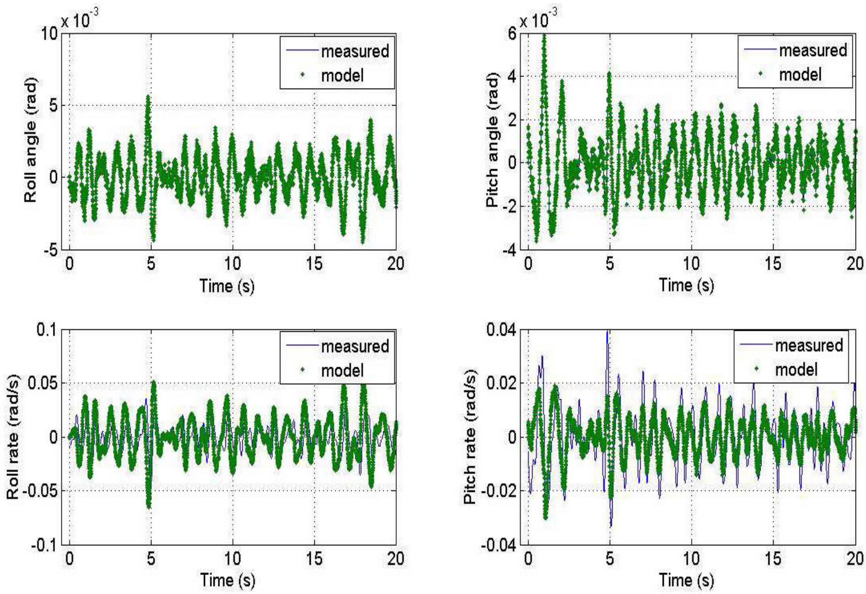

Fig. 3.29 Roll and pitch angle estimation

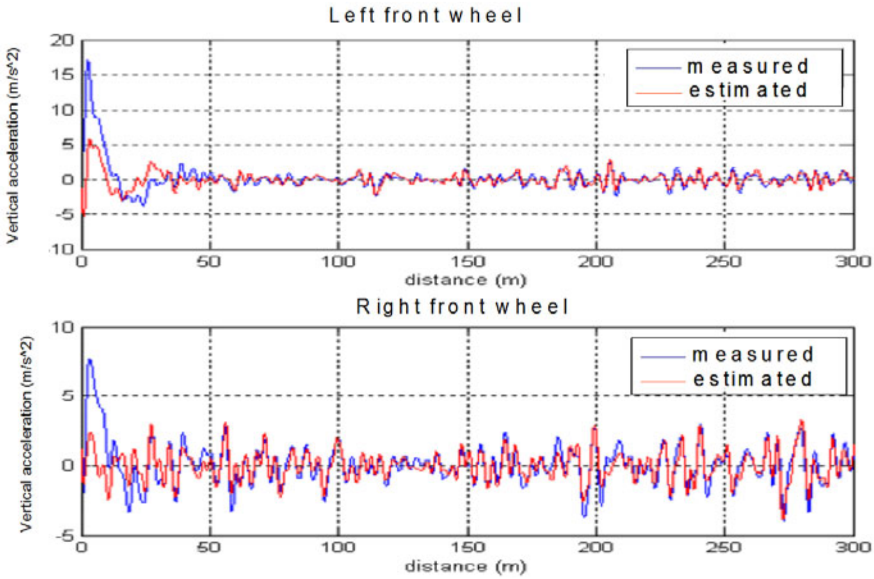

Fig. 3.30 Vertical acceleration of the wheels

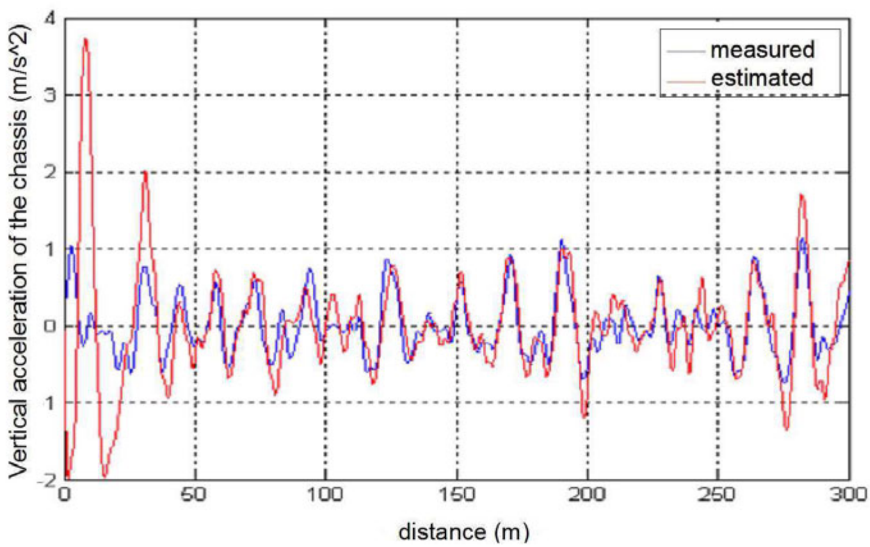

Fig. 3.31 Vertical acceleration of the chassis

The speeds of the wheels are illustrated in Fig. 3.32.

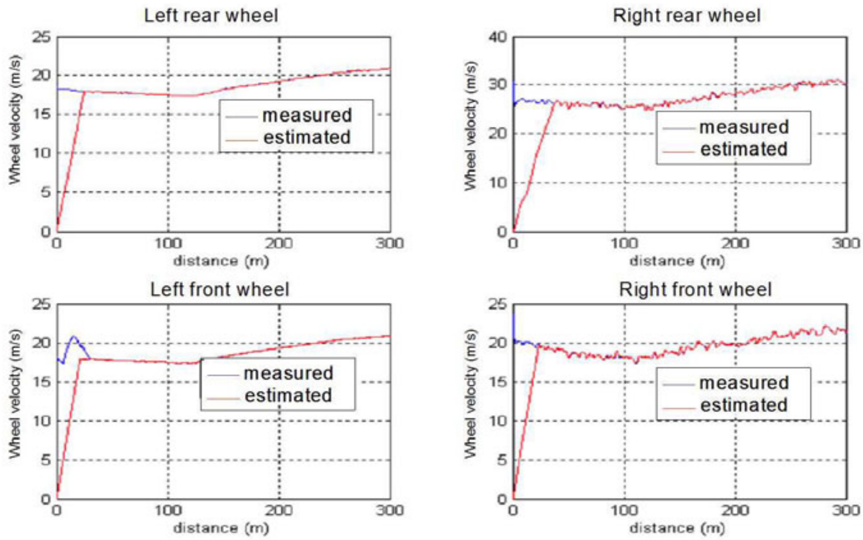

Fig. 3.32 Wheels velocities

One notices that the velocities coming from the model are quite close to the measured ones.

3.7 Conclusion

In this chapter a dynamic model of vehicle is presented. This model is important and necessary in order to design the estimation strategies that will be presented in the following chapters. The presented dynamic model is composed of several interconnected sub-models. Nevertheless, it is noted that some elements of the vehicle have not been studied. For example, a model for the power train has not been considered... The model is validated by the simulator ve-DYNA, and also by real time measurements using an instrumented vehicle. Several validation scenarios have been carried out (straight line motion, two lane passage). Obtained results are reasonable and one can conclude then that the model can be used for the development and design of model based strategies (estimation, control, diagnosis, etc.). That is the aim of next chapters 3 and 4.

Chapter 4
States and Parameters Estimation

Abstract. In this chapter, a first order SM observer and an observer based on the adaptation of a quality function have been developed in order to estimate the vehicle dynamics such as side slip angle, the unknown forces and identification of parameters of the vehicle. The advantage and the inconvenient of each method is then noticed

4.1 Introduction

Effective intelligent control systems are implemented on a vehicle to obtain a certain desired trajectory and to provide safety. For that purpose, a mathematical model representing, with a good precision, the states describing the real system should be obtained, and also corresponding sensors should be implemented on the vehicle in order to give a correct image of the states. In fact it is not simple to measure all the states and all the forces due to the high costs of some sensors, or the non existence of some others. That is why observers for state estimation and parameter identification should be designed to be an intermediate stage before the control.

Braking and traction control systems must be able to stabilize the car during cornering or in critical situations. For this reason important researches have been performed on the study of traction and braking control, sliding control using SM techniques or using Lageurre approach ([UK99], [SOA05a]). Nevertheless, for complicated analytical models the control design for the global vehicle is complicated due to the presence of contact forces which have complex forms. To avoid these complications, and the high costs of the sensors measuring these forces, estimation and identification strategies are proposed. Another important term which is used for the control is the side slip angle, which is a key variable in vehicle dynamics. In the Electronic Stability Program (ESP) or the Dynamic Stability Control (DSC) the vehicle side slip angle is used as a control reference.

H. Imine et al.: Sliding Mode Based Analysis, LNCIS 414, pp. 61–81.
springerlink.com

Table 4.1 Nomenclature.

Symbol	Physical Meaning
Ω_i	angular velocity of the wheel
M	total mass of the vehicle
r_i	radius of the wheel i
COG	center of gravity of the vehicle
r_{1i}	dynamical radius of the wheel i
Fz_i	vertical force at wheel i
Fz_{i0}	vertical nominal Force of the wheel i
Fx_i	longitudinal force applied at the wheel i
Fy_i	lateral force applied at the wheel i
C_{fi}	braking torque applied at wheel i
C_{mi}	motor torque applied at wheel i
$torque_i$	$C_{mi} + C_{fi}$
I_Z	moment of inertia around Z axis
ψ	yaw angle
$\dot{\psi}$	yaw velocity
δ_f	front steering angle
δ_r	rear steering angle
Vx	longitudinal velocity of the center of gravity
Vy	lateral velocity of the center of gravity
a_x	longitudinal acceleration of the center of gravity
a_y	lateral acceleration of the center of gravity
I_{ri}	moment of inertia of the wheel i
v_{COG}	total velocity of the center of gravity
L_1	distance between COG and the front axis
L_2	distance between COG and the rear axis
L	$L_1 + L_2$
C_{ij}	tire side slip constants (i:front (F), rear (R),j:right (R), left (L))
X_{COG}	longitudinal position of COG in a fixed reference
Y_{COG}	lateral position of COG in a fixed reference
α_{ij}	slip angle of the wheel i
β	slip angle of the COG
H	height of COG
t_f	front half gauge
t_r	rear half gauge
F_{xwind}	air resistance in the longitudinal direction
F_{ywind}	air resistance in the lateral direction
A_L	front vehicle area
ρ	air density
C_{aer}	coefficient of aerodynamic drag

However, the vehicle side slip angle cannot be measured with standard sensors. Several approaches can be found in the literature for the estimation of the vehicle side slip angle ([HCB+01], [SCD05]) in which a bicycle model is used for the vehicle. For small lateral acceleration their observers show good results, but for larger lateral acceleration, however, the bicycle model is no longer capable of describing the vehicle side slip angle properly. Consequently the observers do not provide a good estimation any more.

In [VHK05], an observer with adaptation of a quality function is used for the estimation of the vehicle side slip angle using a model linearized around the states.

The main contributions of this work reside in the estimation of wheel contact forces with the ground, vehicle side slip angle and velocities using a complete model and taking as inputs only some measurements. These estimations are made using two classes of SM observers.

- In the first part, the estimation of the angular velocity and the identification of the longitudinal force of each wheel are realised using a second-order SM observer based on the modification of the super-twisting algorithm with finite time convergence. Only partial knowledge of the system model is required.

  Due to the finite time convergence of the observer and the properties of equivalent control, the proposed observer allows solving simultaneously the presented identification problems.
- In the second part, the identified longitudinal forces are used as inputs. The vehicle side slip angle is estimated using a classical SM observer and then compared to the one estimated by an observer with adaptation of a quality function used in [VHK05]. Lateral forces at the contact areas are also deduced by applying the simplified relations relating them to side slip of each wheel [KN05]. Vertical forces are estimated using measurements of the accelerations (lateral and longitudinal). Finally, the position of the contact point (the center) of each wheel on the surface of contact with the ground can be found in order to be injected in the equation representing the yaw rate.

SM observer designs have been proposed by various authors; they have received much attention recently and have been shown to be effective when applied to nonlinear systems (see for example recent tutorials ([ESH02], [BDB03], [Poz03]). These types of observers are widely used due to their finite time convergence, robustness with respect to uncertainties and the possibility of uncertainty estimation.

On the other hand the use of first order sliding mode observers for mechanical systems with unknown inputs based on standard first order sliding mode approach have the following disadvantages:

1. for the observation of velocity, filtration is needed,
2. for the uncertainties and parameter identification a second filtration is necessary, leading to a bigger corruption of results.

In [Lev98], a robust exact differentiator was designed as an application of the second order sliding mode super twisting algorithm [Lev93] ensuring the best possible approximation of the derivative for a given sampling step and level for deterministic noise. These differentiators are, for example, successfully used in ([Ram02], [BPPU03]).

In [DFL05b] it is shown that the second order sliding mode observers provide the best possible approximation of the velocity for the given sampling step or measurement step.

Simulations results are compared with those obtained using the simulator VE-DYNA.

The chapter is organized as follows: in section 2, the problem statement is discussed. Section 3 shows the modeling of the vehicle in the (X, Y) plane. In section 4, the second order SM observer is proposed. At the end of this section, simulations and comments are made. In section 5, a reduced model is used for the global vehicle, and it is validated by the simulator VE-DYNA. In this section, a classical first order SM observer and an observer based on the adaptation of a quality function are presented in order to estimate the side slip angle of the center of gravity. Then, velocities of the center of gravity and lateral contact forces are directly found and validated by the simulator. At the end of this section, simulations and comments are made. Finally in section 6 a conclusion is shown.

4.2 Problem Statement

The task is to design a virtual sensor (observer) for the vehicle in order to estimate some unknown parameters, states and forces when it is not easy to measure all of them, be it for cost purposes or for the complexity of their implantation. Some example are contact forces with the ground, side slip angle, lateral and longitudinal velocities, all of which are needed especially in fields of diagnosis and control. For that reason, several steps are proposed (see Fig. 4.1):

1. estimate the angular velocity of each wheel, and identify the longitudinal forces which are assumed as unknown inputs. In this part a second-order SM observer based on the modification of the super twisting algorithm is used,
2. to use the results of the first estimation as inputs to the second step, a classical SM observer and an observer based on the adaptation of a quality function are used for the estimation of the side slip angle of the center of gravity of the vehicle using the complete vehicle model. Observers results are compared.
3. find the lateral and the longitudinal velocities of the center of gravity using validated relations relating them through the side slip angle,
4. find the side slip angle of each wheel based on the above estimated values,
5. find the lateral forces using the relations relating them to the side slip angle of each wheel,

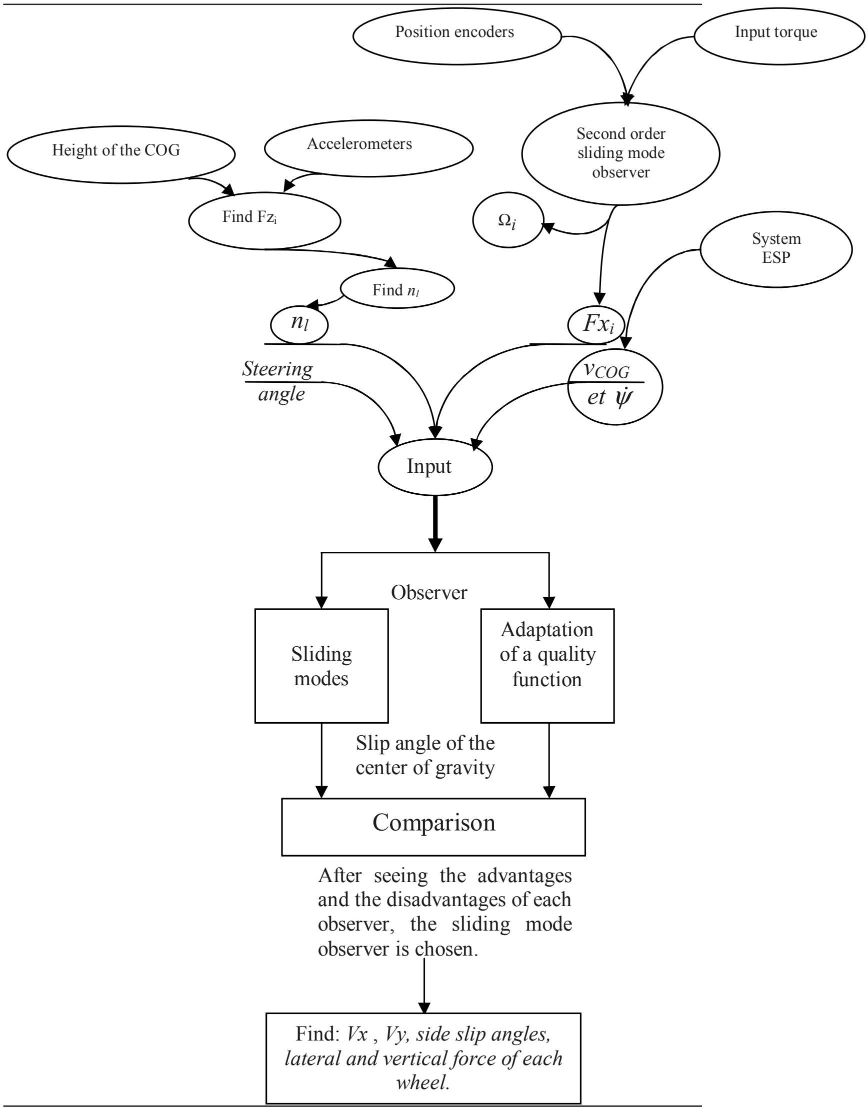

Fig. 4.1 Graphical description of the proposed work

4.3 A Second Order Sliding Mode Observer Design

In this part, the angular velocities equations are used to estimate the longitudinal force and the angular velocity of each wheel. Furthermore, a second order SM observer based on the modification of super-twisting algorithm [DFL05b] is proposed. It takes as measured values the angular position of each wheel and the applied torques and assumes that the longitudinal forces are unknown inputs to be identified.

We have seen in the chapter 2 that the equations for the angular velocity of the wheels are given by:

$$\begin{cases} Ir_1 \times \dot{\Omega}_1 = -r_{11} \times Fx_1 + torque_1 \\ Ir_2 \times \dot{\Omega}_2 = -r_{12} \times Fx_2 + torque_2 \\ Ir_3 \times \dot{\Omega}_3 = -r_{13} \times Fx_3 + torque_3 \\ Ir_4 \times \dot{\Omega}_4 = -r_{14} \times Fx_4 + torque_4 \end{cases} \tag{4.1}$$

where Ω_i and $\dot{\Omega}_i$ are the angular position and the angular velocity of the wheel $i, .i = 1..4$, $torque_i$ is the applied torque and Fx_i is the longitudinal force.

The dynamic equations of the wheels 4.1 can be rewritten in the following state form:

$$\begin{cases} \dot{x}_1 = x_2 \\ \dot{x}_2 = f(t, x_1, x_2, u) \end{cases} \tag{4.2}$$

where $x_1 = [\Omega_1, \Omega_2, \Omega_3, \Omega_4]$ and $x_2 = [\dot{\Omega}_1, \dot{\Omega}_2, \dot{\Omega}_3, \dot{\Omega}_4]$.

The proposed observer has the following form (see the chapter 1):

$$\begin{cases} \dot{\hat{x}}_1 = \hat{x}_2 + z_1 \\ \dot{\hat{x}}_2 = f_1(t, x_1, \hat{x}_2, u) + z_2 \end{cases} \tag{4.3}$$

where $\hat{x}_1$ and $\hat{x}_2$ are the state estimations of the angular positions and the angular velocities of the four wheels respectively, f_1 is a nonlinear function containing only the known terms, z_1 and z_2 are the correction factors based on the super twisting algorithm defined in the previous chapter 1.

This observer ensures the finite time convergence of the estimated states to the real states i.e. $(\hat{x}_1, \hat{x}_2) \to (x_1, x_2)$ [DFL05b].

4.3.1 Unknown Parameter Identification

The convergence of x_2 in a finite time ensures that the equality

$$\dot{\hat{x}}_2 = F(t, x_1, x_2, \hat{x}_2, u) - z_2 = 0$$

holds after some finite time, i.e. when $f_1(t, x_1, \hat{x}_2, u)$ converges to the known part of $f(t, x_1, x_2, u)$, z_2 will be equal to the unknown part, which is assumed from equations 4.1 to be equal to $(-r_i/I_i) \times Fx_i$, so the longitudinal force of the wheel can be found after filtering through a low-pass filter.

4.3.2 Simulation Results

Simulations are made and results are compared by those provided by simulator VE-DYNA. The same observer is applied on the four wheels but, for sake of similarity, we present only one observer corresponding to the front left wheel.

The simulator uses a car with two rear wheel drives.

The Fig. 4.2 shows the input torque for the two rear wheels and Fig. 4.3 the torque for the two front wheels.

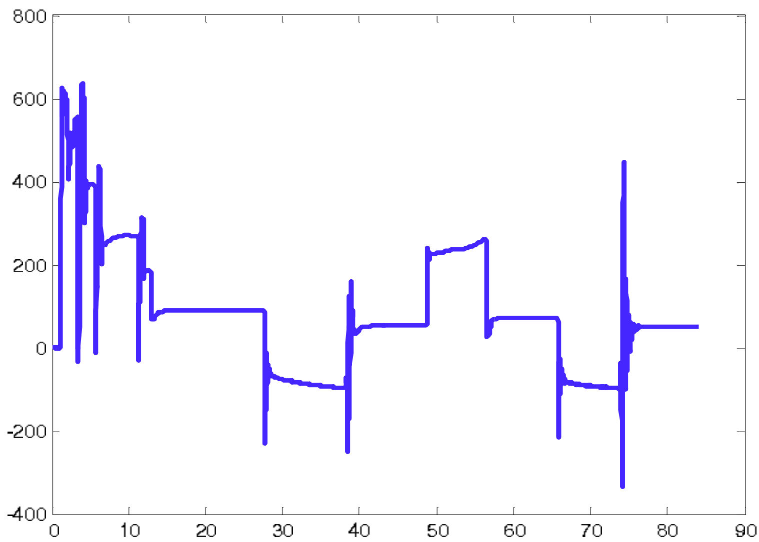

Fig. 4.2 Motor and braking torque (N.m) applied at the two rear wheels

In Fig. 4.4 and Fig. 4.5 the angular position θ_1 and angular velocity w_1 given by the simulator VE-DYNAand those computed by the proposed observer are compared.

In these figures, one remarks the quick convergence of the observer in spite of the initial values: $\theta_{10} = 0$ radians, $\hat{\theta}_{10} = 50$ radians, $w_{10} = 0$ rad/sec and $\hat{w}_{10} = 100$ rad/sec.

The values used for the observer are $\alpha = 420$ and $\lambda = 1.5\sqrt{420}$.

In Fig. 4.6, the unknown function is filtered through a low pass filter.

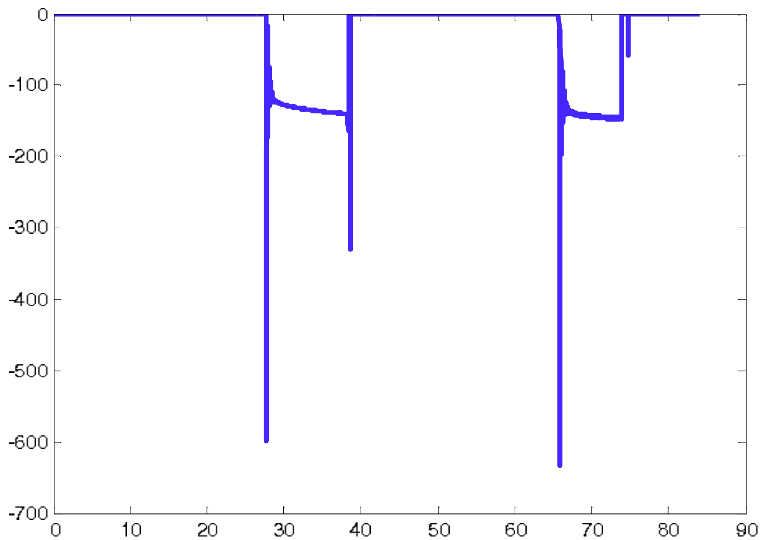

Fig. 4.3 Motor and braking torque (N.m) applied at the two front wheels

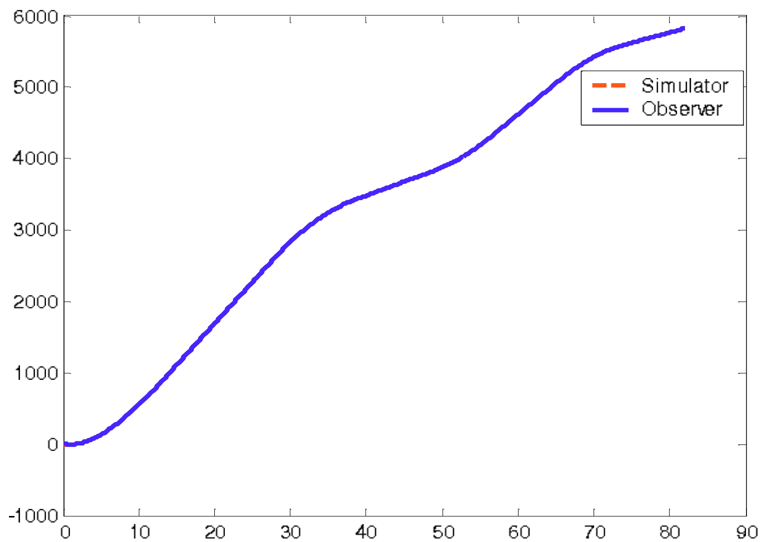

Fig. 4.4 Angular position (rad) by the simulator VE-DYNA (dashed line), and that estimated by the observer (solid line)

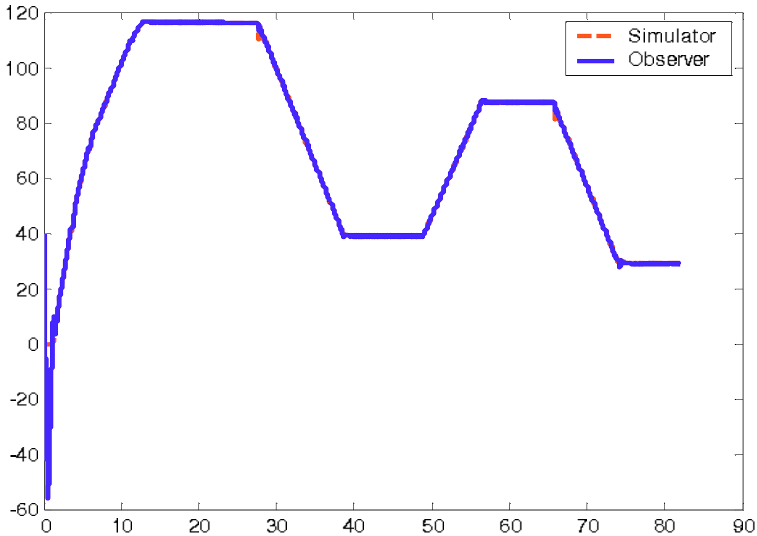

Fig. 4.5 Angular velocity (rad/sec) by the simulator VE-DYNA (dashed line), and that estimated by the observer (solid line)

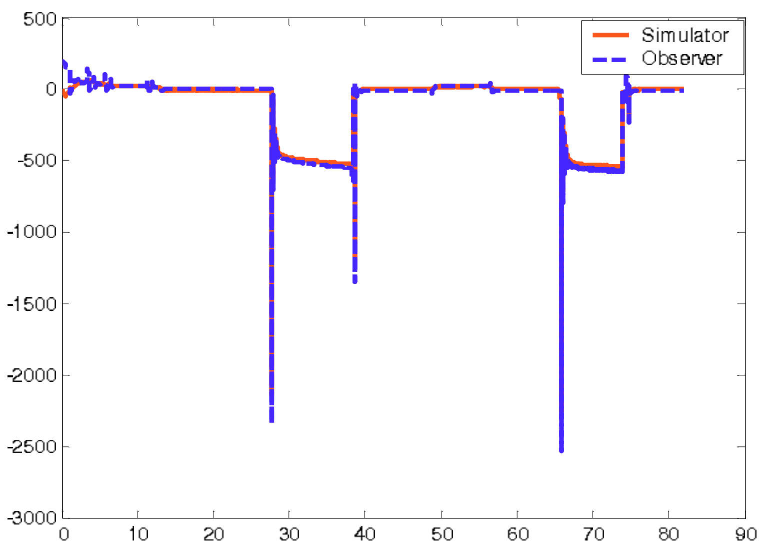

Fig. 4.6 The unknown input after filtration (N) (solid line), and the longitudinal force from the simulator (dashed line)

One notices that the filtered function approximately coincides with the longitudinal force given by the simulator.

4.4 Side Slip Angle

In order to estimate vehicle side slip angle, the wheel side forces are approximated to be proportional to the tire side slip angles α_{ij}:

$$\begin{cases} Fy_1 = C_{FL} \times \alpha_{FL} = C_{FL} \times \left(\delta_f - \beta - \frac{L_1 \times \dot{\psi}}{v_{COG}}\right) \\ Fy_2 = C_{FR} \times \alpha_{FR} = C_{FR} \times \left(\delta_f - \beta - \frac{L_1 \times \dot{\psi}}{v_{COG}}\right) \\ Fy_3 = C_{RL} \times \alpha_{RL} = C_{RL} \times \left(-\beta + \frac{L_2 \times \dot{\psi}}{v_{COG}}\right) \\ Fy_4 = C_{RR} \times \alpha_{RR} = C_{RR} \times \left(-\beta + \frac{L_2 \times \dot{\psi}}{v_{COG}}\right) \end{cases} \tag{4.4}$$

Then, the model of the vehicle will be rewritten as:

$$\begin{aligned} \dot{v}_{COG} = \tfrac{1}{M} \{ & (Fx_1 + Fx_2)cos(\delta_f - \beta) - (C_{FL} + C_{FR}) \\ & (\delta_f - \beta - \tfrac{L_1\dot{\psi}}{v_{COG}})sin(\delta_f - \beta) + \\ & (F_{x3} + F_{x4} - C_a er A_L v_{COG}^2 \tfrac{\rho}{2})cos(\beta) + \\ & (C_{RL} + C_{RR}) \left(-\beta + \tfrac{L_2\dot{\psi}}{v_{COG}}\right) sin(\beta) \Big\} \end{aligned} \tag{4.5}$$

$$\begin{aligned} \dot{\beta} = \tfrac{1}{M v_{COG}} \{ & (F_{x1} + F_{x2})\, sin(\delta_f - \beta) + (C_{FL} + C_{FR}) \\ & (\delta_f - \beta - \tfrac{L_1\dot{\psi}}{v_{COG}})cos(\delta_f - \beta) - \\ & (F_{x3} + F_{x4} - C_a er A_L v_{COG}^2 \tfrac{\rho}{2})sin(\beta) + \\ & (C_{RL} + C_{RR}) \left(-\beta + \tfrac{L_2\dot{\psi}}{v_{COG}}\right) cos(\beta) \Big\} - \dot{\psi} \end{aligned} \tag{4.6}$$

$$\begin{aligned} \ddot{\psi} = \tfrac{1}{I_Z} \{ & (L_1 - n_{lf} cos(\delta_f))(F_{x1} + F_{x2})sin(\delta_f) + \\ & (\delta_f - \beta - \tfrac{L_1\dot{\psi}}{v_{COG}})cos(\delta_f)(C_{FL} + C_{FR}) \\ & (L_1 - n_{lf})cos(\delta_f)) + t_f(F_{x2} - F_{x1})cos(\delta_f) \\ & - t_f(C_{FR} - C_{FL}) \left(\delta_f - \beta - \tfrac{L_1\dot{\psi}}{v_{COG}}\right) sin(\delta_f) \\ & - (L_2 + n_{lr})(C_{RL} + C_{RR}) \left(-\beta + \tfrac{L_2\dot{\psi}}{v_{COG}}\right) \\ & + t_r(F_{x4} - F_{x3}) \} \end{aligned} \tag{4.7}$$

where the positions of the centers of the contact patches n_{lf} and n_{lr} that are used in 4.7 have been calculated as follows.

$$\begin{cases} n_{li} = \frac{1}{2} \left(l_0 + l_1 \frac{Fz_i}{Fz_0}\right) \\ n_{si} = 3 n_{li} tan(\alpha_{ij}) + \frac{Fz_i}{c_{press}} \end{cases} \tag{4.8}$$

The positions of the centres of the contact are shown in the Fig. 4.7.

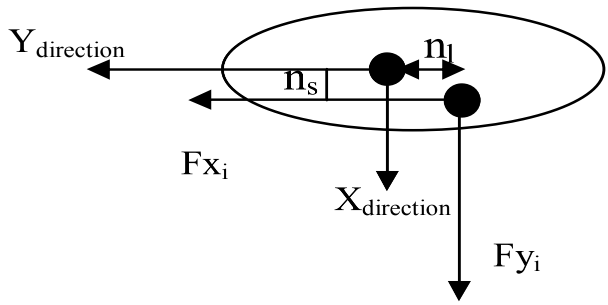

Fig. 4.7 Position of the center of contact with the road

Due to the existence of the sensors measuring the accelerations (accelerometers) and that of the height of the center of gravity, the vertical forces of each wheel can be calculated by applying these relations:
For the front left wheel:

$$F_{ZFL} = \frac{1}{2}M\left(\frac{L_2}{L} - \frac{H}{L}a_x\right) - M\left(\frac{L_2}{L} - \frac{H}{L}a_x\right)\frac{H.a_y}{t_f.g} \tag{4.9}$$

For the front right wheel:

$$F_{ZFR} = \frac{1}{2}M\left(\frac{L_2}{L} - \frac{H}{L}a_x\right) + M\left(\frac{L_2}{L} - \frac{H}{L}a_x\right)\frac{H.a_y}{t_f.g} \tag{4.10}$$

For the rear left wheel:

$$F_{ZRL} = \frac{1}{2}M\left(\frac{L_2}{L} + \frac{H}{L}a_x\right) - M\left(\frac{L_2}{L} + \frac{H}{L}a_x\right)\frac{H.a_y}{t_f.g} \tag{4.11}$$

For the rear right wheel:

$$F_{ZRL} = \frac{1}{2}M\left(\frac{L_2}{L} + \frac{H}{L}a_x\right) + M\left(\frac{L_2}{L} + \frac{H}{L}a_x\right)\frac{H.a_y}{t_f.g} \tag{4.12}$$

Using the three differential equations 4.5, 4.6 and 4.7, one can define the nonlinear state space model as:

$$\dot{x} = f(x, u) \tag{4.13}$$

where

$$x = \begin{bmatrix} v_{COG} & \beta & \dot{\psi} \end{bmatrix} \tag{4.14}$$

The control input vector is:

$$u = [F_{x1} \quad F_{x2} \quad F_{x3} \quad F_{x4} \quad \delta_f] \tag{4.15}$$

and the output vector is defined by:

$$y = \begin{bmatrix} v_{COG} & \dot{\psi} \end{bmatrix} \tag{4.16}$$

The proposed model for the side slip angle and the yaw rate is validated by the simulator VE-DYNA. It is seen that the reduced model is valid in all the tested cases using simulator. A two lane trajectory is used to validate the model. The input for the steering angle is shown in the figure 4.8 and the input rear wheels torque is represented in the figure 4.9.

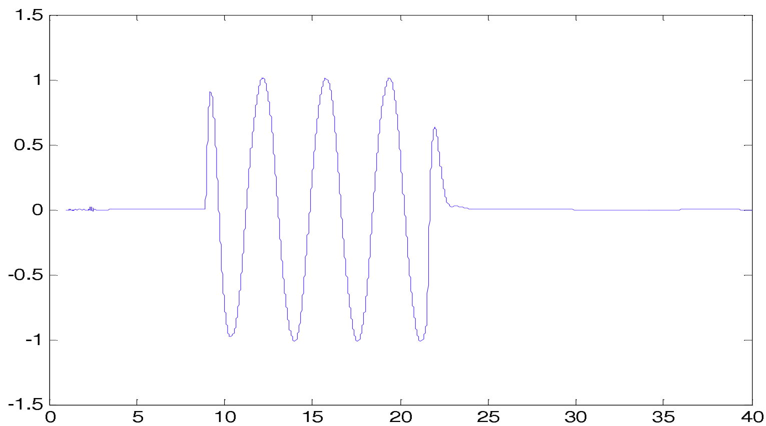

Fig. 4.8 The input steering angle (radians)

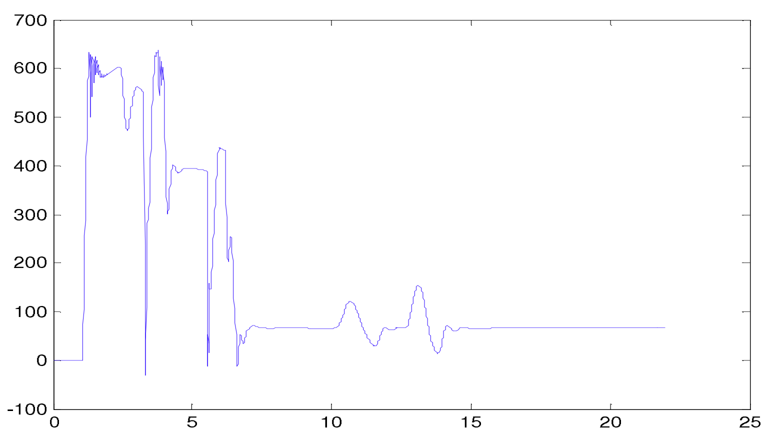

Fig. 4.9 The input torque applied at the two rear wheels (N.m)

The output of the model gives the side slip angle 4.10 and the yaw rate 4.11.

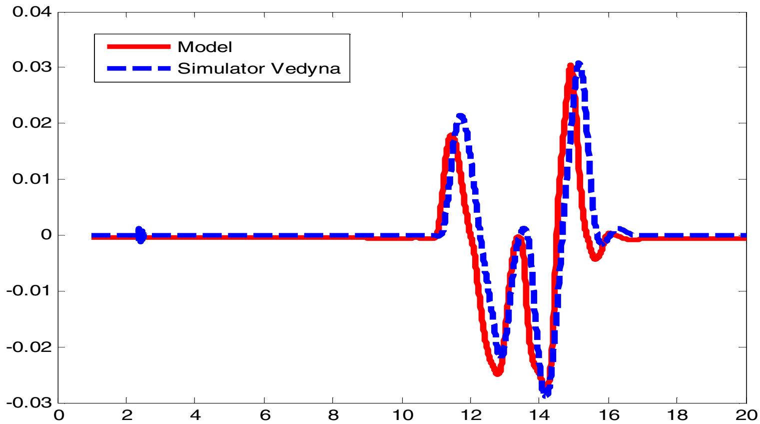

Fig. 4.10 Validation side slip angle (rad/sec) of the proposed model and that of the simulator VE-DYNA

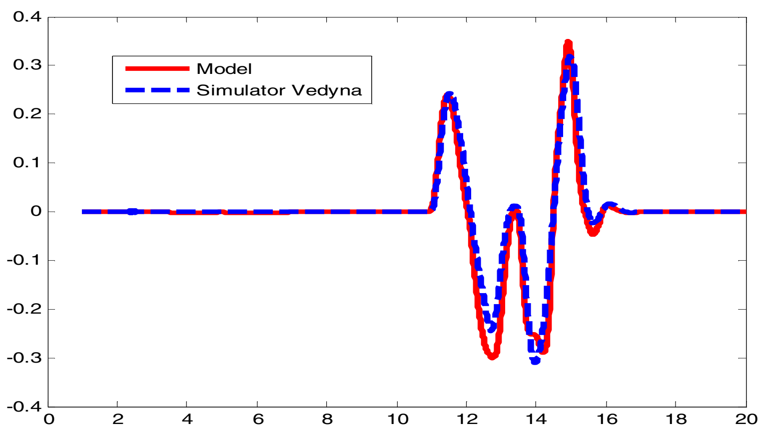

Fig. 4.11 Validation yaw rate (rad/sec) of the proposed model and that of the simulator VE-DYNA

4.4.1 Two Track Model and Observability Study

In this part, the sliding mode observer is compared to the observer with adaptation of a quality function which is restricted to models with specific structure, so the model may be written as a reduced nonlinear two track model ([KN05], [VHK05]):

$$\begin{aligned} \dot{x} &= A(x,u)x + B(x,u)u \\ y &= C(x,u)x \end{aligned} \tag{4.17}$$

As described clearly in [KN05] and in order to restructure the nonlinear double track model the differential equations 4.5, 4.6 and 4.7, or the three state variables, are linearized with respect to the unknown vehicle side slip angle β.

The equation 4.7 for the yaw rate is a linear function with respect to β. The effect of the linearization of the other two equations was analyzed by the of simulations for several test drives. For the side slip angle, the linearized state and the original nonlinear one are almost identical. For the velocity, however, there are significant deviations. Consequently, the velocity is no longer regarded as a state space variable but as an input variable, and thus the corresponding differential equation is no longer required and the system order reduces from 3 to 2. The new state space variables are:

$$x = \begin{bmatrix} \beta & \dot{\psi} \end{bmatrix} \tag{4.18}$$

and the six input variables are

$$u = [F_{x1} \quad F_{x2} \quad F_{x3} \quad F_{x4} \quad \delta_f \quad v_{COG}] \tag{4.19}$$

Then, equation 4.17 will be rewritten as

$$\begin{aligned} \dot{x} &= A(y,u^*)x + B(u^*) \\ y &= C(x,u^*) = Cx = [0 \quad 1]\, x \end{aligned} \tag{4.20}$$

with

$$A = \begin{bmatrix} a_{11} & a_{12} \\ a_{21} & a_{22} \end{bmatrix}$$

$$\begin{aligned} a_{11} = \tfrac{1}{Mv_{COG}} \{&(C_{FL} + C_{FR})[-cos(\delta_f) + sin(\delta_f)(\delta_f \\ &-\tfrac{L_1\psi}{v_{COG}}] - (C_{RL} + C_{RR}) - (Fx_3 + Fx_4 - \\ &C_aerA_L \tfrac{\rho}{2} v_{COG}^2) - (Fx_1 + Fx_2)cos(\delta_f)\} \end{aligned}$$

$$\begin{aligned} a_{12} = \tfrac{1}{Mv_{COG}^2} \{&L_2(C_{RL} + C_{RR}) - \\ &L_1 cos(\delta_f)(C_{FL} + C_{FR})\} - 1 \end{aligned}$$

$$\begin{aligned} a_{21} = \tfrac{1}{I_Z} \Big\{&-\tfrac{2t_f}{2} sin(\delta_f)(C_{FL} - C_{FR}) - \\ &(C_{FL} - C_{FR})(L_1 - n_{lf} cos(\delta_f))cos(\delta_f) + \\ &(C_{RL} + C_{RR})(L_2 + n_{lr})\} \end{aligned}$$

$$a_{22} = \frac{1}{I_Z v_{COG}} \left\{ -\frac{2t_f L_1}{2} sin(\delta_f)(C_{FL} - C_{FR}) - \right.$$
$$L_1(C_{FL} + C_{FR})(L_1 - n_{lf} cos(\delta_f)) cos(\delta_f) -$$
$$L_2(C_{RL} + C_{RR})(L_2 + n_{lr})\}$$

and

$$B = \begin{bmatrix} b_1 \\ b_2 \end{bmatrix}$$

$$b_1 = \frac{1}{M v_{COG}} \{\delta_f cos(\delta_f)(C_{FL} + C_{FR}) +$$
$$sin(\delta_f)(Fx_1 + Fx_2)\}$$

$$b_2 = \frac{1}{I_Z} \left\{ -\frac{2t_f}{2} cos(\delta_f)(Fx_2 - Fx_1) + \delta_f cos(\delta_f) \right.$$
$$(C_{FL} + C_{FR})(L_1 - n_{L1} cos(\delta_f)) + (Fx_2 + Fx_1)$$
$$sin(\delta_f)(L_1 - n_{L1} cos(\delta_f)) + (C_{FL} - C_{FR})$$
$$\delta_f t_f sin(\delta_f) + (Fx_4 - Fx_3) t_r\}$$

Before designing the sliding mode observer, the observability of the model must be investigated and tested. The criteria for the observability of nonlinear systems can be found in [Zei87].

The observability definition is local and uses the Lie derivative. It is a function of state trajectory and inputs applied to the model. For the system described by equation 4.20 the observability function is:

$$observability(x, u^*) = \begin{bmatrix} C(x) \\ L_f C(x, u^*) \\ L_f^2 c(x, u) \end{bmatrix}$$

where

$$L_f C(x, u^*) = \frac{dc_j(x)}{dx} f(x, u^*)$$

The system is observable if its Jacobian matrix $J_{observability}$ has a full rank (which is 2 in our case).

$$J_{observability} = \frac{d}{dx} observability(x, u)$$

By applying these notions to the system described by equation 4.17, we see that its rank is 2 and it is therefore observable.

4.4.1.1 Sliding Mode Observer Design

The proposed sliding mode observer is:

$$\begin{cases} \dot{\hat{x}} = A(y, u^*)\hat{x} + B(u^*) + \Delta sign(y - \hat{y}) \\ \hat{y} = C\hat{x} \end{cases} \tag{4.21}$$

where Δ is the gain of the sliding mode observer. The convergence of this observer is explained briefly in [ILMD01] in which the same type of observer is used for a bicycle model.

4.4.1.2 Observer by Adaptation of a Quality Function

The basic idea of the observer of adaptation of a quality function is the adaptation of a quality function of the nonlinear estimation error dynamics to the one of a linear reference system.

$$\begin{cases} \dot{\hat{x}} = A(y,u^*)\hat{x} + B(u^*) + L(y,u^*)(y-\hat{y}) \\ \hat{y} = C\hat{x} \end{cases} \tag{4.22}$$

The differential equation for the estimation error becomes [VHK05]:

$$\dot{\tilde{x}} = \left[A(y,u^*) - L(y,u^*)C\right]\tilde{x} \tag{4.23}$$

For the determination of an appropriate observer gain $L(y,u^*)$, the nonlinear estimation error is adapted to a linear reference model. This reference model is derived by linearizing the nonlinear state space model 4.20 around an equilibrium point(x_R, u_R^*).

4.4.2 Comparison between the Observers

The main differences between the proposed observer and the nonlinear observer with adaptation of a quality function are:

1. the nonlinear observer with adaptation of a quality function needs to linearize the equation 4.20 around an equilibrium point which is to be found.
2. the simplicity of the sliding observer in its construction and the proof of its convergence.
3. the fast convergence velocity of the sliding mode observer: at each iteration the nonlinear observer with adaptation of a quality function calculates its gain while the sliding mode observer takes the same value for its gain for a certain process.

4.4.3 Simulation Results and Discussions

In this part, the estimated vehicle side slip angle using the sliding modes observer and using the observer with adaptation of a quality function are compared to that of the simulator VE-DYNA. It is seen that the errors are practically very small and may be neglected. Several simulations are made covering most of drive cases; two simulations are shown where the side slip angle varies strongly. The gains of the observers are chosen as follows:

For the sliding mode observer Δ=20. For the observer of the adaptation of a quality function:

$$L(y,u^*) = \begin{bmatrix} 1.41 & 0.33 & 1 & 0 \\ -0.10 & 1.03 & 0 & 1 \end{bmatrix} \begin{bmatrix} a_{11} \\ a_{12} \\ a_{21} \\ a_{22} \end{bmatrix} + \begin{bmatrix} 109.9 \\ 117.4 \end{bmatrix}$$

Good and reasonable results are shown.

A simulation of 20 seconds is made, taking as inputs those defined in the figures 4.8 and 4.9.

The simulation results are shown in the figures 4.12, 4.13, 4.15 and 4.14.

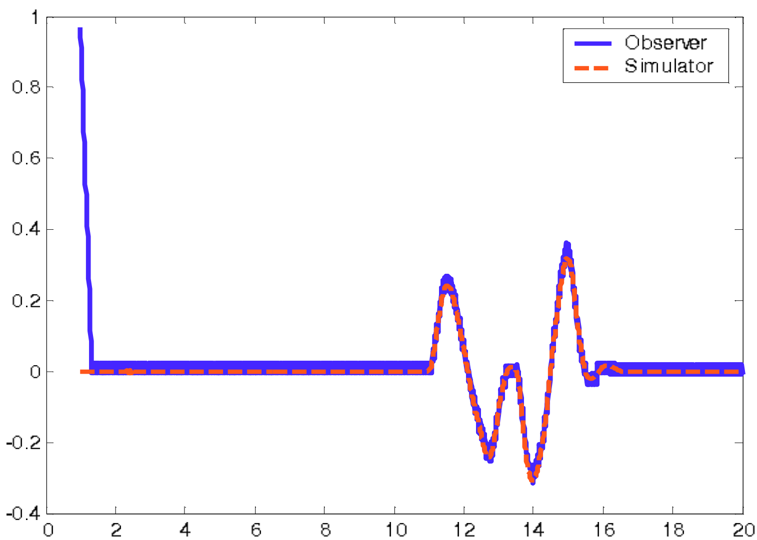

Fig. 4.12 Reconstructed yaw using sliding modes obserever and that of the simulator VE-DYNA

By estimating the slip angle of the center of gravity, and taking its global velocity as an input value (this value can be calculated directly from the velocities of the wheels), the velocities of the center of gravity in (X, Y) can be directly found by:

The lateral velocity:

$$Vy = v_{COG} sin(\beta) \tag{4.24}$$

The result of this estimation is shown in the figure 4.16.

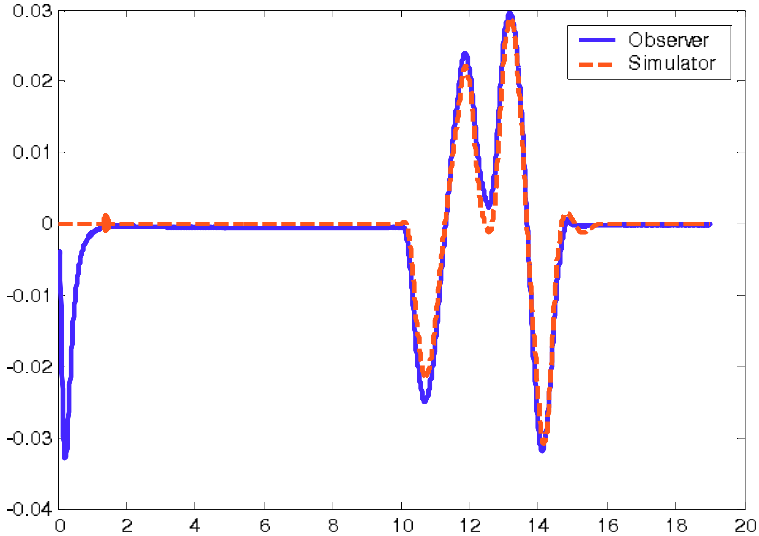

Fig. 4.13 Estimated side slip angle using sliding modes and that of the simulator VE-DYNA

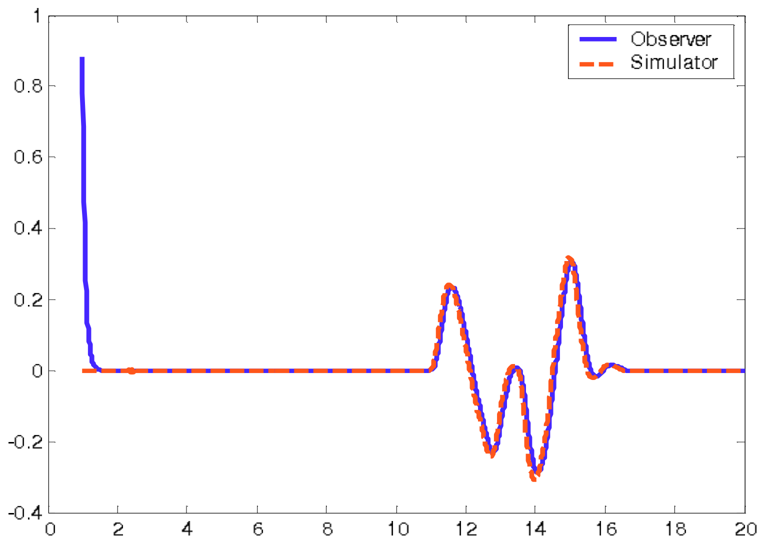

Fig. 4.14 Estimated yaw rate using observer with adaptation quality function and that of the simulator VE-DYNA

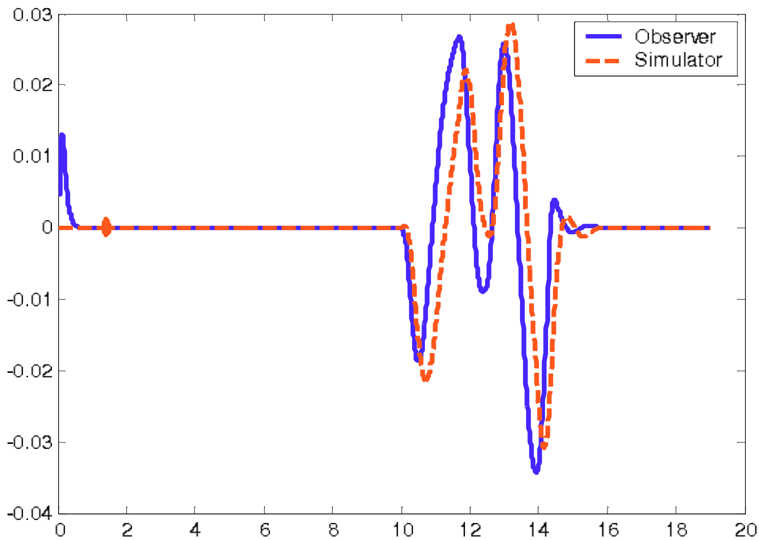

Fig. 4.15 Estimated side slip angle using observer with adaptation of a quality function and that of the simulator VE-DYNA

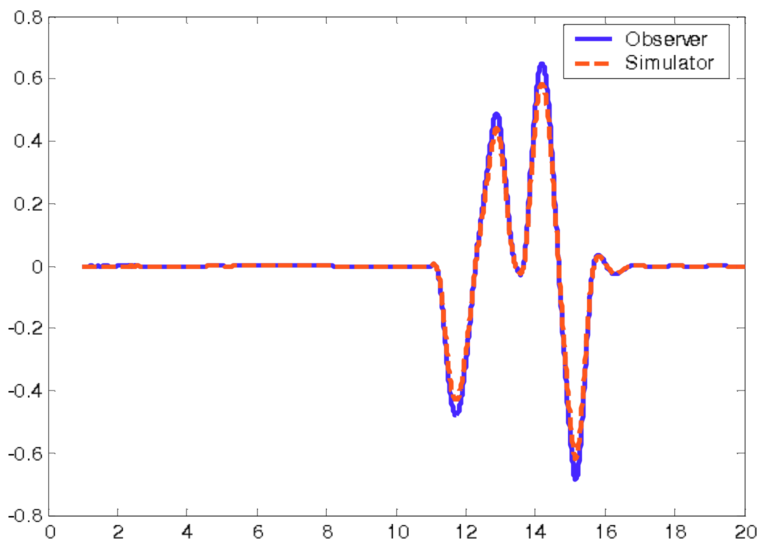

Fig. 4.16 Estimated vy (m/sec) and that of the simulator VE-DYNA

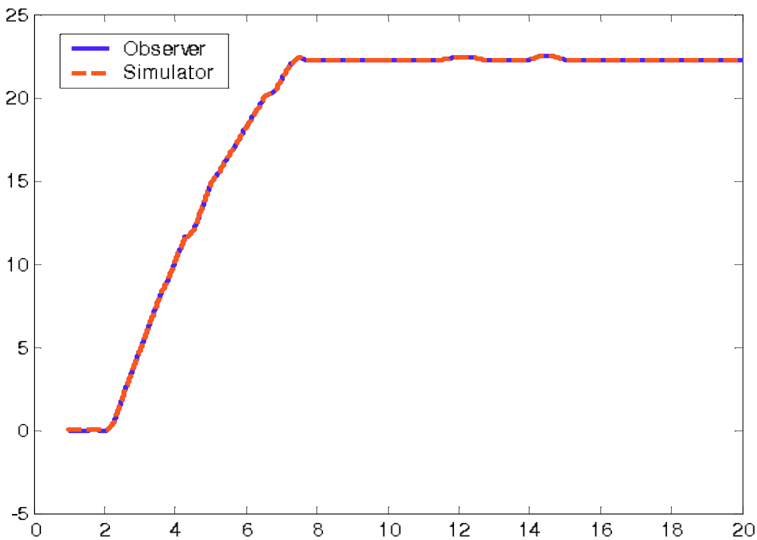

Fig. 4.17 Estimated vx (m/sec) and that of the simulator VE-DYNA

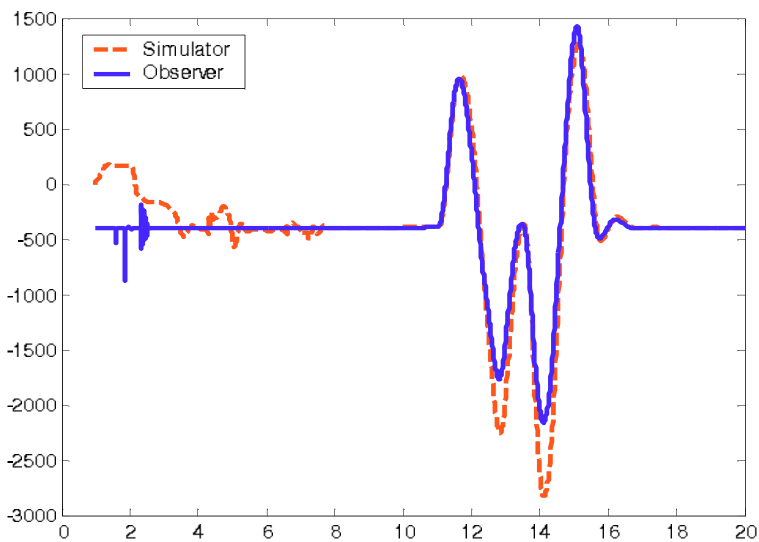

Fig. 4.18 Estimated lateral force (N) for the front left wheel and that of the simulator VE-DYNA

The longitudinal velocity which coincides with that of the simulator is calculated using:

$$Vx = v_{COG} cos(\beta) \tag{4.25}$$

The estimation of Vx is shown in the figure 4.17.

The lateral forces can be calculated using the equations defined in 4.4.

The result of estimating of the lateral force of the front left wheel is shown in the figure 4.18.

4.5 Conclusion

The estimation of vehicle parameters, states and forces, which need expensive measuring devices (expensive sensors), are presented in this chapter. In this work, two classes of sliding mode observers are used:

1. A second order sliding mode with a super-twisting algorithm observer is used in order to design the angular velocity observer for each wheel of the vehicle, and then to identify longitudinal forces between the wheels and the road.
2. A classical sliding mode observer is used in order to estimate the side slip angle of the center of gravity of the vehicle, and then to find its velocities in the (X, Y) plane and the lateral force of each wheel.

The use of the second order sliding mode observer allows to solve the problems of disturbance and parameters identification which appear in the first part. In the second part, a classical sliding mode observer is used to estimate the side slip angle of the center of gravity, then, comparison between the proposed observer and an observer with adaptation of a quality function is made. Velocities of the center of gravity and the lateral forces are deducted directly after the side slip angle. Vertical forces can be found by using measurements of the accelerations given by the accelerometers. Simulations to demonstrate the performance of the proposed sliding mode observers are made and their efficiency are shown by the comparison with the output of the simulator VE-DYNA.

Chapter 5
Estimation of Road Profile and External Forces as Unknown Inputs

Abstract. This chapter is devoted to the application of sliding mode observers to estimate the unknown inputs of the road. Vehicle motion simulation accuracy, such as in accident reconstruction or vehicle controllability analysis on real roads, can be obtained only if valid road profile and tire-road friction models are available. Regarding road profiles, a new method based on Sliding Mode Observers has been developed and is compared to two inertial methods. Experimental results are shown and discussed to evaluate the robustness and the quality of the proposed approach.

5.1 Introduction

Road profile unevenness through road/vehicle dynamic interaction and vehicle vibration affects safety (tyre contact forces), ride comfort, energy consumption and wear. The road profile unevenness is consequently a basic information for road maintenance management systems [VP91]. In order to obtain this road profile, several methods have been developed. Measurement of road roughness has been a subject of numerous research for more than 70 years ([Har83], [MW86], [Mis90]). Methods developed can be classified into two types: response type and profiling method. Nowadays profiling methods giving a road profile along a measuring line are generally preferred. These methods belong to two basic techniques: rolling beam or inertial profiling method. The last method, which was first proposed in 1964 [SK64], is now used worldwide. Inertial profiling methods consist in analyzing the signal coming from displacement sensors and accelerometers ([Kar84], [GSH87]). One problem with the inertial profiling method, as currently used, is that it is impossible to build a $3D$ profile from elementary measurements needed for road/vehicle interaction simulation package. It is worthwhile mentioning that these methods do not take into consideration the dynamic behavior of the vehicle. However, it has been shown that modifications of the dynamic behavior may lead to biased results.

H. Imine et al.: Sliding Mode Based Analysis, LNCIS 414, pp. 83–102.
springerlink.com

Finding a way to get a $3D$ profile from the dynamic response of an instrumented car driven on a chosen road section is the general purpose of a research carried out at Roads and Bridges Central Laboratory (in French: LCPC) in cooperation with the Robotics Laboratory of Versailles (in French: LRV) [Imi03].

The proposed method estimates the unknown inputs of the system corresponding to the height of the road through the use of sliding mode observers ([BZ88], [XG88], [Dra92], [BBD96], [DBB99], [DB02]).

Design of such observers requires a dynamic model. As a first step, a dynamic model of a vehicle is built up ([Men97], [Imi03]). This model has been experimentally validated comparing the estimated and measured dynamics in the response of a Peugeot 406 vehicle (as a test car). The longitudinal forces which depend on the road adhesion coefficients are estimated using a sliding mode observer (see [Can98], [IDM03]).

The second section of this chapter deals with the vehicle description and modeling. Then the observer design is presented in the third section in order to estimate the unknown inputs. Some simulation and experimental results are given in this section. The estimation of unknown forces is presented in the section four and a second approach to estimate the unknown inputs is presented. The main experimental results are presented in order to show the accuracy of the estimated road profile coming from the observer based method. Finally, the last section concludes on the effectiveness of the presented methods.

5.2 Vehicle Modeling

In this section, we are interested in the excitations of pavement and the vehicle/road interaction. The model is established while making the following simplifying hypotheses:

- The vehicle is rolling with a constant speed.
- The wheels are rolling without slip and without contact loss.

The vertical motion of the vehicle model can be described by the following equation:

$$M\,\ddot{q} + C\,\dot{q} + Kq = AU + \Omega, \tag{5.1}$$

where $q = \begin{bmatrix} z_1 \; z_2 \; z_3 \; z_4 \; z \; \theta \; \phi \; \psi \end{bmatrix}^T$ is the coordinates vector , $\dot{q}$ represent the velocities vector and $\ddot{q}$ the accelerations vector.

The vector $U = \begin{bmatrix} u_1 \; u_2 \; u_3 \; u_4 \; \dot{u}_1 \; \dot{u}_2 \; \dot{u}_3 \; \dot{u}_4 \end{bmatrix}^T$ is the road inputs vector.

The vector $\Omega = [0\ 0\ 0\ 0\ 0\ 0\ 0\ f(\delta_f, \beta)]^T$ is a function of the steering angle δ_f and the side slip angle β. The function $f(\delta_f, \beta)$ is given by:

$$f(\delta_f, \beta) = -2(r_1 C_{yf} - r_2 C_{yr})\beta + 2 r_1 C_{yf} \delta_f. \tag{5.2}$$

$M \in \mathbb{R}^{8\times 8}$ represent the mass matrix:

$$M = \begin{bmatrix} m_1 & 0 & 0 & 0 & 0 & 0 & 0 & 0 \\ 0 & m_2 & 0 & 0 & 0 & 0 & 0 & 0 \\ 0 & 0 & m_3 & 0 & 0 & 0 & 0 & 0 \\ 0 & 0 & 0 & m_4 & 0 & 0 & 0 & 0 \\ 0 & 0 & 0 & 0 & m & 0 & 0 & 0 \\ 0 & 0 & 0 & 0 & 0 & J_{xx} & 0 & 0 \\ 0 & 0 & 0 & 0 & 0 & 0 & J_{yy} & 0 \\ 0 & 0 & 0 & 0 & 0 & 0 & 0 & J_{zz} \end{bmatrix}. \tag{5.3}$$

where m_i is the mass of the wheel i, m is the spring mass, J_{xx}, J_{yy} and J_{zz} are respectively the moments of inertia along X, Y and Z axis.

$C \in \mathbb{R}^{8\times 8}$ is the damping matrix:

$$C = \begin{bmatrix} (B_1 + B_{r1}) & 0 & 0 & 0 & -B_1 & C_{16} & C_{17} & 0 \\ 0 & (B_2 + B_{r2}) & 0 & 0 & -B_2 & C_{26} & C_{27} & 0 \\ 0 & 0 & (B_3 + B_{f1}) & 0 & -B_3 & C_{36} & C_{37} & 0 \\ 0 & 0 & 0 & (B_4 + B_{f2}) & -B_4 & C_{46} & C_{47} & 0 \\ -B_1 & -B_2 & -B_3 & -B_4 & C_{55} & C_{56} & C_{57} & 0 \\ B_1 p_r & -B_2 p_r & B_3 p_f & -B_4 p_f & C_{65} & C_{66} & C_{67} & 0 \\ B_1 r_2 & B_2 r_2 & -B_3 r_1 & -B_4 r_1 & C_{75} & C_{76} & C_{77} & 0 \\ C_{81} & C_{82} & C_{83} & C_{84} & C_{85} & C_{86} & C_{87} & C_{88} \end{bmatrix} \tag{5.4}$$

The matrix $K \in \mathbb{R}^{8\times 8}$ is function of spring coefficients:

$$K = \begin{bmatrix} k_1 + k_{r1} & 0 & 0 & 0 & -k_1 & k_1 p_r & k_1 r_2 & 0 \\ 0 & k_2 + k_{r2} & 0 & 0 & -k_2 & -k_2 p_r & k_2 r_2 & 0 \\ 0 & 0 & k_3 + k_{f1} & 0 & -k_3 & k_3 p_f & -k_3 r_1 & 0 \\ 0 & 0 & 0 & k_4 + k_{f2} & -k_4 & -k_4 p_f & -k_4 r_1 & 0 \\ -k_1 & -k_2 & -k_3 & -k_4 & K_{55} & K_{56} & K_{57} & 0 \\ k_1 p_r & -k_2 p_r & k_3 p_f & -k_4 p_f & K_{65} & K_{66} & K_{67} & 0 \\ k_1 r_2 & k_2 r_2 & -k_3 r_1 & -k_4 r_1 & K_{75} & K_{76} & K_{77} & 0 \\ K_{81} & K_{82} & K_{83} & K_{84} & K_{85} & K_{86} & K_{87} & K_{88} \end{bmatrix}. \tag{5.5}$$

The matrix $A \in \mathbb{R}^{8\times 8}$ is composed of spring and damping coefficients:

$$A = \begin{bmatrix} k_{r1} & 0 & 0 & 0 & B_{r1} & 0 & 0 & 0 \\ 0 & k_{r2} & 0 & 0 & 0 & B_{r2} & 0 & 0 \\ 0 & 0 & k_{f1} & 0 & 0 & 0 & B_{f1} & 0 \\ 0 & 0 & 0 & k_{f2} & 0 & 0 & 0 & B_{f2} \\ 0 & 0 & 0 & 0 & 0 & 0 & 0 & 0 \\ 0 & 0 & 0 & 0 & 0 & 0 & 0 & 0 \\ 0 & 0 & 0 & 0 & 0 & 0 & 0 & 0 \\ 0 & 0 & 0 & 0 & 0 & 0 & 0 & 0 \end{bmatrix} . \tag{5.6}$$

We then rewrite the model in the state form as (5.1) :

$$\begin{cases} x_1 = q \\ \dot{x}_1 = x_2 \\ \dot{x}_2 = \ddot{x}_1 = \ddot{q} = M^{-1}(-Cx_2 - Kx_1 + Ax_3 + \Omega) \\ \dot{x}_3 = x_4 = \dot{U} \\ y = x_1 \end{cases} . \tag{5.7}$$

where y is the output vector:

$$y = \begin{bmatrix} z_1 \; z_2 \; z_3 \; z_4 \; z \; \theta \; \phi \; \psi \end{bmatrix}^T . \tag{5.8}$$

In the following section, a sliding mode observer is developed in order to estimate the unknown inputs of the system.

5.3 Sliding Mode Observer and Estimation of Unknown Inputs

The construction of the observer is done using 3 steps as we explain in this section. After that, we present and we discuss some simulation results.

5.3.1 Observability Study

In order to study the observability of the system (5.1), let us define the functions f and h as:

$$\begin{cases} f(x,U) = M^{-1}(-Cx_2 - Kx_1 + AU + \Omega) \\ y = h(x) \end{cases} . \tag{5.9}$$

where $x = (x_1, x_2)^T$ is a vector of dimension n.

The system is considered to be observable if the matrix MO defined below is of rank n (see [Bou97]) (in our case $n = 16$):

$$MO = \begin{bmatrix} dh(x) \\ dL_f h(x) \\ \vdots \\ \vdots \\ dLf^{\ 15} h(x) \end{bmatrix}. \tag{5.10}$$

where $dh = (\frac{\partial h}{\partial x_1}, \frac{\partial h}{\partial x_2}, ..., \frac{\partial h}{\partial x_{16}})$ and $L_f(h)(x) = \sum_{i=1}^{16} f_i \frac{\partial h}{\partial x_i}$.

The calculation of this matrix using Matlab shows that the rank of MO is 16. We deduce that the system (5.1) is observable.

5.3.2 Observer Design

This section is devoted to sliding mode observer design in order to estimate the vectors $\dot{q}$ and $\ddot{q}$ and to then reconstruct the unknown inputs vector U ([SHM86], [ILMD02a]).

Before developing the observer, we notice that the system satisfies the following hypothesis:

a) The state of the system is bounded ($\| x(t) \| < \infty \ \forall\ t \geq 0$). The vehicle states are bounded.

b) The system is input bounded (for $i = 1..4$ a constant $\mu_i \in \mathbb{R}$ $exists such that$ $\|\dot{u}_i\| < \mu_i$);

c) The amplitude of the inputs representing the road are very low and not greater than $10^{-3}m$. We can then assume that their accelerations are small and neglected $\ddot{x}_3 = \dot{x}_4 = \ddot{U} = 0$.

Assuming that the dynamic parameters of the vehicle are well known, we can write the observer as:

$$\begin{cases} \dot{\hat{x}}_1 = \hat{x}_2 + H_1 sign(\tilde{x}_1) \\ \dot{\hat{x}}_2 = M^{-1}(-C\hat{x}_2 - K\hat{x}_1 + A\hat{x}_3 + \Omega) + H_2 sign(\tilde{x}_1) \\ \dot{\hat{x}}_3 = \hat{x}_4 + H_3 sign(\tilde{x}_1) \end{cases}. \tag{5.11}$$

where $\hat{x}_i$ represents the observed state vector of x_i.

$H_i \in \mathbb{R}^{8\times 8}$, $i = 1, 2$, are diagonal positive gains matrices and the "$sign$" are defined as follows:

$$\begin{cases} H_1 = diag\{H_{1_1}, H_{1_2}, H_{1_3}, H_{1_4}, H_{1_5}, H_{1_6}, H_{1_7}, H_{1_8}\} \\ H_2 = diag\{H_{2_1}, H_{2_2}, H_{2_3}, H_{2_4}, H_{2_5}, H_{2_6}, H_{2_7}, H_{2_8}\} \\ sign(\tilde{x}_1) = diag\{\tilde{x}_{1_1}, \tilde{x}_{1_2}, \tilde{x}_{1_3}, \tilde{x}_{1_4}, \tilde{x}_{1_5}, \tilde{x}_{1_6}, \tilde{x}_{1_7}, \tilde{x}_{1_8}\}^T \end{cases} \tag{5.12}$$

The matrix $H_3 \in \mathbb{R}^{8\times 8}$ is to be defined during the convergence study.

The estimation error of the variable x_i is obtained by:

$$\tilde{x}_i = x_i - \hat{x}_i, \quad i = 1..3. \tag{5.13}$$

The dynamic error of the observer is obtained through the difference between systems (5.7) and (5.11) as following:

$$\begin{cases} \dot{\tilde{x}}_1 = \tilde{x}_2 - H_1 sign(\tilde{x}_1) \\ \dot{\tilde{x}}_2 = -M^{-1}(C\ \tilde{x}_2 + K\ \tilde{x}_1) + M^{-1}A\ \tilde{x}_3 - H_2 sign(\tilde{x}_1) \\ \dot{\tilde{x}}_3 = \tilde{x}_4 - H_3 sign(\tilde{x}_1) \end{cases}. \tag{5.14}$$

5.3.3 Convergence Study

As we showed previously, and in order to study the convergence of the observer, we proceed step by step. We first prove the convergence of the position ($\tilde{x}_1 = 0$). We must prove that the sliding surface is attractive ($\tilde{x}_1 = 0$). Then, we will study the convergence of the speed $\tilde{x}_2$. At this moment, we can deduce that the estimation error of the input ($\tilde{x}_3$) converges towards 0.

5.3.3.1 Convergence of the Position

Let us consider the following Lyapunov function:

$$V_1 = \frac{1}{2}\tilde{x}_1^T \tilde{x}_1, \tag{5.15}$$

Its derivative gives:

$$\dot{V}_1 = \tilde{x}_1^T \dot{\tilde{x}}_1, \tag{5.16}$$

From (5.14), we obtain:

$$\dot{V}_1 = \tilde{x}_1^T (\tilde{x}_2 - H_1 sign(\tilde{x}_1)). \tag{5.17}$$

Choosing the gain matrices $H_1 = diag(h_{i1})$, as $h_{i1} > |\tilde{x}_{i2}|$ for $i = 1...8$, we prove that $\dot{V}_1 < 0$. Then, $\hat{x}_1$ converges towards x_1 in finite time t_0. In this case, $\dot{\tilde{x}}_1 = 0\ \forall\ t > t_0$.

This implies, from relationship (5.17), that we obtain:

$$sign_{eq}(\tilde{x}_1) = H_1^{-1}\tilde{x}_2 \qquad , \tag{5.18}$$

where $sign_{eq}$ is the equivalent mean of the $sign$ function in the sliding surface:

Taking into account (5.18) and since $\tilde{x}_4$ is bounded, then equations (5.14) become:

$$\begin{cases} \dot{\tilde{x}}_1 = \tilde{x}_2 - H_1 sign(\tilde{x}_1) \to 0 \\ \dot{\tilde{x}}_2 = -M^{-1}C\ \tilde{x}_2 + M^{-1}A\ \tilde{x}_3 - H_2 H_1^{-1}\tilde{x}_2 \\ \dot{\tilde{x}}_3 = -H_3 H_1^{-1}\tilde{x}_2 \end{cases}. \tag{5.19}$$

5.3.3.2 Speed Convergence

Consider now a following second Lyapunov function:

$$V_2 = \frac{1}{2}\tilde{x}_2^T M \tilde{x}_2 + \frac{1}{2}\tilde{x}_3^T P_1 \tilde{x}_3, \tag{5.20}$$

where $P_1 \in \mathbb{R}^{8\times 8}$ is a diagonal positive matrix:

The calculation of $\dot{V}_2$ gives, using the equations (5.19),:

$$\dot{V}_2 = -\tilde{x}_2^T C \tilde{x}_2 - \tilde{x}_2^T M H_2 H_1^{-1} \tilde{x}_2 + \tilde{x}_2^T A \tilde{x}_3 - \tilde{x}_3^T P_1 H_3 H_1^{-1} \tilde{x}_2. \tag{5.21}$$

Choosing the gains ($P_1 = diag(P_{1i})$, $i = 1..8$) such as $A^T = P_1 H_3 H_1^{-1}$, the matrix H_3 is deduced as follows:

$$H_3 = P_1^{-1} A^T H_1. \tag{5.22}$$

Replacing the matrices P_1, A^T and H_1 by their respective values, we obtain the elements of the matrix H_3 :

$$H_3 == \begin{bmatrix} H_{11}k_{r1}/P_{11} & 0 & 0 & 0 & 0\ 0\ 0\ 0 \\ 0 & H_{22}k_{r2}/P_{22} & 0 & 0 & 0\ 0\ 0\ 0 \\ 0 & 0 & H_{33}k_{f1}/P_{33} & 0 & 0\ 0\ 0\ 0 \\ 0 & 0 & 0 & H_{44}k_{f2}/P_{44} & 0\ 0\ 0\ 0 \\ H_{11}B_{r1}/P_{55} & 0 & 0 & 0 & 0\ 0\ 0\ 0 \\ 0 & H_{22}B_{r2}/P_{66} & 0 & 0 & 0\ 0\ 0\ 0 \\ 0 & 0 & H_{33}B_{f1}/P_{77} & 0 & 0\ 0\ 0\ 0 \\ 0 & 0 & 0 & H_{44}B_{f2}/P_{88} & 0\ 0\ 0\ 0 \end{bmatrix}. \tag{5.23}$$

$\dot{V}_2$ becomes:

$$\dot{V}_2 = -\tilde{x}_2^T (C + M H_2 H_1^{-1}) \tilde{x}_2. \tag{5.24}$$

We defined a matrix Q as:

$$Q = C + M H_2 H_1^{-1}. \tag{5.25}$$

The gains of matrix H_2 are chosen in order to satisfy that matrix Q be definite positive . In this case, we have $\dot{V}_2 < 0$ and the observation error is decreasing, which implies that the condition $h_{i1} > |\tilde{x}_{i2}|$ is always verified for $t > t_0$. The surface $\tilde{x}_2 = 0$ is then attractive and thus means that $\hat{x}_2$ converges asymptotically toward x_2.

Equations (5.19) allow deducing that the estimation errors of the derivative of the road profile tend towards 0.

5.3.4 Estimation Results

In order to validate the proposed approach, some simulation experimental results are given.

5.3.4.1 Simulation Results

In this section we give some simulation results obtained using sliding mode observers. These observers make it possible to reconstruct the states of the system, and thus to consider the unknown inputs of the road. It is assumed that the deflection of the chassis and the four wheels and also the rotation of the chassis (roll, pitch and yaw angle) are measured by sensors. That being said, several other signals are assumed to be known, such as the vehicle speed and steering angle.

The main estimate is shown in Fig. 5.1.

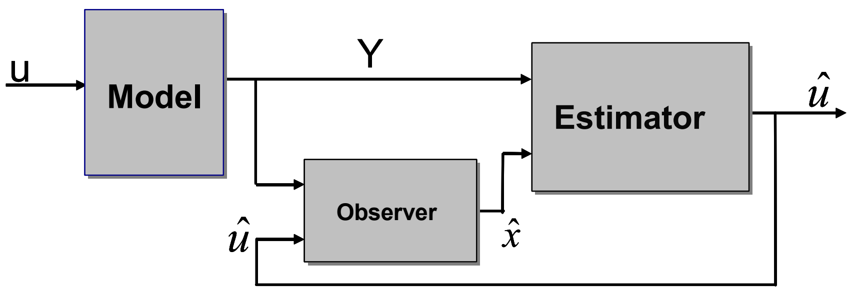

Fig. 5.1 Estimation principle

The input signals used in this simulation are those measured by Selcom sensors during tests done at LCPC with an instrumented *Peugeot* 406 rolling at a constant speed of about $72km/h$.

The estimated vertical displacement of the chassis (z) and the estimated roll angle (θ) and their equivalent measurements are represented in Fig. 5.2.

These figures show the accurate estimation of the displacement and also of the roll angle since the correlation of the figures is clearly shown.

The other figures of the second line represent, respectively, the vertical speed of the chassis and the roll rate. One can notice that the estimates follow closely the speeds given by the model.

However, a small variation exists on the estimated roll rate. The estimation of the road profile is given in Fig. 5.3 and Fig. 5.4 which represent, respectively, the right and the left road profile compared to the LPA measurements.

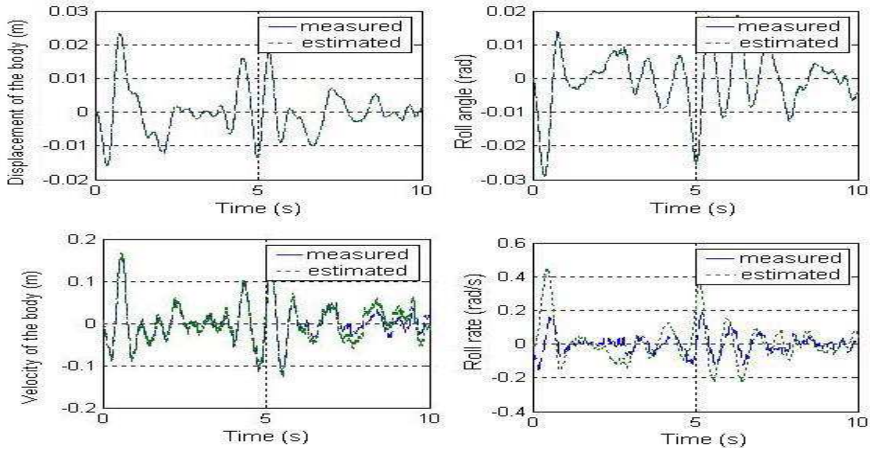

Fig. 5.2 Vehicle states estimation: roll angle and displacement of the chassis

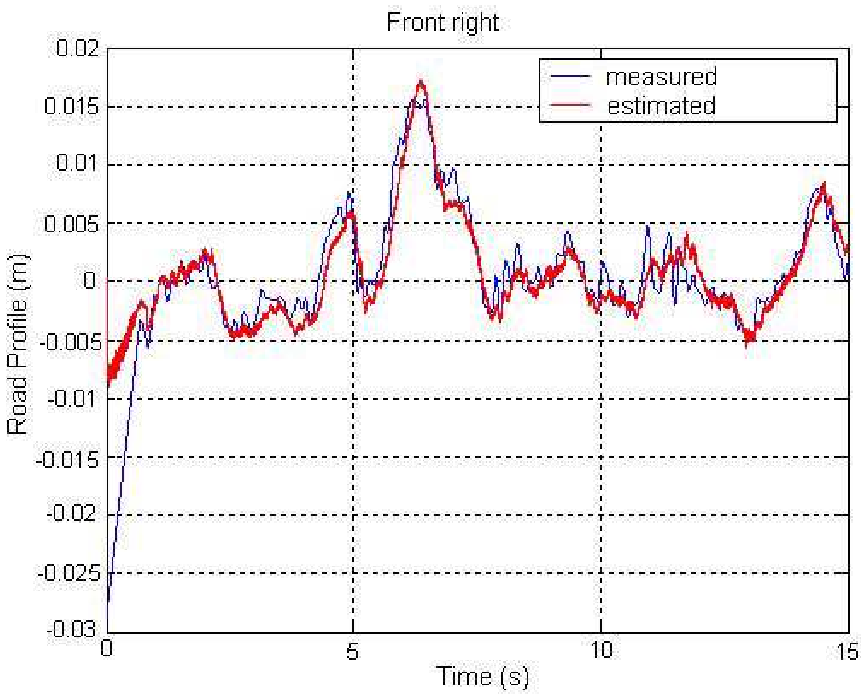

Fig. 5.3 Road profile estimation: front right

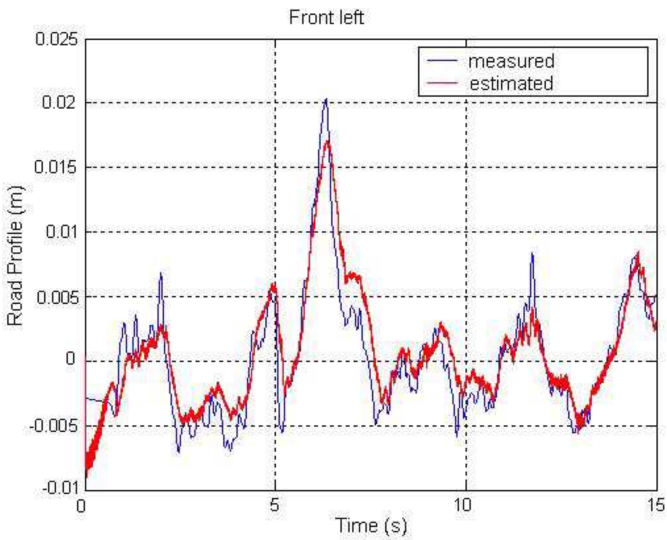

Fig. 5.4 Road profile estimation: front left

One can remark from these figures that the estimated road profile is correct compared to those measured by APL.

5.3.4.2 Experimental Results

In this part, the measured signals coming from sensors are compared to those estimated by the observer.

The estimation principle is shown in Fig. 5.5.

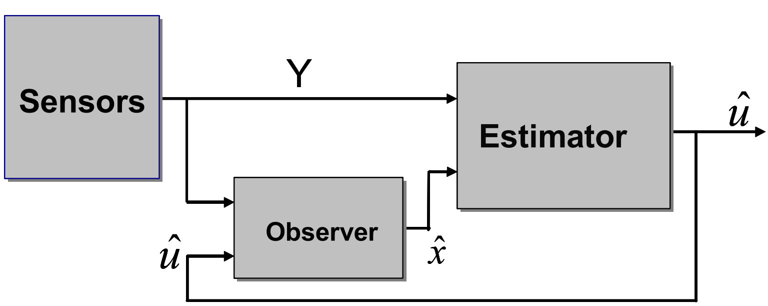

Fig. 5.5 Estimation principle

The following gains are used: $P_1 = diag(100, 100, 100, 100, 100, 100, 100, 100)$, $H_1 = diag(1, 1, 1, 1, 1, 1, 1, 1)$, the elements of matrix H_3 are given by: $H_3(1, 1) = 1000$, $H_3(2, 2) = 1000$, $H_3(3, 3) = 1000$, $H_3(4, 4) = 1000$, $H_3(5, 1) = 5$, $H_3(6, 2) = 5$, $H_3(7, 3) = 5$, $H_3(8, 4) = 5$.

The vertical displacement and the yaw angle are shown in Fig. 5.6.

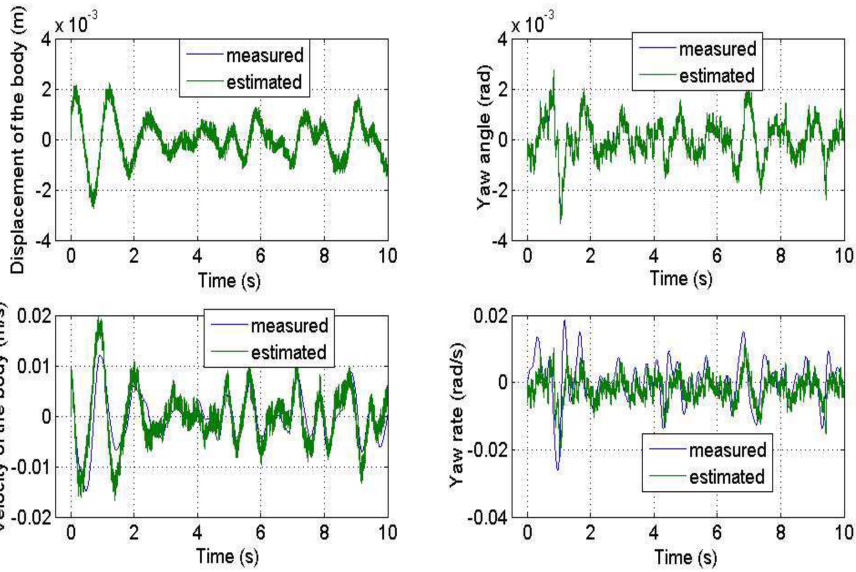

Fig. 5.6 States estimation: experimental case

The convergence is quick and in finite time. In the second line, the equivalent speeds are represented.

A well estimation of the vertical speed can be noticed. However some chattering exist concerning the estimated yaw rate. This is due to sensor errors.

In Fig. 5.7 the estimated road profile is shown.

This figures shows that the unknown input is well estimated compared to LPA measure with some chattering due to the *sign* function used in the observer.

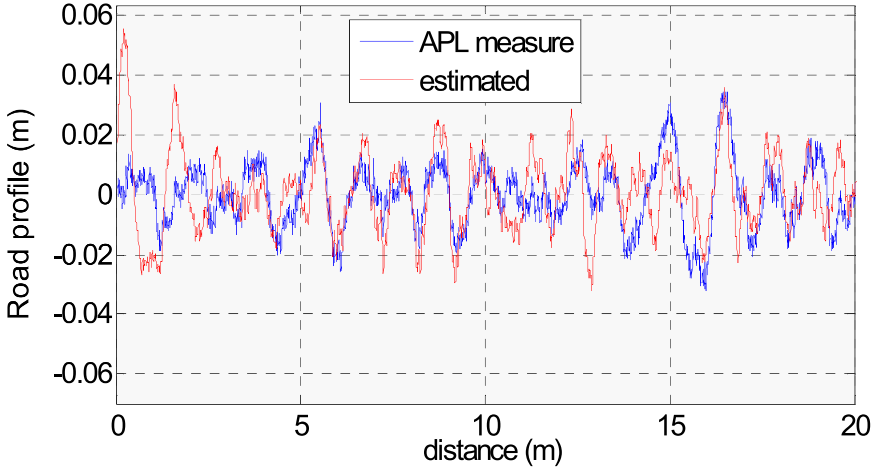

Fig. 5.7 Road profile estimation: experimental case

5.4 Unknown Forces Estimation

The parameters used in our vehicle model are considered constant and measured. However, some parameters depend on the type and the quality of the road and are generally not well known.

Coefficients intervening in the calculation of the adhesion are included in this category. Our idea consists in considering the longitudinal forces of the wheels which are a function of the road adhesion coefficient jointly as unknown states ([HI01], [MT99], [HCB+01], [HCM01], [HCBM02], [IMD03], [IDM03]).

In our case, four measurements of the speeds of the wheels are added to the previously measured vector.

The vector y becomes:

$$y = \begin{bmatrix} z_1 \ z_2 \ z_3 \ z_4 \ z \ \theta \ \phi \ \psi \ w_{r1} \ w_{r2} \ w_{f1} \ w_{f2} \end{bmatrix}^T \tag{5.26}$$

Before developing the observer, let us define the new state vector $x = [x_1, x_2, x_3, x_4]^T$ as follows:

$$\begin{cases} x_1 = \begin{bmatrix} z_1 \ z_2 \ z_3 \ z_4 \ z \ \theta \ \phi \ \psi \end{bmatrix}^T \\ x_2 = \begin{bmatrix} \dot{z}_1 \ \dot{z}_2 \ \dot{z}_3 \ \dot{z}_4 \ \dot{z} \ \dot{\theta} \ \dot{\phi} \ \dot{\psi} \ w_{r1} \ w_{r2} \ w_{f1} \ w_{f2} \end{bmatrix}^T \\ x_3 = U = \begin{bmatrix} u_1 \ u_2 \ u_3 \ u_4 \ \dot{u}_1 \ \dot{u}_2 \ \dot{u}_3 \ \dot{u}_4 \end{bmatrix}^T \\ x_4 = \dot{x}_3 \end{cases} \tag{5.27}$$

where

$$\begin{cases} \dot{x}_1 = \Lambda_1 = [\dot{z}_1 \ \dot{z}_2 \ \dot{z}_3 \ \dot{z}_4 \ \dot{z} \ \dot{\theta} \ \dot{\phi} \ \dot{\psi}]^T = E_1 x_2 \\ \dot{\Lambda}_1 = M^{-1}(-C\Lambda_1 - Kx_1 + Ax_3 + \Omega) \end{cases} \tag{5.28}$$

$E_1 \in \mathbb{R}^{8\times12}$ is a definite positive matrix such that its elements $E_{ij} \in \{0,1\}$.

The rotational movement of the wheels are given by:

$$\dot{\Lambda}_2 = J^{-1}(\Gamma + R\Psi), \tag{5.29}$$

where $\Lambda_2 = \begin{bmatrix} w_{r1} & w_{r2} & w_{f1} & w_{f2} \end{bmatrix}^T = E_2 x_2$ is the vector of wheel speeds, $E_2 \in \mathbb{R}^{4\times12}$ is a positive matrix where its elements E_{ij} are defined in the domain $\{0,1\}$. $\Psi = [F_{xr1}, F_{xr2}, F_{xf1}, F_{xf2}]^T$ represent the longitudinal vector forces. We assume that the derivative of these forces are neglected ($\dot{\Psi} = 0$).

J is a diagonal matrix composed of the inertia of the wheels:

$$J = \begin{bmatrix} J_r & 0 & 0 & 0 \\ 0 & J_r & 0 & 0 \\ 0 & 0 & J_f & 0 \\ 0 & 0 & 0 & J_f \end{bmatrix}, \tag{5.30}$$

where Γ is matrix composed of the engine torquesM_{f1}, M_{f2} :

$$\Gamma = \begin{bmatrix} 0 & 0 & 0 & 0 \\ 0 & 0 & 0 & 0 \\ 0 & 0 & M_{f1} & 0 \\ 0 & 0 & 0 & M_{f2} \end{bmatrix}, \tag{5.31}$$

with $R = r * I$ where r is the wheel radius and $I \in \mathbb{R}^{4\times4}$ is identity matrix:

The variable state $\dot{x}_2$ is then given by:

$$\dot{x}_2 = A_1\dot{\Lambda}_1 + A_2\dot{\Lambda}_2. \tag{5.32}$$

The matrices $A_1 \in \mathbb{R}^{12\times8}$ and $A_2 \in \mathbb{R}^{12\times4}$ are defined in the Appendix.

The proposed observer is:

$$\begin{cases} \dot{\hat{x}}_1 = \hat{\Lambda}_1 + H_1 sign(\tilde{x}_1) \\ \dot{\hat{\Lambda}}_1 = M^{-1}(-C\ \hat{\Lambda}_1 - K\ \hat{x}_1 + A\ \hat{x}_3 + \Omega) + H_2 sign(\tilde{x}_1) \\ \dot{\hat{\Lambda}}_2 = J^{-1}\Gamma + J^{-1}R\ \hat{\Psi} \\ \dot{\hat{x}}_3 = \hat{x}_4 + H_3 sign(\tilde{x}_1) \\ \dot{\hat{\Psi}} = \mu \end{cases} . \tag{5.33}$$

where μ is an adaptation term to be defined. $H_i \in \mathbb{R}^{8\times8}$, $i = 1..3$ are diagonal positive gains matrices and the "$sign$", defined as follows:

$$\left\{ \begin{array}{l} H_1 = diag\{H_{1_1}, H_{1_2}, H_{1_3}, H_{1_4}, H_{1_5}, H_{1_6}, H_{1_7}, H_{1_8}\} \\ H_2 = diag\{H_{2_1}, H_{2_2}, H_{2_3}, H_{2_4}, H_{2_5}, H_{2_6}, H_{2_7}, H_{2_8}\} \\ H_3 = diag\{H_{3_1}, H_{3_2}, H_{3_3}, H_{3_4}, H_{3_5}, H_{3_6}, H_{3_7}, H_{3_8}\} \\ sign(\tilde{x}_1) = diag\{\tilde{x}_{1_1}, \tilde{x}_{1_2}, \tilde{x}_{1_3}, \tilde{x}_{1_4}, \tilde{x}_{1_5}, \tilde{x}_{1_6}, \tilde{x}_{1_7}, \tilde{x}_{1_8}\}^T \end{array} \right| \tag{5.34}$$

The variable $\tilde{x}_i = x_i - \hat{x}_i,\ \ i = 1..4$ represents the estimation error of x_i, $\tilde{\Lambda}_i = \Lambda_i - \hat{\Lambda}_i$ is the estimation error of $\Lambda_i (i = 1..2)$. $\tilde{\Psi} = \Psi - \hat{\Psi}$ is the estimation error of longitudinal forces.

The dynamic observation error is given by:

$$\begin{cases} \dot{\tilde{x}}_1 = \tilde{\Lambda}_1 - H_1 sign(\tilde{x}_1) \\ \dot{\tilde{\Lambda}}_1 = M^{-1}(-C\ \tilde{\Lambda}_1 - K\ \tilde{x}_1 + A\ \tilde{x}_3) - H_2 sign(\tilde{x}_1) \\ \dot{\tilde{\Lambda}}_2 = J^{-1} R\ \tilde{\Psi} \\ \dot{\tilde{x}}_3 = \tilde{x}_4 - H_3 sign(\tilde{x}_1) \\ \dot{\tilde{\Psi}} = -\mu \end{cases} . \tag{5.35}$$

5.4.1 Convergence Study

The convergence study of the observer is done step by step. First the convergence of the position x_1 is done.

Let us define the following Lyapunov function:

$$V_1 = \frac{1}{2} \tilde{x}_1^T \tilde{x}_1 \tag{5.36}$$

Its derivative is given by:

$$\dot{V}_1 = \tilde{x}_1^T \dot{\tilde{x}}_1 \tag{5.37}$$

Using (5.35), we obtain:

$$\dot{V}_1 = \tilde{x}_1^T (\tilde{\Lambda}_1 - H_1 sign(\tilde{x}_1)) \tag{5.38}$$

The gain matrix $H_1 = diag(h_{i1})$ is chosen such that $h_{i1} > \left| \tilde{\Lambda}_{i1} \right|$ for $i = 1...8$. We then have $\dot{V}_1 < 0$, which implies that $\hat{x}_1$ tends toward x_1 in finite time t_0. We the obtain $\dot{\tilde{x}}_1 = 0\ \forall\ t > t_0$.

The function $sign_{eq}$ is then defined as the *sign* function in the sliding surface.

$$sign_{eq}(\tilde{x}_1) = H_1^{-1} \tilde{\Lambda}_1 \tag{5.39}$$

The equation system defined in (5.35) becomes $\forall\ t > t_0$:

$$\begin{cases} \dot{\tilde{x}}_1 = 0 \\ \dot{\tilde{\Lambda}}_1 = M^{-1}(-C\ \tilde{\Lambda}_1 + A\ \tilde{x}_3) - H_2 H_1^{-1} \tilde{\Lambda}_1 \\ \dot{\tilde{\Lambda}}_2 = J^{-1} R\ \tilde{\Psi} \\ \dot{\tilde{x}}_3 = \tilde{x}_4 - H_3 H_1^{-1} \tilde{\Lambda}_1 \\ \dot{\tilde{\Psi}} = -\mu \end{cases} \tag{5.40}$$

In order to prove the convergence of x_2 and then estimate the unknown input vector $\hat{U}$ and the unknown forces vector $\hat{\Psi}$, a second Lyapunov function is considered:

$$V_2=\frac{1}{2}\tilde{\Lambda}_1^T M\tilde{\Lambda}_1+\frac{1}{2}\tilde{\Lambda}_2^T\tilde{\Lambda}_2+\frac{1}{2}\tilde{x}_3^T P_1\tilde{x}_3+\frac{1}{2}\tilde{\Psi}^T P_2\tilde{\Psi} \tag{5.41}$$

where $P_1 \in \mathbb{R}^{8\times 8}$ and $P_2 \in \mathbb{R}^{4\times 4}$ are diagonal positive matrices:

Its derivative gives:

$$\dot{V}_2 = \tilde{\Lambda}_1^T\dot{\tilde{\Lambda}}_1 + \tilde{\Lambda}_2^T\dot{\tilde{\Lambda}}_2 + \tilde{x}_3^T P_1\dot{\tilde{x}}_3 + \tilde{\Psi}^T P_2\dot{\tilde{\Psi}} \tag{5.42}$$

From equation (5.40) and since $\tilde{x}_4$ is bounded, we obtain:

$$\begin{aligned}\dot{V}_2 = &-\tilde{\Lambda}_1^T C\tilde{\Lambda}_1 - \tilde{\Lambda}_1^T MH_2H_1^{-1}\tilde{\Lambda}_1 + \tilde{\Lambda}_1^T A\tilde{x}_3 \\ &-\tilde{x}_3^T P_1 H_3 H_1^{-1}\tilde{\Lambda}_1 + \tilde{\Lambda}_2^T J^{-1}R\,\tilde{\Psi} - \tilde{\Psi}^T P_2\mu\end{aligned} \tag{5.43}$$

Choosing matrix P_1 such that $A^T = P_1H_3H_1^{-1}$, we obtain the gain matrix H_3 as:

$$H_3 = P_1^{-1}A^T H_1 \tag{5.44}$$

The function $\dot{V}_2$ becomes:

$$\dot{V}_2 = -\tilde{\Lambda}_1^T C\tilde{\Lambda}_1 - \tilde{\Lambda}_1^T MH_2H_1^{-1}\tilde{\Lambda}_1 + \tilde{\Lambda}_2^T J^{-1}R\,\tilde{\Psi} - \tilde{\Psi}^T P_2\mu \tag{5.45}$$

The adaptive term μ is then deduced as follows:

$$\begin{aligned}\mu &= P_2^{-1}(J^{-1}R)^T\tilde{\Lambda}_2^T \\ &= P_2^{-1}\Omega^T\tilde{\Lambda}_2^T\end{aligned} \tag{5.46}$$

where $\Omega = J^{-1}R$.

We finally obtain:

$$\dot{V}_2 = -\tilde{\Lambda}_1^T(C + MH_2H_1^{-1})\tilde{\Lambda}_1 \tag{5.47}$$

The gain matrix H_2 is chosen such that the matrix $Q_1 = C + MH_2H_1^{-1}$ is definite positive. Consequently, $\dot{V}_2 < 0$, which implies the asymptotic convergence of $\tilde{x}_2$ towards 0.

From (5.40), the convergence of the errors $\dot{\tilde{x}}_3$toward 0 is then ensured. We also show that the estimation error of the longitudinal forces is bounded.

In the following paragraph, we give some experimental results to show the quality of the proposed observer.

5.4.2 Experimental Results

In this section, we give some results in order to test and validate our approach. The estimated road profile is compared to the profile measured by an longitudinal profile analyzer (LPA) developed at the LCPC Laboratory [LDG96]. It is equipped with a laser sensor and an accelerometer to measure the elevation of the road profile as shown in the Fig. 5.8.

Fig. 5.8 Longitudinal Profile Analyzer (APL in french)

The model parameters are measured. However, the pneumatic parameters C_1, C_2 and C_3 are not well known. To mitigate this disadvantage, we use observers to estimate the longitudinal forces which are related to these parameters. The system outputs are the displacements of the wheels and the chassis, which correspond to the signals given by the sensors. Different measurements are done with the vehicle moving at several speeds.

Fig. 5.9 shows the average vehicle speed of $70km/h$ $(20m/s)$ with an error which does not exceed $1.2m/s$.

This figure shows the measured and the estimated displacements. In the first two subplot on top of figure (5.10), the vertical displacement (z) and the yaw angle (ψ) of the chassis respectively are presented.

It is shown that the estimation of these displacements is fast and of good quality.

The bottom of this figure represent the velocities. We can see that the estimated vertical velocity $(\dot{z})$ is accurate compared to the true signal.

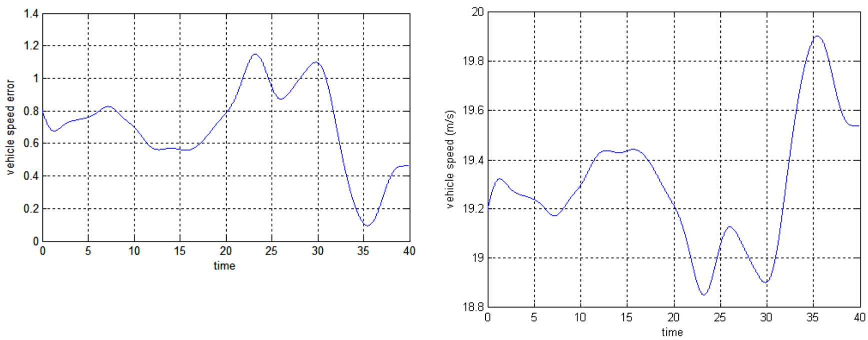

Fig. 5.9 Vehicle speed

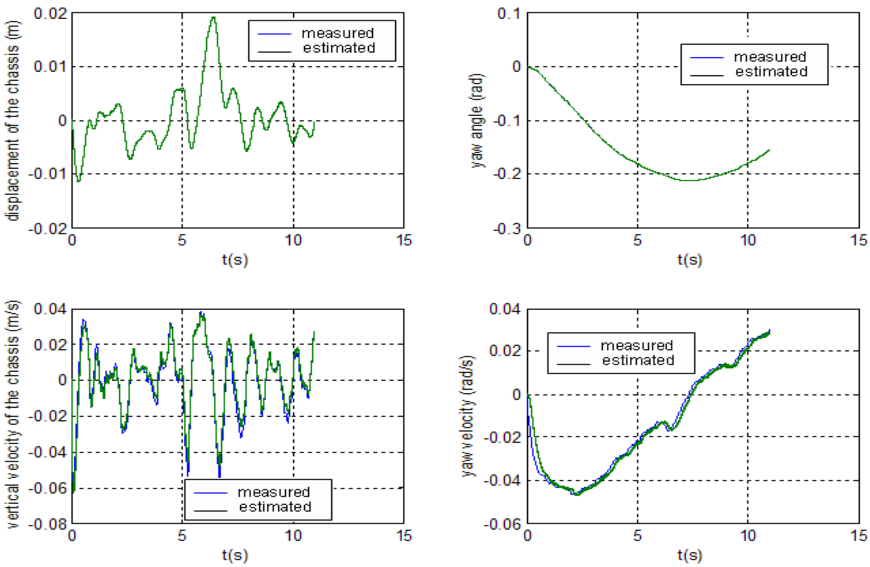

Fig. 5.10 Estimated and measured states: chassis and yaw angle

However, some error occurs concerning the estimation of $\dot{\psi}$. This error is mainly due to sensor calibration (the sensor that we used in our measurement presented an error of calibration that we could not correct).

In Fig. 5.11 we notice that the estimated angular velocity of the wheel converges well towards the actual ones in finite time.

Indeed, we get only 1 *second* for the convergence time.

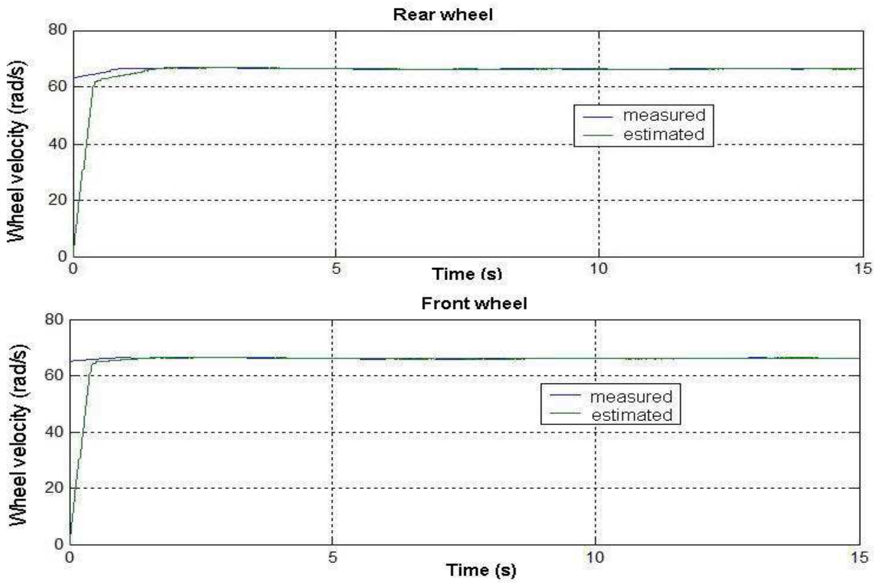

Fig. 5.11 Estimated and measured wheels velocities

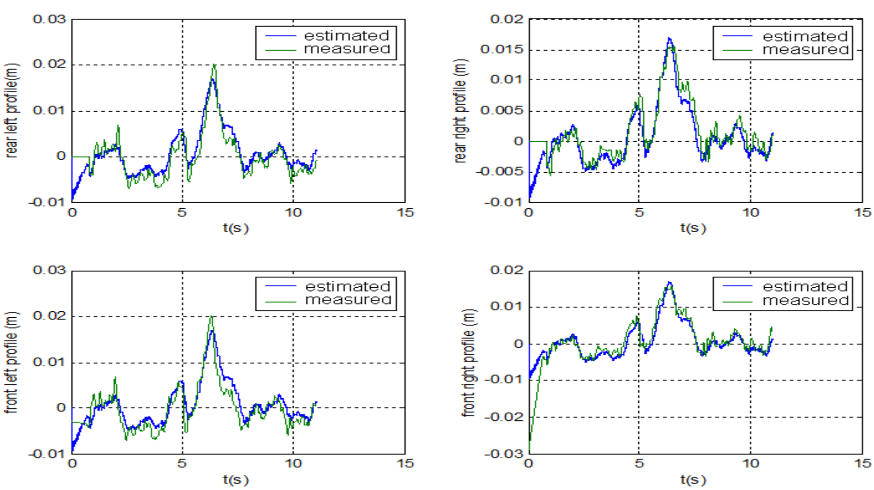

Fig. 5.12 Comparison between the LPA measured profile and estimated one

The convergence of the states is very fast and the estimation is of high quality. The good reconstruction of these states allows estimating the unknown inputs.

In Fig. 5.12 we show the behavior of the road profile estimator.

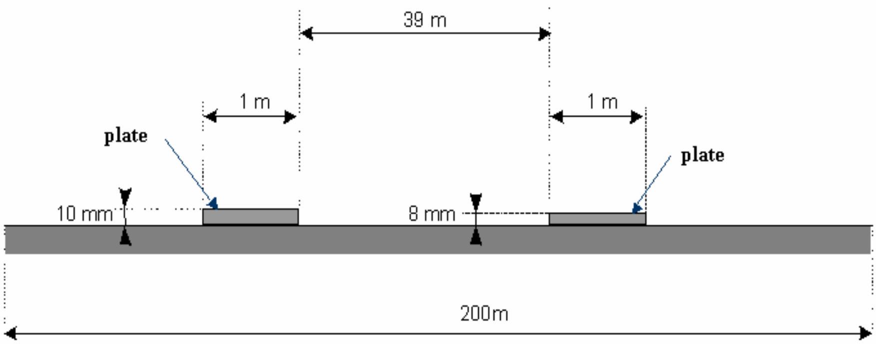

Fig. 5.13 Postions of the plates on the track

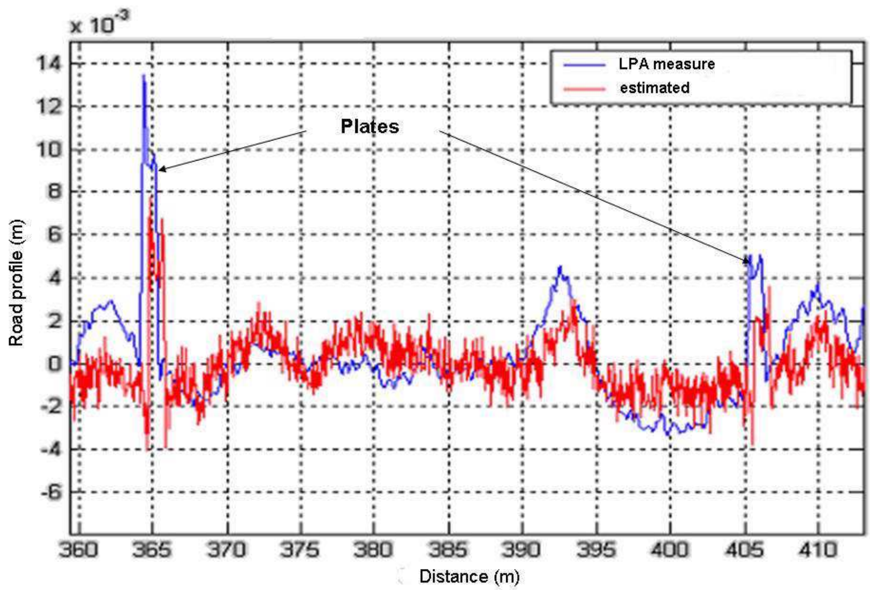

Fig. 5.14 Plates estimation

This figure presents both the measured road profile and the estimated one.

As a further example, two plates are located on the track as shown in Fig.5.13.

Fig. 5.14, shows that these plates of height, respectively, of $10mm$ and $8mm$, are well reconstructed by the observers approach compared to the LPA measurements.

We compare now, the results of each method developed earlier.

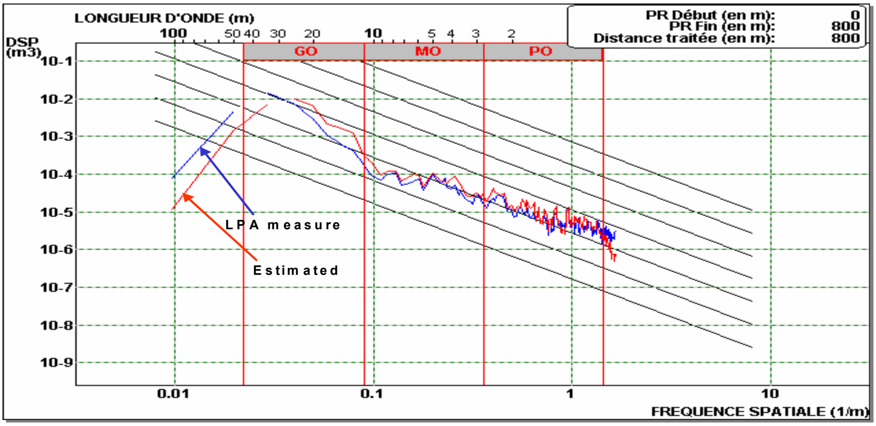

Fig. 5.15 Power Spectral Density (PO: low wave, MO: average wave, GO: high wave

One can then observe that the estimated values are quite close to the true ones. These profiles have the same pace and the differences are not important.

Fig. 5.15 shows the power spectral density of the estimated road profile and the measured one given by LPA instrument.

One notices that the low and average waves of the road (high and average frequency) are well reconstructed. However there are limitations of our method to estimate the high waves of the road.

5.5 Conclusion

In this chapter sliding mode observers have been developed in order to estimate the longitudinal tire/road forces of the system and the unknown inputs which correspond to the road profile.

The parameters of the system are presumedly measured and known. However, the pneumatic coefficients which intervene in the calculation of the longitudinal forces are unknown. This is why we built another observer to directly consider these longitudinal forces. We noticed that the profile estimated by our approach is very close to that measured by the LPA instrument. However, local variations appear. It is then important to know if these variations do not penalize the capability of these profiles (of a band-width broader than APL) to determine the dynamic response of the vehicle (previous studies have shown that in the profile measured by LPA, it is not correct to consider this dynamic response). We consider, in the future work, these profiles as inputs of a dynamic model of the vehicle to estimate the instantaneous loads of the wheels. We thus compare the dynamic responses measured on an instrumented vehicle and those estimated by the simulator of the vehicle.

Chapter 6
Conclusions

In this first work concerning variable structure systems in automotive application, one tried to show the utility of use of such tools in the field of vehicle dynamics. Some applications have been developed. Simulation and experimental results have been shown.

Before to develop some application using sliding mode techniques, a complete definition of vehicle with its different components has been given. A dynamic model with 16 degrees of freedom is developed and validated through simulations and experimental results obtained on an instrumented vehicle.

Then sliding mode observers have been developed in order to:

- observe the dynamics of the vehicle such as the yaw rate, the height of the centre of gravity and the vertical acceleration

- estimate some dynamic parameters of the vehicle such as the side slip angle.

- estimate the unknown inputs

- estimate the impact forces

We have seen that, using sliding mode observers, first or high order, we are able to reconstruct all the state vector of the vehicle and also estimation of its centre height of gravity. This estimation

allows to estimate the unknown inputs. In this work, the estimation of the road profile is shown. This last is compared to the measures coming from Longitudinal Profile Analyzer instrument. This comparison shows that the estimation is of quality with some errors due to the noises coming from the road.

Another application of sliding mode observer is the estimation of contact forces which are, as seen in the previous chapters, very important in the description of the behavior of the vehicle. We have also seen that these forces are very hard and expansive to measure. The developed observer seems then to be an interesting method to estimate theses forces. Indeed, the presented results show an interesting correlation between the estimated forces and those coming from the reference which is, in our case, the vehicle simulator. This

H. Imine et al.: Sliding Mode Based Analysis, LNCIS 414, pp. 103–104.
springerlink.com

confirms that the observers are able to estimate the longitudinal and lateral forces in finite time and with small errors.

This book is the first of long series of books in the field of variable structure system in automotive application. Some other results and tools will be proposed and explained in the next work.

Some of these future works will be the application of sliding mode control in order to control the behavior of the vehicle in longitudinal and lateral axis. Our challenge is also to show the quality of such tools in the field of heavy vehicles.

References

[AFTV10] Amodeo, M., Ferrara, A., Terzaghi, R., Vecchio, C.: Wheel slip control via second-order sliding-mode generation. IEEE Transactions on Intelligent Transportation Systems 11(1), 122–131 (2010)

[BBD96] Barbot, J.P., Boukhobza, T., Djemai, M.: Triangular input observer form and sliding mode observer. In: IEEE Conf. On Decision and Control, pp. 1489–1491 (1996)

[BDB03] Barbot, J.P., Djemai, M., Boukhobza, T.: Implicit triangular observer form dedicated to a sliding mode observer for systems with unknown inputs. Asian Journal of Control, 513–527 (2003)

[BFP07] Bejarano, F.J., Fridman, L., Poznyak, A.S.: Estimation of unknown inputs, with application to fault detection, via partial hierarchical observation. In: European Control Conference 2007, Kos, Greece, pp. 5154–5161 (2007)

[BNP87] Bakker, E., Nyborg, L., Pacejka, H.: Tire modeling for use in vehicle dynamic studies. SAE International, P. 870421 (1987)

[Bou97] Boukhobza, T.: Observateurs à modes glissants et formes d'observabilité et analyse et synthèse des commandes par ordres supérieurs. PhD thesis, Université de Paris Sud Orsay (1997)

[BPPU03] Bartolini, G., Pisano, A., Punta, E., Usai, E.: Survey of applications of second order sliding control to mechanical systems. International Journal of Control 76, 875–892 (2003)

[BSW77] Bernard, J.E., Segel, L., Wild, R.E.: Tire shear force generation during combined steering and braking manouevres. SAE International 8, 2935–2969 (1977)

[BZ88] Bestle, D., Zeitz, M.: Canonical form observer design for nonlinear time varying systems. International Journal of Control 47, 1823–1836 (1988)

[Can98] De Canudas Wit, C.: Dynamic tire friction models for vehicle traction control. In: American Control Conference, Philadelphia (June 1998)

[CB98] Clover, C.L., Bernard, J.E.: Longitudinal tire dynamics. Vehicle System Dynamics 29, 231–259 (1998)

[CBW90] Captain, K.M., Boghani, A.B., Wormley, D.N.: Analytical tire models for dynamic vehicle simulation. Vehicle System Dynamic 8, 1–32 (1990)

[CH99] De Canudas Wit, C., Horowitz, R.: Observer for tire road contact friction using only wheel angular velocity information. In: 38th IEEE Conference on Decision and Control, CDC (1999)

[DB02] Djemaï, M., Barbot, J.P.: Smooth manifolds and high order sliding mode control. In: IEEE-CDC Conf., Proceedings of the 41st IEEE Conference on Decision and Control, vol. 1, pp. 335–339 (2002)

[DBB99] Djemaï, M., Barbot, J.P., Boukhobza, T.: Some comments on higher order sliding modes utilities. In: Proc ECC (1999)

[DFL05a] Davila, J., Fridman, L., Levant, A.: Second-order sliding-mode observer for mechanical systems. IEEE Trans. Automat. Contr. 50(11), 1785–1789 (2005)

[DFL05b] Davila, J., Fridman, L., Levant, A.: Survey of applications of second order sliding control to mechanical systems. IEEE Transactions on Automatic Control 50, 1785–1789 (2005)

[DFP06] Davila, J., Fridman, L., Poznyak, A.: Observation and identification of mechanical systems via second order sliding modes. International Journal of Control 79(10), 1251–1262 (2006)

[Dix96] Dixon, J.C.: Tires, Suspension and Handling, 2nd edn. SAE, Warrendale (1996)

[Dra92] Drakunov, S.V.: Sliding-mode observers based on equivalent control method. In: Proc. 31st IEEE Conf. Decision and Control, Tucson, Arizona, pp. 2368–2369 (1992)

[DS70] Dugoff, P.F.H., Segel, L.: An analysis of tire traction properties and their influence on vehicle dynamic performance. SAE International 3, 1219–1243 (1970)

[dwTV+03] De Canudas Wit, C., Tsiotras, P., Velenis, E., Basset, M., Gissinger, G.: Dynamic friction models for road/tire longitudinal interaction. Vehicle Syst. Dynamics 39, 189–226 (2003)

[EFT07] Edwards, C., Fridman, L., Thein, M.-W.L.: Fault reconstruction in a leader/follower spacecraft system using higher order sliding mode observers. In: IEEE American Control Conference 2007, NewYork, USA, pp. 408–413 (2007)

[EKL93] Emelyanov, S.V., Korovin, S.K., Levant, A.: Higher-order sliding modes in control systems. differential equations. Differential Equations 11, 1627–1647 (1993)

[Eme67] Emelyanov, S.V.: Variable structure control systems. CRC Press, Boca Raton (1967)

[ESH02] Edwards, C., Spurgeon, S.K., Hebden, R.G.: On development and applications of sliding mode observers, variable structure systems. In: Towards xxist century. LNCIS, pp. 1785–1789 (2002)

[FB06] Floquet, T., Barbot, J.: A canonical form for the design of unknown input sliding mode observers. In: Edwards, C., Fossas, E., Fridman, L. (eds.) Advances in Variable Structure and Sliding Mode Control. LNCIS, pp. 271–292. Springer, Berlin (2006)

[FBPD04] Floquet, T., Barbot, J.P., Perruquetti, W., Djemaï, M.: On the robust fault detection via sliding mode perturbation observer. International Journal of Control 77(7), 622–629 (2004)

[Fil60] Fillipov, A.F.: Application of the theory of diiferential equations with discontinuous right hand side to non linear problems in automatic control. American Mathematic Society Transactions 62, 199–231 (1960)

[Fil88] Filippov, A.F.: Differential Equations with Discontinuos Right-hand Sides. Kluwer Academic Publishers, Dordrecht (1988)

[FLD07] Fridman, L., Levant, A., Davila, J.: High-order sliding-mode observation and fault detection via weakly unobservable subspace reconstruction. In: European Control Conference 2007, Kos, Greece, pp. 5139–5146 (2007)

[FLD08] Fridman, L., Levant, A., Davila, J.: Observation and identification via high-order sliding modes. In: Bartolini, G., Fridman, L., Pisano, A., Usai, E. (eds.) Modern Sliding Mode Control Theory: New Perspectives and Applications. LNCIS, vol. 375, pp. 293–319. Springer, London (2008)

[Fri99] Fridman, L.: The problem of chattering: an averaging approach. In: Young, K.D., Ozguner, U. (eds.) Variable Structure, Sliding Mode and Nonlinear Control. LNCIS, vol. 247, pp. 363–386. Springer, London (1999)

[GFP02] Gissenger, G., Le Fort-Pait, N.: Contrôle-commande de la voiture. Hermès Science Publications (2002)

[Gil92] Gillespie, T.D.: Fundamentals of vehicle dynamics. In: 400 Commonwealth Drive, pp. 427–446. SAE, Society of Automotive Engineers, Inc. (1992)

[GMR01] Gaddouna, B., Maquin, D., Ragot, J.: Fault detection observers for systemes with unknown inputs. In: Safeprocess (2001)

[GN90] Gim, G., Nikravesh, P.: Analytical model of pneumatic tyres for vehicle dynamic simulations part 1: pure slips. International Journal of Vehicle Design 11, 589–618 (1990)

[GSH87] Gillespie, T.D., Sayers, M.W., Hagan, M.R.: Methodology for road roughness profiling and rut depth measurement. Federal Highway Administration, The University of Michigan Transportation Research Institute 87-042 (1987)

[Har83] Harrison, R.F.: The Non-Stationary Response of Vehicles on Rough Ground. PhD thesis, Institute of Sound and Vibration Research Faculty of Engineering an Applied Science, University of Southampton (1983)

[HCB+01] El Hadri, A., Cadiou, J.C., Beurier, G., M'Sirdi, N.K., Delanne, Y.: Whell slip regulation based on sliding mode approach. In: SAE, Detroit, Michigan, pp. 2001–01–0602 (March 2001)

[HCBM01] El Hadri, A., Cadiou, J.C., Beurier, G., M'Sirdi, N.K.: Vehicle/road interaction and tire lateral performance identification. In: ROMAN (2001)

[HCBM02] El Hadri, A., Cadiou, J.C., Beurier, G., M'Sirdi, N.K.: Adaptive sliding mode control for vehicle traction. In: IFAC World Congress, Barcelone, Espagne (2002)

[HCM01] El Hadri, A., Cadiou, J.C., M'Sirdi, N.K.: Tire forces estimation based non linear observer. In: 3rd IFAC Workshop, Advanced Automative Control, Karlsrhue, Germany (2001)

[HI01] Husain, I., Islam, M.S.: Observers for positions and speed estimations in switched reluctance motors. In: Proceedings of the 40th Conference on Decision and Control, Florida, Orlando, pp. 2217–2222 (Decenber 2001)

[ID07] Imine, H., Dolcemascolo, V.: Rollover risk prediction of heavy vehicle in interaction with infrastructure. IJHVS, International Journal of Heavy Vehicle Systems 14(3), 294–307 (2007)

[IDM03] Imine, H., Delanne, Y., M'sirdi, N.K.: Adaptive observers and estimation of the road profile. SAE Transactions Journal of Passenger Cars - Mechanical Systems 112(6), 1312–1317 (2003)

[IF08] Imine, H., Fridman, L.: Road profile estimation in heavy vehicle dynamics simulation. IJVD, International Journal of Vehicle Design 47(1, 2, 3, 4), 234–249 (2008)

[ILMD01] Imine, H., Laval, L., M'sirdi, N.K., Delanne, Y.: Observers with unknown inputs for estimation of the road profiles. In: ICAR 2001, IEEE International Conference On Advanced Robotics, Budapest, Hongrie, pp. 22–25 (Aout 22-25, 2001)

[ILMD02a] Imine, H., Laval, L., M'Sirdi, N.K., Delanne, Y.: Sliding mode observers with unknown inputs to estimate the road profile. In: International Conference on Control and Applications, IASTED 2002, Cancun, Mexico, (May 20-22, 2002)

[ILMD02b] Imine, H., Laval, L., M'Sirdi, N.K., Delanne, Y.: Observateurs à entrées inconnues par mode glissant appliqués à l'estimation du profil de route. In: Conférence Internationale Francophone d'Automatique, CIFA, Nantes, France, pp. 883–888 (Juillet 2002)

[IMD03] Imine, H., M'Sirdi, N.K., Delanne, Y.: Adaptive observers and estimation of the road profile. In: SAE World Congress, Detroit, Michigan, USA, pp. 175–180, (March 2003)

[Imi03] Imine, H.: Observation d'état d'un véhicule pour l'estimation des traces de roulement. PhD thesis, Doctorat de Université de Versailles Saint Quentin en Yvelines (2003)

[ISM08] Imine, H., Srairi, S., Madani, T.: Experimental validation of rollover risk prediction of heavy vehicles. In: TRA 2008 Transport Research Arena, Ljubljana, Slovenia, (April 21-25, 2008)

[Kar84] Karunasena, W.G.: Determination of Road Roughness from Inertial Profilometer Data. PhD thesis, The Pennsylvania State University (1984)

[Kha92] Khalil, H.K.: Nonlinear Systems. Mac Milan Ed. (1992)

[KID10a] Khemoudj, O., Imine, H., Djemaï, M.: Estimation of the tyre-forces and control theory approach applied for monitoring heavy vehicle. In: HVTT 2011, International Heavy Vehicle Symposium, Melbourne, Australia, March 15-17, pp. 278–289 (2010)

[KID10b] Khemoudj, O., Imine, H., Djemaï, M.: Variable gain sliding mode observer for heavy duty vehicle tyre forces estimation. In: 11th International Workshop on Variable Structure Systems, VSS 2010, Mexico city, Mexico (June 26-28, 2010)

[KID10c] Khemoudj, O., Imine, H., Djemaï, M.: Robust observation of tractor-trailer vertical forces using inverse model and exact differentiator. SAE, International Journal of Materials and Manufacturing 3(1), 278–289 (2010)

[KN05] Kiencke, U., Nielsen, L.: Automotive Control Systems: For Engine, Driveline and Vehicle. Springer, Heidelberg (2005)

[Kol62] Kolmogoroff, A.N.: On inequalities between upper bounds of consecutive derivatives of an arbitrary function defined on an infinite interval. Amer. Math. Soc. Transl. 2, 233–242 (1962)

[KR95] Krishnaswami, V., Rizzoni, G.: Vehicle steering system state estimation using sliding mode observers. In: Proceedings of the 34th Conference on Decision and Control, New Orleans, LA, pp. 3391–3396 (December 1995)

[LDG96] Legeay, V., Daburon, P., Gourraud, C.: Comparaison de mesures de l'uni par l'analyseur de profil en long et par compensation dynamique. Bulletin interne, Laboratoire Central des Ponts et Chaussées, DGER/IRVAR (Décembre 1996)

[Lev85] Levantovsky, L.V.: Second order sliding algorithms: Their realization in dynamic of heterogeneous systems. In: Institute for System Studies, Moscow, pp. 32–34 (1985)

[Lev93] Levant, A.: Sliding order and sliding accuracy in sliding mode control. International Journal Control 58(6), 1247–1263 (1993)

[Lev98] Levant, A.: Robust exact differentiation via sliding mode technique. Automatica 34(3), 379–384 (1998)

[Lev03] Levant, A.: High-order sliding modes: differentiation and output-feedback control. International Journal of Control 76(9-10), 924–941 (2003)

[Lue64] Luenberger, D.G.: Observing the state of a linear system. IEEE Trans. Mil. Electron. (8), 74–80 (1964)

[Mam02] Mammar, S.: Contrôle latérale assisté et automatisé des véhicules: Approche par commandes robustes. Habilitaion à diriger la recherche, HDR de l'Université d'Evry-Val d'Essonne (Septembre 2002)

[MDSP10] Marouf, A., Djemaï, M., Sentouh, C., Pudlo, P.: Driver torque and road reaction force estimation of an electric power assisted steering using sliding mode observer with unknown inputs. In: IEEE Conference on Intelligent Transportation Systems (ITSC 2010), adeira Island, Portugal (September 19-22, 2010)

[Men97] Mendoza, R.: Sur la modélisation et la commande des véhicules automobiles. PhD thesis, Institue National Polytechnique de Grenoble, Laboratoire d'Automatique de Grenoble (Juillet 1997)

[Mis90] Misun, V.: Simulation of the interaction between vehicle wheel and the unevenness of the road surface. Vehicle System Dynamics 19, 237–253 (1990)

[MNMSm00] Mammar, S., Nouvelière, L., M'sirdi, N.K., Saint-marie, J.: Contrôle intgré d'un véhicule en automatisation basse vitesse. In: Conférence Internationale Francophone d'Automatique, Villeneuve d'Ascq (2000)

[MT99] Marino, R., Tomei, P.: Robust adaptive observers for nonlinear systems with bounded disturbances. In: 38th IEEE Conference on Decision and Control, CDC 1999, Phoenix, Arizona (1999)

[MW86] Meau, F.P., Wambold, J.C.: Evaluation of computation methods for accelerometer-established inertial profiling reference systems. Technical Report 1348, Transportation Research Record (1986)

[MYWL02] Ma, L., Yang, Y., Wang, F., Lu, N.: A sliding mode observer approach for fault detection and diagnosis in uncertain nonlinear systems. In: Proceedings of the 4th World Congress on Intelligent Control and Automation, Shanghai, ChinaL (June 2002)

[NMS+10] Nehaoua, L., Marouf, A., Santin, J.J., Pudlo, P., Djemai, M.: Towards an electrical power-assisted steering simulator: Modelisation specifications. In: 5th IFAC Symposium on Mechatronic Systems, Cambridge Massachusetts, USA, pp. 957–962 (September 13-15, 2010)

[Pac89] Pacejka, H.: Modeling of the pneumatic tyre and its impact on vehicle dynamic behavior. Technical report, Vehicle Research Laboratory, Delft University of Technologie, Netherlands (1989)

[Pet03] Petersen, I.: Wheel slip control in abs brakes using gain scheduled optimal control with constraints. PhD thesis, Department of Engineering Cybernetics, Norwegian University of Science and Technology Trondheim (2003)

[Poz03] Poznyak, A.S.: Stochastic output noise effects in sliding mode estimations. International Journal of Control 76, 986–999 (2003)

[PSF+06] Poznyak, A., Shtessel, Y., Fridman, L., Davila, J., Escobar, J.: Identification of dynamic systems parameters via sliding-mode technique. In: Edwards, C., Fossas, E., Fridman, L. (eds.) Advances in Variable Structure and Sliding Mode Control. LNCIS, vol. 334, pp. 313–347. Springer, London (2006)

[Poz08] Poznyak, A.: Advanced Mathematical Tools for Control Engineers: Deterministic Techniques, vol. 1. Elsevier, Amsterdam (2008)

[Ram02] Sira Ramirez, H.: Dynamic second order sliding mode control of the hovercraft vessel. IEEE Trans. on Control System Technology 10, 860–865 (2002)

[RMFD06] Rabhi, A., M'Sirdi, N., Fridman, L., Delanne, Y.: Second order sliding mode observer for estimation of road profile. In: IEEE Workshop on Variable Structure Systems, Alghero, Italy, pp. 161–165 (2006)

[SAF+06] Shraim, H., Ananou, B., Fridman, L., Noura, H., Ouladsine, M.: Sliding mode observers for the estimation of vehicle parameters. In: Proc. 45th IEEE Conf. Decision Control, San Diego, CA, USA, pp. 1635–1640 (2006)

[SCD05] Stéphant, J., Charara, A., Dominique, M.: Evaluation of sliding mode observer for vehicle side slip angle. In: 16th IFAC World Congress (2005)

[SFAO07] Shraim, H., Fridman, L., Ananou, B., Ouladsin, M.: A new diagnosis strategy based on the online estimation of the tire pressure. In: European Control Conference, Kos, Greece, pp. 3437–3443 (2007)

[SH97] Stotsky, A., Hu, X.: Control of car-like robots using sliding observers for steering angle estimation. In: Proceedings of the 36th Conference on Decision and Control, San Diego, California USA (December 1997)

[SHM86] Slotine, J.J.E., Hedrick, J.K., Misawa, E.A.: Nonlinear state estimation using sliding observers. In: 25th IEEE Conference on Decision and Controle, Greece, pp. 332–339 (1986)

[Sie97] Sienel, W.: Estimation of the tire cornering stiffness and its application to active car steering. In: 36th IEEE Conf. Decision and Control, San Diego, California, vol. 5, pp. 4744–4749 (1997)

[SK64] Spangler, E.B., Kelly, W.J.: Gmr road profilometer method for measuring road profile. Technical Report GMR-452, General Motors Research Publication (1964)

[SLD+06] Saadaoui, H., De Leon, J., Djemai, M., Manamanni, N., Barbot, J.P.: High order sliding mode and adaptive observers for a class of switched systems with unknown parameter: A comparative study. In: Proc. 45th IEEE Conf. Decision Control, San Diego, USA (2006)

[SNA05] Shraim, H., Ouladsine, M., Noura, H., Ananou, B.: Modeling and validation of ground contact forces and their influence on the movement of the center of gravity. In: Integrated Modeling and Analysis in Applied Control and Automation, Marseille (2005)

[SOA05a] Shraim, H., Ouladsine, M., El Adel, M.: Longitudinal slip control using laguerre approach. In: IEEE International Conference on Mechatronics and Automation, pp. 184–186 (2005)

[SOA05b] Shraim, H., Ouladsine, M., El Adel, M.: A new nonlinear control strategy for a vehicle trajectory tracking in the presence of faults. In: 44th IEEE Conference on Decision and Control CDC and European Control Conference ECC (2005)

[SOF07] Shraim, H., Ouladsine, M., Fridman, L.: Sliding mode observers to replace vehicles expensivesensors and to preview driving critical situations. Int. J. Vehicle Autonomous Systems 5(3/4), 345–361 (2007)

[SS89] Soderstrom, T., Stoica, P.: System Identification. Prentice-Hall International, Cambridge (1989)

[UK99] Unsal, C., Kachroo, P.: Sliding mode measurement feedback control for antilock braking systems. IEEE Transactions on Control Systems Technology 7, 271–281 (1999)

[Utk77] Utkin, V.I.: Variable structure systems with sliding mode. IEEE Transactions on Automatic Control 26, 212–222 (1977)

[Utk92] Utkin, V.I.: Sliding Modes in Control and Optimization. Springer, Berlin (1992)

[VHK05] Von Vietinghoff, A., Hiemer, M., Kiencke, U.: Non linear observer design for lateral vehicle dynamics. In: 16th IFAC World Congress, pp. 687–692 (2005)

[VP91] Van Der Jagt, P., Parsons, A.: Road surface correction of tire test data. In: 1st International Colloqium on Tyre Models for Vehicles Dynamics Analysis, Delft, The Netherlands (October 21-22, 1991)

[XG88] Xia, X.H., Gao, W.B.: Nonlineare observer design by observer canonical forms. International Journal of Control 47(4), 1081–1100 (1988)

[YS95] Yang, H., Saif, M.: Fault detection in a class of nonlinear systems via adaptive sliding observer design. In: IEEE Conference on Systems, Man and Cybernetics, Vancouver, BC, pp. 2199–2204 (1995)

[Zei87] Zeitz, M.: The extended luenberger observer for nonlinear systems. Systems and Control Letters (1987)

[ZEP95] Van Zanten, A., Erhardt, R., Pfaff, G.: The vehicle dynamics control system of bosch. In: SAE International, P. 950759 (1995)

[ZWR90] Van Zanten, A., Lutz, A., Ruf, W.D.: The measurement and simulation of transient in longitudinal and lateral tire forces. SAE International, P. 900210 (1990)

Appendix A
Recalls on Sliding Modes Techniques

In this appendix we will recall some sliding modes principle, precisely the finite time convergence and the notion of equivalent vector.

Let us consider the following system input:

$$\dot{x} = F(x, t, u) \tag{A.1}$$

where $x \in \Re^n$ is the state, and $u \in \Re$ is the control vector.
For this system, we define the discontinuous control given by:

$$u_i(x,t) = \begin{cases} u^+(x,t) \text{ si } s(x) > 0 \\ u^-(x,t) \text{ si } s(x) < 0 \end{cases}$$

where $s(x) \in \Re$ is a function.
the closed loop system is then noted

$$\dot{x} = f(x, t) \tag{A.2}$$

If there exists a positive constant k such that the Lyapunov function defined by

$$v = \frac{s^2}{2}$$

verifies

$$\dot{v} \leq -k|s| = -k\sqrt{(v)}$$

then the sliding mode occurs (i.e $s(x) = 0$) after a finite time inteval. We will establish this using a comparison method.
In fact , the existence of such a constant k implies that there exists another constant μ such that

$$\begin{array}{l} v(t) \leq \rho(t),\ \dot{\rho} = \mu\sqrt{(\rho)},\ \rho(0) = v(0) \\ 0 < v(t) = \rho(t) = (v(0) - \mu t/2)^2, \\ v(t) = 0(s(t) = 0) \text{ for } t > t_1 = 2v(0)/\mu(\text{ because} v \geq 0) \end{array}$$

Another demonstration in [Kha92] (chapter 7) establishes that $t_1 leq|s(t=0)|/k$ by integrating

$$\frac{1}{2}\frac{d}{dt}s^2 \leq -k|s|$$

Now, we interest to the dynamics of the system on the sliding surface. The system's motion on the sliding surface can give an interesting geometric problem interpretation as an average of the system's dynamics on both sides of the surface. Thus, by solving formally the equation $\dot{s}=0$ for the control input, we obtain an expression for u called the equivalent control denoted by u_{eq}, which can be interpreted as the continuous control law that would maintain $\dot{s}=0$.

This result is a consequent of the Fillipov theorem [Fil60]. The trajectories of the system (A.2) on the sliding surfaces are not defined as the control vector is also not defined on $s=0$. Filippov [Fil60] defined a solution of (A.2) in terms of differential inclusions:

Definition A.1. (Solution of (A.2) in the sens of Filippov) The stae vector $x(t)$ défined on $[t_1, t_2]$ is a solution of (A.2) in the Filippov's sens, if $x(t)$ is absolutely continuous, and if for almost all $t \in [t_1, t_2]$,

$$\dot{x}(t) \in \bigcap_{\delta>0}\bigcap_{\mu N=0} \overline{conv}\, f(B(x,\delta)-N,t) \tag{A.3}$$

where $\overline{conv}$ designes the close convex envelope, $B(x,\delta)$ is the ball centered in x and of ray δ, μ is the Lebegue's measure. The notation,

$$\bigcap_{\mu N=0}$$

indicates the intersection of all the null measure sets.

So in the Filippov sense, the differential equation (A.2) is substituted by the differential inclusion (A.3).

• The dynamics of the system on the sliding surface

For sake of simplicity, we take the following notation:

$$S = \{x \in \Re^n \ : \ s(x) = 0\}$$

The surface S separates the state space into two parts S^+ ($s(x)>0$) and S^- ($s(x)<0$). We suppose that the functions $f^+(x,t)$ and $f^-(x,t)$ defined by

$$\lim_{s\to 0^+} f(x,t) = f^+(x,t)$$
$$\lim_{s\to 0^-} f(x,t) = f^-(x,t)$$

exist for all given t.

Let $f_0^+(x,t) =< \nabla s, f^+(x,t) >$ (resp. $f_0^-(x,t) =< \nabla s, f^-(x,t) >$) the projection of f^+ (resp. f^-) in the normal direction of the sliding surface S oriented to S^- (resp. S^+).
with these notations, we announce the Fillipov theorem

Theorem A.2. *Let $x(t)$ absolutely continuous such that $x(t) \in S$, verify $f_0^-(x,t) \geq 0$, $f_0^+(x,t) \leq 0$ and $f_0^-(x,t) - f_0^+(x,t) > 0$, then $x(t)$ is a solution solution of (A.2) (in the sens of the definition A.1), if and only if*

$$\dot{x}(t) = \alpha(t)f^+(x,t) + (1-\alpha(t))f^-(x,t) \quad \textit{whith} \tag{A.4}$$

$$\alpha(t) = \frac{f_0^-(x,t)}{f_0^-(x,t) - f_0^+(x,t)} \tag{A.5}$$

The right hand of the equation (A.4) is orthogonal to ∇s. In fact, we verify that $< \nabla s, \alpha f^+ + (\alpha - 1)f^- >= 0$.

Consequently the solution $x(t)$ remains on the surface S. The values of $f(x,t)$ in the neighborhood of S generate solutions which are constraint to slide on the surface S (see figures A.1 and A.2).

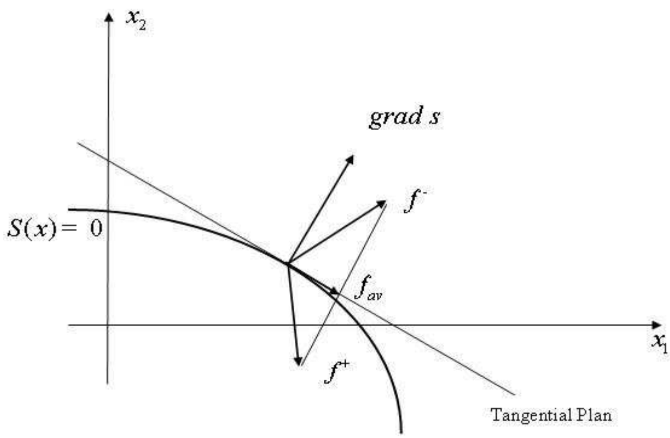

Fig. A.1 Filipppov definition of the sliding mode equations

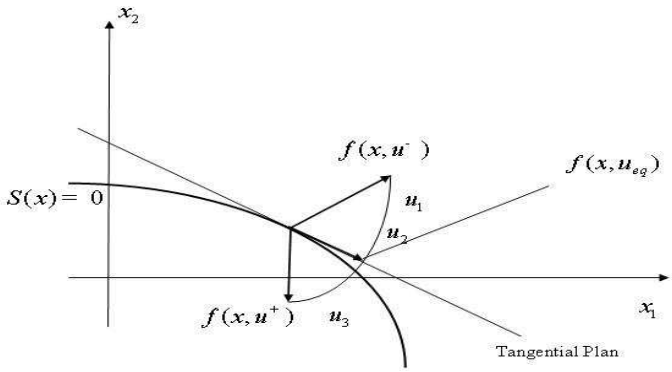

Fig. A.2 Equivalent control method definition of the sliding mode equations

Appendix B
Equivalent Control Concept

B.1 Motivation

When using SM control, one of the most interesting practical problems appearing is that of finding the trajectory of the state variables, so called, the sliding equations [Utk92].

A formal approach is that of solution of differential inclusions in the Filippov sense [Fil60]. However, a simpler way to study the effect of a discontinuous control acting on the system is the *equivalent control method (ECM)* which, in fact, for affine systems, it turns out to give the same results as studying differential inclusion in the Filippov sense. In this chapter a short description of the ECM is introduced.

B.2 Equivalent Control Method

Let us consider the system described by the following differential equation:

$$\dot{x}(t) = f(x,t) + B(x,t)\,u(t)\,,\ t \geq t_0 \tag{B.1}$$

where $x \in \mathbb{R}^n$ and $u \in \mathbb{R}^m$, and they represent the state vector and the control vector, respectively. Moreover, $f(x,t)$ and $B(x,t)$ are continuous vector and matrix functions, respectively, with respect to all the arguments. Here, u is to be designed as a discontinuous control to compel the trajectories of (B.1) to enter into the sliding manifold $S = \{x : s(x) = 0\}$ and to be maintained there for all the time forward. The function $s(x) \in \mathbb{R}^m$ is to be designed according to some specific requirements, we will called it sliding variable. Once the trajectories of (B.1) are into the manifold S, i.e. $s(x) = 0$, we say that (B.1) is on a sliding mode (SM). An u achieving the SM will be called sliding mode control.

Let us assume that $s(x) \equiv 0$, then its derivative would be also identical to zero. Thus, we have that

$$\dot{s}(x) = \frac{\partial s}{\partial x}\left[f(x,t) + B(x,t)\, u\right] = 0 \tag{B.2}$$

Assuming that $G(x) := \frac{\partial s}{\partial x}$ fulfills with the condition $\det G(x)\, B(x) \neq 0$. The function u taken from (B.2) is the so-called equivalent control, thus we have that,

$$u_{\mathrm{eq}} = -\left[G(x)\, B(x,t)\right]^{-1}\left[G(x)\, f(x,t)\right] \tag{B.3}$$

What the EC method asserts is that the dynamics of (B.1) can be calculated by the substitution of u_{eq} in the place of u, i.e., on the sliding mode the system is governed by the following equations,

$$\dot{x}(t) = f(x,t) - B(x,t)\left[G(x)\, B(x,t)\right]^{-1}\left[G(x)\, f(x,t)\right] \tag{B.4}$$

Let us consider the following simple scalar example:

$$\dot{x}(t) = ax + bu + \gamma(t) \tag{B.5}$$

where a and $b \neq 0$ are real scalars and $\gamma(t)$ is a disturbance. Let say that we wish to constrain $x(t)$ to the origin in a finite time and in spite of the lack of knowledge of $\gamma(t)$. This can be achieved by selecting $u = -b^{-1}M(t)\,\mathrm{sign}\, x$ and $M(t) > |ax| + |\gamma(t)| + \epsilon$, for some arbitrarily small ϵ. By deriving $V = \frac{1}{2}|x|^2$ we get that

$$\begin{aligned}\dot{V} &= |x|\left(ax + bu + \gamma(t)\right) \leq -|x|\left(M(t) - |ax| - |\gamma(t)|\right)\\ &\leq -|x|\,\epsilon = -\sqrt{2}\epsilon\sqrt{V}\end{aligned}$$

By using the comparison principle, we obtain that

$$V(t) \leq \left(V(t_0) - \frac{\epsilon}{\sqrt{2}}(t - t_0)\right)^2 \text{ for all } t \geq t_0 \tag{B.6}$$

Since $V(t)$ is by definition a positive function, from (B.6) we can calculate an upper-estimation of the time t_s when $V(t)$ vanishes and consequently also $x(t)$ do it. Thence, we obtain that

$$t_s \leq \frac{\sqrt{2}}{\epsilon}V(t_0) + t_0$$

Thus in this example the EC is obtain from (B.5) when $\dot{x}$ and x are identical to zero, i.e. $u_{\mathrm{eq}} = -b^{-1}\gamma(t)$. We immediately, notice that the disturbance $\gamma(t)$ might be estimated by means of the equivalent control, a way to do it will be given below.

Notice that with the control u being a signum function the right-hand side of (B.5) is not Lipschitz, therefore, we can not use the theory of differential equations. To overcome such a complexity, we can use the theory of differential inclusions treated extensively in [Fil60]. Thus, we can obtain a solution of (B.5) in the Filippov sense.

Nevertheless, the effects of real devices, let say small delays, uncertainties, hysteresis, digital computations, etc., always avoid to achieve the identity $s(x) \equiv 0$. And the trajectories are constraint to some region around the origin, i.e., $\|s(x)\| \leq \Delta$. That is why, that we can ask for the limit solution of (B.1) when Δ tends to zero. That solution is in fact the solution of (B.1) on the sliding mode and it will be found using the equivalent control method, which will be justified by means of Theorem B.1.

Let $\tilde{u}$ be a control for which we obtain the boundary layer $\|s(x)\| \leq \Delta$, we could say that $\tilde{u}$ is the *real control* with which we obtain a real sliding mode. Thus, the dynamic equations are,

$$\dot{x}(t) = f(x,t) + B(x,t)\,\tilde{u}(t) \tag{B.7}$$

Let us notate by x^* the state vector obtained using the EC method, i.e. the trajectories whose dynamics is governed by (B.4). Let us assume that the distance of any point in the set $S_r = \{x : \|s(x)\| \leq \Delta\}$ to the manifold S is estimated by the inequality

$$d(x,S) \leq P\Delta, \;\; for\; P > 0.$$

Such a number P always exists if all gradients of functions $s_i(x)$ are linearly independent and are lower bounded in the norm by some positive number. In fact the first condition follows from the assumption that $\det(GB) \neq 0$.

Theorem B.1. *Let us assume that the following 4 conditions are satisfied:*

1. *there is a solution $x(t)$ of system (B.7) which, on the interval $[0,T]$, fulfills the inequality $\|s(x)\| \leq \Delta$;*
2. *for the right-hand part of (B.4), rewritten using x^* as*

$$\dot{x}^*(t) = f(x^*,t) - B(x^*,t)\left[G(x^*)\,B(x^*,t)\right]^{-1}\left[G(x^*)\,f(x^*,t)\right], \tag{B.8}$$

   a Lipschitz constant exists;
3. *partial derivatives of the function $B(x,t)\left[G(x)\,B(x,t)\right]^{-1}$ with respect to all arguments exist and are bounded in every bounded domain, and*
4. *for the right-hand part (B.7) there exist positive numbers M and N such that*

$$\|f(x,t) + B(x,t)\,\tilde{u}\| \leq M + N\,\|x\|\,. \tag{B.9}$$

Then for any pair of solutions to eqs. (B.8) and (B.7) with their initial conditions satisfying

$$\|x(0) - x^*(0)\| \leq P\Delta$$

there exists a positive number H such that

$$\|x(t) - x^*(t)\| \leq H\Delta \text{ for all } t \in [0, T].$$

Proof. For (B.7) we will obtain the following derivative on time of $s(x)$,

$$\dot{s}(x) = G(x)\, f(x,t) + G(x)\, B(x,t)\, \tilde{u}(t) \tag{B.10}$$

since we have assumed that $\det(GB) \neq 0$, from (B.10) we obtain that

$$\tilde{u}(t) = [G(x)\, B(x,t)]^{-1}\, \dot{s}(x) - [G(x)\, B(x,t)]^{-1}\, G(x)\, f(x,t) \tag{B.11}$$

The substitution of $\tilde{u}(t)$ into (B.7) yields

$$\dot{x} = f - B\,[GB]^{-1}\, Gf + B\,[GB]^{-1}\, \dot{s} \tag{B.12}$$

Thus, we have that (B.8) and (B.12) differ from a term depending on $\dot{s}$. By integrating, x^* and x can be written by the following integral equations,

$$x^*(t) = x^*(0) + \int_0^t \left\{ f(x^*, \tau) - B(x^*, \tau)\, [G(x^*)\, B(x^*, \tau)]^{-1}\, [G(x^*)\, f(x^*, \tau)] \right\} d\tau, \tag{B.13}$$

$$\begin{aligned} x(t) = x(0) + \int_0^t \left\{ f(x, \tau) - B(x, \tau)\, [G(x)\, B(x, \tau)]^{-1}\, [G(x)\, f(x, \tau)] \right\} d\tau + \\ + \int_0^t B(x, \tau)\, [G(x)\, B(x, \tau)]^{-1}\, \dot{s}(x)\, d\tau \end{aligned} \tag{B.14}$$

By integrating the last term of (B.14) by parts, and taking into account the hypothesis of the theorem, we can obtain the following estimation of the difference of the two solutions,

$$\begin{aligned} \|x(t) - x^*(t)\| \leq P\Delta + \int_0^t L\, \|x(\tau) - x^*(\tau)\|\, d\tau \\ + \left\| B(x, \tau)\, [G(x)\, B(x, \tau)]^{-1}\, s(x) \right\| \Big|_0^t \\ + \int_0^t \left\| \frac{d}{d\tau} B(x, \tau)\, [G(x)\, B(x, \tau)]^{-1} \right\| \|s(x)\|\, d\tau \end{aligned} \tag{B.15}$$

By the assumption (B.9), we have that the norm of $x(t)$ is bounded in a interval $[0,T]$, indeed, since

$$\|x(t)\| \leq \|x(0)\| + MT + \int_0^t N\|x(\tau)\| \, d\tau.$$

According to the Bellman-Gronwall lemma (see, e.g. [Poz08]) the following inequality is satisfied,

$$\|x(t)\| \leq (\|x(0)\| + MT)\, e^{NT}, \text{ for all } t \in [0,T]. \tag{B.16}$$

Thus by the continuity of f and B, and taking into account hypothesis 3 of the theorem, the inequality (B.15) may be represented as follows,

$$\|x(t) - x^*(t)\| \leq Q\Delta + \int_0^t L\|x(\tau) - x^*(\tau)\| \, d\tau$$

where Q is a positive number. Using again the Bellman-Gronwall lemma, we obtain the inequality

$$\|x(t) - x^*(t)\| \leq Q\Delta e^{LT}$$

Taking $H = Qe^{LT}$, the theorem is proven.

Thus, from the theorem we have that $\lim_{\Delta\to 0} x(t) \to x^*(t)$ in a finite interval. This justifies the equivalent control method.

We have say the equivalent control method might be used for the estimation of the matched disturbances, as in the example where $u_{\mathrm{eq}} = -\gamma$. Next, we will see how to estimate the function u_{eq} by means of a first-order low-pass filter. We will make use of the following lemma.

Lemma B.2. *Let the differential equation be as follows*

$$\tau\dot{z}(t) + z(t) = h(t) + H(t)\,\dot{s} \tag{B.17}$$

where τ is a scalar constant and z, h and s are m-dimensional function vectors. If the following assumptions are satisfied,

i) *the functions $h(t)$ and $H(t)$, and their first order derivatives are bounded in magnitude by a certain number M and*
ii) $\|s(t)\| \leq \Delta$, *Δ being a constant positive value,*

then, for any pair of positive numbers Δt and ε, there exists a number $\delta = \delta(\varepsilon, \Delta t, z(0))$ such that the following inequality is fulfilled

$$\|z(t) - h(t)\| \leq \varepsilon$$

provided that $0 < \tau \leq \delta$, $\Delta/\tau \leq \delta$ and $t \geq \Delta t$.

Proof. Let us write the solution of (B.17).

$$z(t) = e^{-t/\tau} z(0) + \frac{1}{\tau} \int_0^t e^{-(t-\sigma)/\tau} \left[h(\sigma) + H(\sigma) \dot{s}(\sigma) \right] d\sigma$$

By integrating by parts we obtain,

$$\begin{aligned} z(t) = {} & e^{-t/\tau} z(0) + h(t) - h(0) e^{-t/\tau} \\ & - \int_{0h}^{t} e^{-(t-\sigma)/\tau} \dot{h}(\sigma) \, d\sigma + H(t) \frac{s}{\tau} - H(0) e^{-t/\tau} \frac{s(0)}{\tau} \\ & - \frac{1}{\tau} \int_0^t e^{-(t-\sigma)/\tau} \left[\dot{H}(\sigma) + \frac{1}{\tau} H(\tau) \right] s(\sigma) \, d\sigma \end{aligned}$$

Then, by the assumptions (i) and (ii), we deduce the following inequality,

$$\|z(t) - h(t)\| \leq \|z(0) - h(0)\| e^{-t/\tau} + M\tau + \frac{2M\Delta}{\tau} + M\Delta + \frac{M\Delta}{\tau}$$

putting similar terms together yields

$$\|z(t) - h(t)\| \leq \|z(0) - h(0)\| e^{-t/\tau} + M(\tau + \Delta) + 3M\frac{\Delta}{\tau} \tag{B.18}$$

Therefore, it is easy to conclude from (B.18) that for any positive number Δt, the following identity is achieved,

$$\lim_{\substack{\tau \to 0 \\ \Delta/\tau \to 0}} z(t) = h(t) \text{ for all } t \geq \Delta t \tag{B.19}$$

Thus, the lemma is proven.

From (B.19), we see that Δ should be much smaller that τ in order to achieve a good estimation of $h(t)$ by means of $z(t)$. Furthermore, (B.18) gives us a more qualitative expression to measure the effect of τ on the estimation. That is, there we can see that if τ is too small then the term depending on the difference on the initial conditions could be considered negligible, i.e. $z(t)$ reaches rapidly a neighborhood around $h(t)$ of order $O(\tau + \Delta) + O\left(\frac{\Delta}{\tau}\right)$. In this case, if Δ is not much smaller than τ, then the neighborhood around $h(t)$ would be big. On the other hand if $\Delta << \tau$, but τ is not so small, then $z(t)$ would last some time before reaching a small neighborhood around $h(t)$. That is why, we can say that an 'ideal' case case is when $\Delta << \tau << 1$.

Thus, the filter designed as

$$\tau u_{\text{av}}(t) + u_{\text{av}}(t) = \tilde{u}(t) \tag{B.20}$$

can be used to estimate u_{eq}. Indeed, from (B.3) and (B.11), (B.20) takes the form

$$\tau u_{\mathrm{av}}\left(t\right)+u_{\mathrm{av}}\left(t\right)=u_{\mathrm{eq}}+\left[G\left(x\right)B\left(x,t\right)\right]^{-1}\dot{s}\left(x\right) \tag{B.21}$$

Hence, by comparing (B.17) with (B.21), lemma implies that

$$\lim_{\substack{\tau\to 0\\ \Delta/\tau\to 0}} u_{\mathrm{av}}=u_{\mathrm{eq}}\ for\ t\in\left(0,T\right] \tag{B.22}$$

provided that u_{eq} and $\left(GB\right)^{-1}$ are bounded and have bounded derivatives, which is fulfilled if conditions of Theorem B.1 are fulfilled.

Now, let us assume that Δ is known (which in general might be not true). In that case we could select $\tau=\Delta^{1/r}$ $(r>1)$, implying that $\Delta/\tau=\Delta^{\frac{r-1}{r}}$. Thus, as Δ tends to zero, Δ/τ tends to zero also. Therefore, in that case, B.22 is still satisfied. For the same qualitative arguments given above, a good estimation of u_{eq} using u_{av} is obtained when it is satisfied that $\Delta<<\tau<<1$. When r is close to 1 then τ is close to Δ; therefore, r near 1 is not a good selection. On the other hand, for $r>>1$, τ is close to 1, then in that case r is not a good choice either. By selecting $r=2$, we obtain, for Δ enough small, that $\Delta<<\tau<<1$. Hence, by selecting $\tau=\Delta^{1/2}$ and provided that Δ is much smaller than 1, we obtain a good estimation of u_{eq}.

Appendix C
Vehicle Parameters Description

C.1 Vehicle Data

Parameter	Value
M	1296 Kg
r_{1i}	0.28 m
I_{ri}	0.9 $Kg.m^2$
l_o	-0.03 m
C_{ij}	50000 N/rad

Parameter	Value
M	1296 Kg
r_{1i}	0.28 m
I_{ri}	0.9 $Kg.m^2$
l_o	-0.03 m
C_{ij}	50000 N/rad

C.2 Friction Parameters Characteristics

Type of cover	c1	c2	c3
Asphalt, dry	1.2801	23.99	0.52
Asphalt, wet	0.857	33.822	0.347
Concrete, dry	1.1973	25.168	0.5373
Cobblestones, dry	1.3713	6.4565	0.6691
Cobblestones, wet	0.4004	33.7080	0.1204
Snow	0.1946	94.129	0.0646
Ice	0.05	306.39	0

Appendix D
Matrices Definitions

The matrices E_1, E_2, A_1 and A_2 have been used in the chapter IV in the section "Unknown Forces Estimation".

The matrices $E_1$and E_2 are defined as follows:

$$E_1 = \begin{bmatrix} 1&0&0&0&0&0&0&0&0&0&0&0 \\ 0&1&0&0&0&0&0&0&0&0&0&0 \\ 0&0&1&0&0&0&0&0&0&0&0&0 \\ 0&0&0&1&0&0&0&0&0&0&0&0 \\ 0&0&0&0&1&0&0&0&0&0&0&0 \\ 0&0&0&0&0&1&0&0&0&0&0&0 \\ 0&0&0&0&0&0&1&0&0&0&0&0 \\ 0&0&0&0&0&0&0&1&0&0&0&0 \end{bmatrix}$$

$$E_2 = \begin{bmatrix} 0&0&0&0&0&0&0&0&1&0&0&0 \\ 0&0&0&0&0&0&0&0&0&1&0&0 \\ 0&0&0&0&0&0&0&0&0&0&1&0 \\ 0&0&0&0&0&0&0&0&0&0&0&1 \end{bmatrix}$$

The matrices A_1 and A_2 are defined as follows:

$$A_1 = \begin{bmatrix} 1&0&0&0&0&0&0&0 \\ 0&1&0&0&0&0&0&0 \\ 0&0&1&0&0&0&0&0 \\ 0&0&0&1&0&0&0&0 \\ 0&0&0&0&1&0&0&0 \\ 0&0&0&0&0&1&0&0 \\ 0&0&0&0&0&0&1&0 \\ 0&0&0&0&0&0&0&1 \\ 0&0&0&0&0&0&0&0 \\ 0&0&0&0&0&0&0&0 \\ 0&0&0&0&0&0&0&0 \\ 0&0&0&0&0&0&0&0 \end{bmatrix}, \quad A_2 = \begin{bmatrix} 0&0&0&0 \\ 0&0&0&0 \\ 0&0&0&0 \\ 0&0&0&0 \\ 0&0&0&0 \\ 0&0&0&0 \\ 0&0&0&0 \\ 0&0&0&0 \\ 1&0&0&0 \\ 0&1&0&0 \\ 0&0&1&0 \\ 0&0&0&1 \end{bmatrix}$$